Effects of Salinity Variations in the Labrador Sea

An evaluation of salinity effects on the Labrador Sea circulation through an idealized model

Storm Woud
Master of Science Thesis

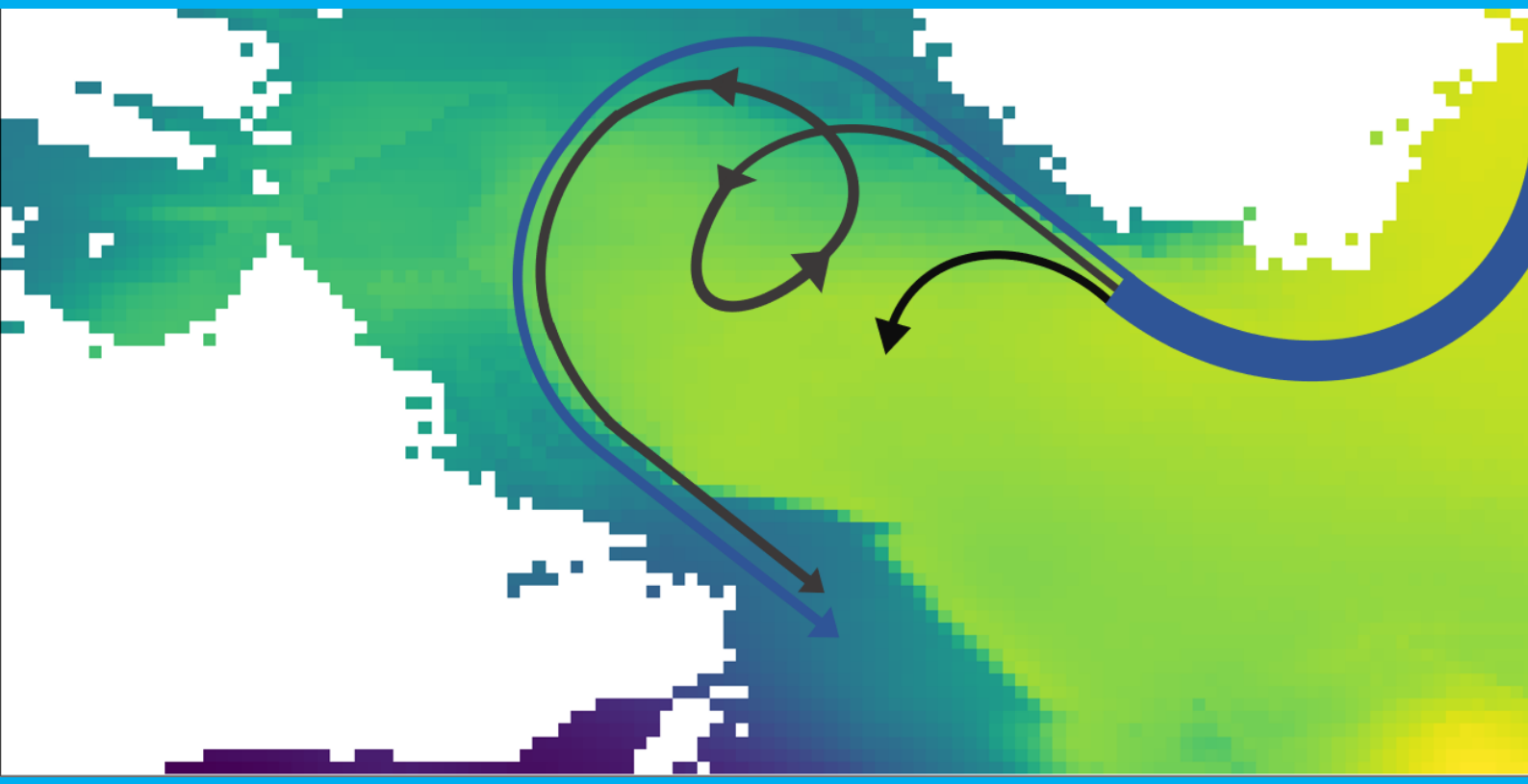

TU Delft

Effects of Salinity Variations in the Labrador Sea

An evaluation of salinity effects on the Labrador Sea circulation through an idealized model

by:
S.T.A.Woud

Project duration: October, 2019 – May, 2020
Supervisors: Dr. C.A. Katsman, TU Delft
Dr. M. Vizcaino TU Delft
Dr. J.M. Sayol TU Delft
Prof. Dr. J.D. Pietrzak TU Delft

Abstract

The Labrador Sea is one of the deep convection sites in the world's oceans and the water masses formed here are an important component of the Atlantic Meridional Overturning Circulation (AMOC). To study this linkage, one study in particular used an idealized model of the Labrador Sea where the density variations consists only of temperature variations [1]. In this study, it is questioned whether the assumption of neglecting salinity is appropriate, by analysing the pathways of water mass and water mass transformation in the Labrador Sea. This is investigated by using that same idealized model (here called the reference run) and comparing this to a model where salinity variations are added whilst keeping density variations the same (Sconstant) to produce a similar circulation pattern. Furthermore, a model configuration is created which investigates if a seasonal cycle in salinity impacts the circulation pattern of the Labrador Sea (Sseasonal). The pathways of water masses in these model configurations are analyzed by Lagrangian particle tracking from A to B. It was found that with the same initial density variations the maximum surface eddy kinetic energy (EKE) increases by 41 % when salinity is incorporated in the model. An increase in EKE is often associated with more water mass leaving the boundary current (BC) due to an increase in instabilities. Surprisingly, the opposite was found: 7.02 and 8.22 Sv are transported through the BC for the reference run and Sconstant, respectively. Furthermore it was found that most of the water mass leaves and re-enters the BC near the maximum EKE for each model configuration. An increase was found in maximum overturning in density space from an Eulerian perspective: from 3.9 to 4.8 Sv for the reference run and Sconstant, respectively, where about 10 % so called density compensation occurred for Sconstant. No significant annual changes are found when adding a seasonal cycle to the model. For all model configurations a large discrepancy exists between Eulerian and Lagrangian calculations in downwelling. This discrepancy is due to Lagrangian particles that reside in the models at the end of their simulation duration Thus the overturning in the Labrador Sea is significantly influenced by particles that have a long residence time (longer than 4 years in these model simulations). Between 22 and 25 % of the Lagrangian volume transport does not reach the outflow of each model simulation. There are also properties that salinity did not influence: no significant changes were found between the model configurations for the overturning in depth space, the annual MLD and barotropic streamfunction. In conclusion adding salinity to the idealized model showed only minor changes in the pathways of water mass and water mass transformation: the order of magnitude of all analyzed properties stays the same. Density compensation however is neglected when no salinity variations are added in the model. This means that for a highly idealized model of the Labrador Sea, salinity variations can be neglected, when density variations due to salinity variations are represented by temperature variations.

Contents

Abstract ii

List of Figures v

List of Tables ix

Acknowledgements x

1 Introduction 1
- 1.1 Atlantic Meridional Overturning Circulation (AMOC) . . . 1
- 1.2 Deep convection and downwelling . . . 2
  - 1.2.1 Deep convection . . . 3
  - 1.2.2 Downwelling . . . 4
- 1.3 Labrador Sea hydrography and circulation . . . 4
  - 1.3.1 Main currents . . . 4
  - 1.3.2 Hydrography of the Labrador Sea . . . 4
  - 1.3.3 (Sub)Mesoscale activity (eddies) . . . 6
  - 1.3.4 Influence of salinity on the circulation . . . 6
- 1.4 Research questions . . . 7

2 Model setup 9
- 2.1 General model configuration . . . 9
- 2.2 Set of model simulations . . . 10
  - 2.2.1 Profiles in the interior initial condition . . . 11
  - 2.2.2 Inflow conditions of the reference run . . . 11
  - 2.2.3 Inflow conditions of Sconstant . . . 13
  - 2.2.4 Inflow conditions of Sseasonal . . . 14
  - 2.2.5 Summary of inflow conditions for each model configuration . . . 14

3 Lagrangian particle tracking 17
- 3.1 CMS description . . . 17
- 3.2 CMS input . . . 17
- 3.3 CMS output . . . 17

4 Main features of idealized Labrador Sea circulation 19
- 4.1 Mean barotropic streamfunction . . . 19
- 4.2 Mixed layer depth . . . 19
- 4.3 Eddy kinetic energy . . . 21
- 4.4 Downwelling . . . 23

5 Lagrangian pathways and volume transport 26
- 5.1 Separating boundary current and interior pathways . . . 26
- 5.2 Comparison pathway transport . . . 27
- 5.3 Overturning depth space based on Lagrangian particles . . . 29
- 5.4 Overturning density space based on Lagrangian particles . . . 29
  - 5.4.1 Overturning density space for Sconstant and Sseasonal . . . 31
  - 5.4.2 Overturning density space for the reference run . . . 32
  - 5.4.3 Closer look at the withinBC particles . . . 32
  - 5.4.4 Closer look at the InteriorShort particles . . . 34
  - 5.4.5 Closer look at particles released in the top 110 m . . . 36
- 5.5 Summary . . . 37

6 Discussion and Conclusion 39

7 Recommendations 43

Bibliography 45

A Appendix A - Derivation inflow conditions for the reference run 48

B Appendix B - Supplementary figures 50
B.1 Bar plots of volume transport at the inflow and outflow 51
B.2 Net and cumulative volume transport 53
B.3 Volume transport separated into inflow and outflow, and net volume transport 54
B.4 Lateral transport of InteriorShort particles in area 1 57
B.5 Net and cumulative volume transport of the top 110m waters 58

List of Figures

1.1 Zonal mean of the absorbed shortwave radiation from the sun (blue line) and the outgoing longwave radiation of the Earth (red line). When more energy is absorbed than is released, the Earth is a net absorber (blue line > red line), which happens at the tropics. Vice versa at the poles the earth is a net emitter (red line > blue line). From: `http://www.met.reading.ac.uk/~sgs02rpa/CONTED/cl-intro.html` 2

1.2 Simplified sketch of the thermohaline Circulation or Ocean Conveyor Belt. The three shaded areas are locations where deep convection occurs. Note that deep convection also occurs int he Mediterranean Sea, but is not indicated in the figure. (from `https://en.wikipedia.org/wiki/Shutdown_of_thermohaline_circulation`) 2

1.3 Simplified sketch of Deep convection due to temperature differences. The black arrows on top indicate cooling and the black arrows in the figure indicate mixing. Left panel: warm and salty water is on top of cold and salty water. Middle panel: the top layer becomes colder due to surface cooling. Right panel: the top layer has cooled enough for its density to be lower than the bottom layer, and thus they mix as the heavier surface layer starts to sink [5]. 3

1.4 Schematic top view of deep convection (from `http://puddle.mit.edu/~helen/oodc.html`). In the plumes vertical mixing occurs with speeds of up to 0.1 m/s. Between the chimney and the stratified waters a horizontal density gradient exists, causing Convective Eddies to be formed due to baroclinic instabilities. 3

1.5 3D view of three currents entering the Labrador Sea. From top to bottom: light blue = West Greenland Current, Orange = Irminger Current, dark blue = Deep Western Boundary Current. (from: `https://www.o-snap.org`) 5

1.6 Hydrography of the Labrador Sea in the year 2005 along the WOCE AR7W section, from [15]. Potential temperature is shown in the upper panel and salinity is shown in the lower panel. The black dotted lines are isopycnals. LSW = Labrador Sea Water, LSW_{2000} = Labrador Sea Water formed in 2000. NEADW = NortEast Atlantic Deep Water, DSOW = Denmark Strait Overflow Water. the black lines are isopycnals [15]. 5

1.7 A schematic of residual overturning in a marginal sea, where strong eddy activity occurs along the boundary current. In the upper part of the boundary current water mass transformation occurs, where the warmer layers outcrop to the surface. This allows for diapycnal processes to occur at the surface due to a horizontal flow. In the interior water masses are transformed trough deep convection. This is connected to the boundary current by means of eddies which transport waters out of the boundary current. This overturning loop is then closed by an isopycnal eddy flow along tilted isopycnals. [13] 7

2.1 (a) Surface mean heat flux of the Labrador Sea, from the climatology of the WHOI AOFlux project [30]. (b) The applied Annual mean surface heat flux in the model configurations (Q < 0 Wm^{-2} means that there is a net surface cooling) (c) Maximum surface heat flux (solid line, occurs at the white marker in b) and average surface heat flux (dashed line) in the model configurations. Adapted from [1]. 10

2.2 a) 36 Years (1984-2020) average salinity in the top layer in the Labrador Sea. The black boxes indicate which data has been used to construct an average vertical salinity profile. The large square represents the data of the interior and the small square that of the boundary current. Data from [31]. b) The 36 years averaged density, temperature and salinity profiles over the vertical of the interior of the Labrador Sea for the model runs. The red line is the density and is the same in each run. The black solid line is the temperature of the reference run. the black dashed and blue lines are the temperature and salinity of the other runs. 12

2.3 36 Years (1984-2020) average salinity (a) and temperature (b) for the boundary current, from (line) observations and (dots) as prescribed in the model. Data from: [31] 12

2.4 36 Years (1984-2020) average salinity (a) and temperature (b) for the boundary current, from (line) observations and (dots) as prescribed in the model. Data from [31] 13

2.5 Blue dots: 36-years average monthly climatology of salinity in the top layer of the boundary current (data from [31]). Red dots: adjusted value such that a stable stratification at the inflow is achieved, which are used for the Sseasonal configuration. Black dotted line: mean of the monthly values. 15
2.6 Vertical density difference (red), adjusted density (red dotted), density difference due to salinity (blue) adjusted density difference due to salinity (blue dotted) and density difference due to temperature (black) 15
2.7 The prescribed annually averaged inflow conditions for all three runs. Top to bottom: zonal velocity, temperature, salinity and horizontal density difference with respect to the initial interior density 16

3.1 a) Release location at the inflow of the particles in meridional direction over the depth b) pathway of particles for a particle that is too close to land (blue line), leaves through the interior (red line), leaves the model domain at the outflow (green line) or stays in the model after 5 years of running time (pink line) 18

4.1 5-Year mean barotropic streamfunction (ψ_B, contour interval is 4 Sv) of each model configuration. The black dashed line is the 19.6 (20.1) Sv contour line for the reference run and Sconstant (Sseasonal). The dark grey lines outline the bathymetry (interval 500 m). 20
4.2 The 5-year mean Mixed Layer Depth (MLD) of February and March of each model configuration (contour interval is 500 m) 20
4.3 Top panel: 5-year average sea surface temperature and salinity (SST and SSS) of the simulations; bottom panel: the maximum mixed layer depth over the last 5 years of the simulations. 21
4.4 Average contour (thick lines) of the winter MLD over the last 5 years of the model simulations (red = reference run, blue = Sconstant, green = Sseasonal). a) MLD level = 500 m. b) MLD level = 1000 m. c) MLD level = 1500 m. The thinner, transparent lines are the MLD per year for five years for each of the model simulations. 22
4.5 Surface Eddy Kinetic Energy (EKE) of for a) reference run b) Sconstant c) Sseasonal (contour interval is 100 cm^2/s^2) 22
4.6 Surface Eddy Kinetic Energy (EKE) comparisons between the model simulations. a) The reference run is compared to Sconstant b) the reference run is compared to Sseasonal. c) Sseasonal is compared to Sconstant. (contour interval is 100 cm^2/s^2)s 22
4.7 Cross section of several eddies that are shed from the boundary current. The colours indicate the temperature and the contour lines the salinity. The map on the bottom left shows the SST and the position of the eddy (green dot). (4.7a-c): an eddy of the reference run in August (a), October (b) and January (c). (4.7d-f) eddy in Sconstant, (4.7g-i) eddy in Sseasonal. 24
4.8 Separation of 4 areas in the basin for all model simulations. Area 1 is the area with the highest EKE. Area 2 is the area with the highest cooling. Area 3 is the area with another smaller EKE peak. Area 4 is the interior of the basin. 25
4.9 Vertical volume transport in Sv for each model simulations. The transport is separated per area as defined in figure 4.8. (a) is the reference run, (b) is Sconstant, (c) is Sseasonal 25

5.1 Example pathways for particles that are defined as withinBC, InteriorShort or Interiorlong, based on method 2 (see text for description of this method). Darkgray is the landmass; lightgray is the BC; white is the interior. Note that one of the withinBC particles sometimes is in the defined interior but is still classified as withinBC 28
5.2 Bar plots of transport of the inflow (blue bars) and outflow (green bars) in depth space binned every 100 m. Figures a-c show the reference run, d-f show Sconstant and g-i show Sseasonal. From top to bottom separations have been made for particles that flow only through the boundary current (a,d,g), InteriorShort particles (b,e,h) and InteriorLong particles (c,f,i). . 30
5.3 Net volume transport (out - in, top panels) and cumulative transport (bottom panels) for Sconstant binned every 100 m for depth space (a,e), 0,1 ^0C for temperature space (b,f) 0.01 PSU for salinity space (c,g) and 0.01 kg/m^3 for density space (d,h). Eulerian is the total calculated net transport (green line), withinBC particles are black, InteriorShort particles are red, their sum is the Lagrangian calculated flow (purple). The transport of the InteriorLong particles is also shown (blue dashed line). 32

5.4 Bar plots of transport of the inflow (blue bars) and outflow (green bars) for Sconstant. Figures a-c show temperature space, binned every 0.1 °C, d-f show salinity space binned every 0.01 PSU and g-i density space binned every 0.01kg/m^3. From top to bottom separations have been made for particles that flow only through the boundary current (a,d,g), InteriorShort particles (b,e,h) and InteriorLong particles (c,f,i). 33
5.5 TS diagrams for withinBC particles along their trajectory for the run Sconstant. The small figure in each plot indicates where data for the TS-diagram is obtained. a) TS-diagram boundary current. b-d) TS-diagram area 1, e,f) TS-diagram area 2, g) TS-diagram area 3, h) TS-diagram at the outflow. The grey lines are the specific density contours 34
5.6 TS diagrams for the InteriorShort particles at the inflow (a) and outflow (b) for the run Sconstant. The grey lines are the specific density contours 35
5.7 Concentration of where volume transport leaves the BC (a), re-enters the BC (b) and net transport (c) of InteriorShort particles in area1 for the Sconstant. The contour lines show the EKE. 36
5.8 Net overturning (top panels) and cumulative overturning (bottom panels) for particles starting in the top 110 m at the inflow for Sconstant binned every 100 m for depth space (a,e), 0,1 ^0C for temperature space (b,f) 0.01 PSU for salinity space (c,g) and 0.01 kg/m^3 for density space (d,h). The withinBC particles are black, InteriorShort particles are red, their sum is the calculated Lagrangian flow (purple). The transport of the InteriorLong particles is also shown (blue dashed line). 38

B.1 Bar plots of transport of the inflow (blue bars) and outflow (green bars) for the reference run in. Figures a-c show temperature space, binned every 0.1 ^0C, d-f show salinity space binned every 0.01 PSU and g-i density space binned every 0.01kg/m^3. From top to bottom separations have been made for particles that flow only through the boundary current (a,d,g), InteriorShort particles (b,e,h) and InteriorLong particles (c,f,i). 51
B.2 Bar plots of transport of the inflow (blue bars) and outflow (green bars) for Sseasonal in. Figures a-c show temperature space, binned every 0.1 ^0C, d-f show salinity space binned every 0.01 PSU and g-i density space binned every 0.01kg/m^3. From top to bottom separations have been made for particles that flow only through the boundary current (a,d,g), InteriorShort particles (b,e,h) and InteriorLong particles (c,f,i). 52
B.3 Net volume transport (out - in, top panels) and cumulative transport (bottom panels) for the reference run binned every 100m for depth space (a,e), 0,1 ^0C for temperature space (b,f) 0.01 PSU for salinity space (c,g) and 0.01 kg/m^3 for density space (d,h). Eulerian is the total calculated net transport (green line), withinBC particles are black, InteriorShort particles are red, their sum is the calculated Lagrangian flow (purple). The transport of the InteriorLong particles is also shown (blue dashed line). 53
B.4 Net volume transport (out - in, top panels) and cumulative transport (bottom panels) for Sseasonal binned every 100m for depth space (a,e), 0,1 ^0C for temperature space (b,f) 0.01 PSU for salinity space (c,g) and 0.01 kg/m^3 for density space (d,h). Eulerian is the total calculated net transport (green line), withinBC particles are black, InteriorShort particles are red, their sum is the calculated Lagrangian flow (purple). The transport of the InteriorLong particles is also shown (blue dashed line). 53
B.5 Net overturning (left column), total inflow (middle column) and total outflow (right column) for the reference run binned every 100m for depth space (a,b,c), 0,1 ^0C for temperature space (d,e,f) 0.01 PSU for salinity space (g,h,i) and 0.01 kg/m^3 for density space (j,k,l). Eulerian is the total calculated net transport (green line), withinBC particles are black, InteriorShort particles are red, their sum is the calculated Lagrangian flow (purple). The transport of the InteriorLong particles is also shown (blue dashed line). The yellow line at the inflow is Lagrangian + InteriorLong. 54
B.6 Net overturning (left column), total inflow (middle column) and total outflow (right column) for Sconstant binned every 100m for depth space (a,b,c), 0,1 ^0C for temperature space (d,e,f) 0.01 PSU for salinity space (g,h,i) and 0.01 kg/m^3 for density space (j,k,l). Eulerian is the total calculated net transport (green line), withinBC particles are black, InteriorShort particles are red, their sum is the calculated Lagrangian flow (purple). The transport of the InteriorLong particles is also shown (blue dashed line). The yellow line at the inflow is Lagrangian + InteriorLong. 55

B.7 Net overturning (left column), total inflow (middle column) and total outflow (right column) for Sseasonal binned every 100m for depth space (a,b,c), 0,1 ^0C for temperature space (d,e,f) 0.01 PSU for salinity space (g,h,i) and 0.01 kg/m^3 for density space (j,k,l). Eulerian is the total calculated net transport (green line), withinBC particles are black, InteriorShort particles are red, their sum is the calculated Lagrangian flow (purple). The transport of the InteriorLong particles is also shown (blue dashed line). The yellow line at the inflow is Lagrangian + InteriorLong. 56
B.8 Concentration of where volume transport leaves the BC (a), re-enters the BC (b) and net transport (c) of InteriorShort particles in area1 for the reference run. The contour lines show the EKE. 57
B.9 Concentration of where volume transport leaves the BC (a), re-enters the BC (b) and net transport (c) of InteriorShort particles in area1 for Sseasonal. The contour lines show the EKE. . . . 57
B.10 Net overturning (top panels) and cumulative overturning (bottom panels) for particles starting in the top 110m at the inflow for the reference run binned every 100m for depth space (a,e), 0,1 ^0C for temperature space (b,f) 0.01 PSU for salinity space (c,g) and 0.01 kg/m^3 for density space (d,h). The withinBC particles are black, InteriorShort particles are red, their sum is the calculated Lagrangian flow (purple). The transport of the InteriorLong particles is also shown (blue dashed line). 58
B.11 Net overturning (top panels) and cumulative overturning (bottom panels) for particles starting in the top 110m at the inflow for Sseasonal binned every 100m for depth space (a,e), 0,1 ^0C for temperature space (b,f) 0.01 PSU for salinity space (c,g) and 0.01 kg/m^3 for density space (d,h). The withinBC particles are black, InteriorShort particles are red, their sum is the calculated Lagrangian flow (purple). The transport of the InteriorLong particles is also shown (blue dashed line). 58

List of Tables

2.1 Several parameters that are used in each of the model configurations 10
2.2 Names of the model configurations, on what the vertical density profile depends for the interior and the inflow conditions (T or S and T), and the transport entering the domain. 11

3.1 Lost volume transport for different criteria. Criteria 1 removes particles that are too close to land. Criteria 2 removes particles which have no data files. Criteria 3 removes particles that left the model but not at the outflow 18
3.2 Lost particles after applying the same criteria as in table 3.1 18

4.1 Sv entering the basin, the chosen contour line and the maximum barotropic streamfunction in the basin for the model simulations. 19

5.1 Method 1: particles and transport for BC, BClong, InteriorShort and InteriorLong particles for the criterion 50, 30 and 10 km offshore from the 2500 m bathymetry line. A total of 396769 particles are calculated carrying 17.42 Sv. 27
5.2 Method 2: particles and transport for BC, BClong, InteriorShort and InteriorLong particles for the criterion 30, 20 and 10 consecutive days offshore of the 19.7 Sv line (20 Sv for Sseasonal). A total of 435313 particles are calculated carrying 17.67 Sv. 27
5.3 Number of particles and transport that occurs for withinBC, BClong, InteriorShort and InteriorLong particles for the reference run, Sconstant and Sseasonal 28
5.4 Total transport and particles for where they leave and re-enter the boundary current, binned per area, as in figure 4.8, where 'inflow' is between the inflow and area1 and 'outflow' is between area 3 and the outflow. 36

Acknowledgements

I would like to thank my supervisors Dr. C.A. Katsman, Dr. J.M. Sayol, Prof. J.D. Pietrzak and Dr. M. Vizcaino for their valuable feedback during the writing of this thesis.
Also thank you to Dr. C.A. Katsman, Dr. J.M. Sayol and S. Georgiou MSc. Because of them, I've learned much more about the field of physical oceanography and modelling, and the conversations about these topics were always interesting with them.

1

Introduction

In this thesis the effects of salinity on the Labrador Sea circulation will be analyzed. This chapter presents the key concepts required to understand the circulation in the Labrador Sea, how salinity could affect it, and why this research is important. First, the main characteristics of the Atlantic Meridional Overturning Circulation (AMOC) and its relevance are outlined (Section 1.1). Second, the connection between the AMOC, deep convection and downwelling is discussed (Section 1.2). Third, the main dynamical features of the Labrador Sea, one of the regions where deep convection occurs and the target area of this thesis, are summarized (Section 1.3). Finally, the research questions for this research are outlined (Section 1.4).

1.1. Atlantic Meridional Overturning Circulation (AMOC)

Solar radiation warms the Earth. This warming is not equally distributed over the Earth's surface. In the tropics, the Earth is warmer as a result of an excess of absorbed solar radiation (blue line in fig 1.1) with respect to the outgoing terrestial radiation (red line in figure 1.1), with values of around 50 W/m^2 between -20 °S and 20 °N latitude. In contrast, at higher latitudes the Earth cools as the outgoing radiation overcomes the absorbed solar radiation with a deficit of around 60 W/m^2 near the poles. Moreover, seasonal differences in the net solar radiation exist due to the angle of Earth's inclination with respect to the ecliptic plane. As a result of this uneven warming, differences between the tropics and the poles would tend to rise indefinitely in the absence of a compensating meridional heat transport. In reality, energy is transported from the equator to the poles through the atmosphere and ocean. This transport is driven by density differences, which are mainly caused by temperature in the current state of the ocean, but can also be caused by salinity variations. For this reason the circulation is also described as the thermohaline circulation (THC). It is often illustrated (and oversimplified) as the Ocean Conveyor Belt whose general circulation pattern around the globe can be seen in figure 1.2 [2]. This circulation consist of four main branches: a transport of waters at depth to the surface due to upwelling processes thought to take place mainly at the Antarctic Circumpolar Current region, transport of relatively light surface waters poleward, formation of deep water where the waters become denser and sink, and a return flow at depth which closes the loop [3].

According to Sandström's theorem [4], this circulation can only exist if there is both a surface cooling and a heating at greater depth. However, the heating occurs normally only at the ocean's surface, and as these waters become lighter than their surroundings they do not sink. In the ocean, heat is being mixed downward due to turbulence coming from wind and tidal energy. This balances the transport of cold waters from the poles.

The volume transport through the North Atlantic Ocean is quantified by means of the Atlantic Meridional Overturning Circulation (AMOC) and is defined as the total circulation in the latitude-depth plane in the Atlantic Ocean [5]. The AMOC consists of both the THC and wind-driven flows, and is an important transporter of heat and chemicals such as carbon dioxide. Furthermore, it exerts a strong control on the stratification of the ocean as well as the distribution of water masses. The AMOC is responsible for 25% of the total meridional heat flux [5], and thus the AMOC is key to the Earth's climate system. In the present, two distinct driving mechanisms are affecting the Meridional Overturning Circulation (MOC). These are wind driven upwelling and vertical mixing. The upper part of the ocean is mainly forced by wind stress, whereas the deep ocean circulation is density driven [3].

The THC, and thus to a large extent the AMOC, is temperature-driven [5]. If the THC was salinity dominated, the flow would be in opposite direction. This is because due to net evaporation at the equator and net precip-

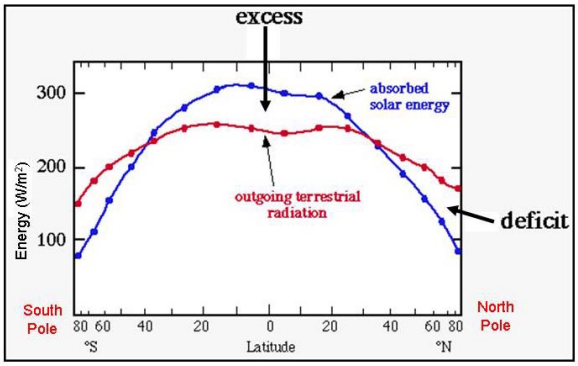

Figure 1.1: Zonal mean of the absorbed shortwave radiation from the sun (blue line) and the outgoing longwave radiation of the Earth (red line). When more energy is absorbed than is released, the Earth is a net absorber (blue line > red line), which happens at the tropics. Vice versa at the poles the earth is a net emitter (red line > blue line). From: `http://www.met.reading.ac.uk/~sgs02rpa/CONTED/cl-intro.html`

itation around the poles the waters become denser at the equator, as they are more saline. A density driven flow due to salinity is thus in the opposite direction [5]. This means that for the THC at least two equilibria can exist [6].

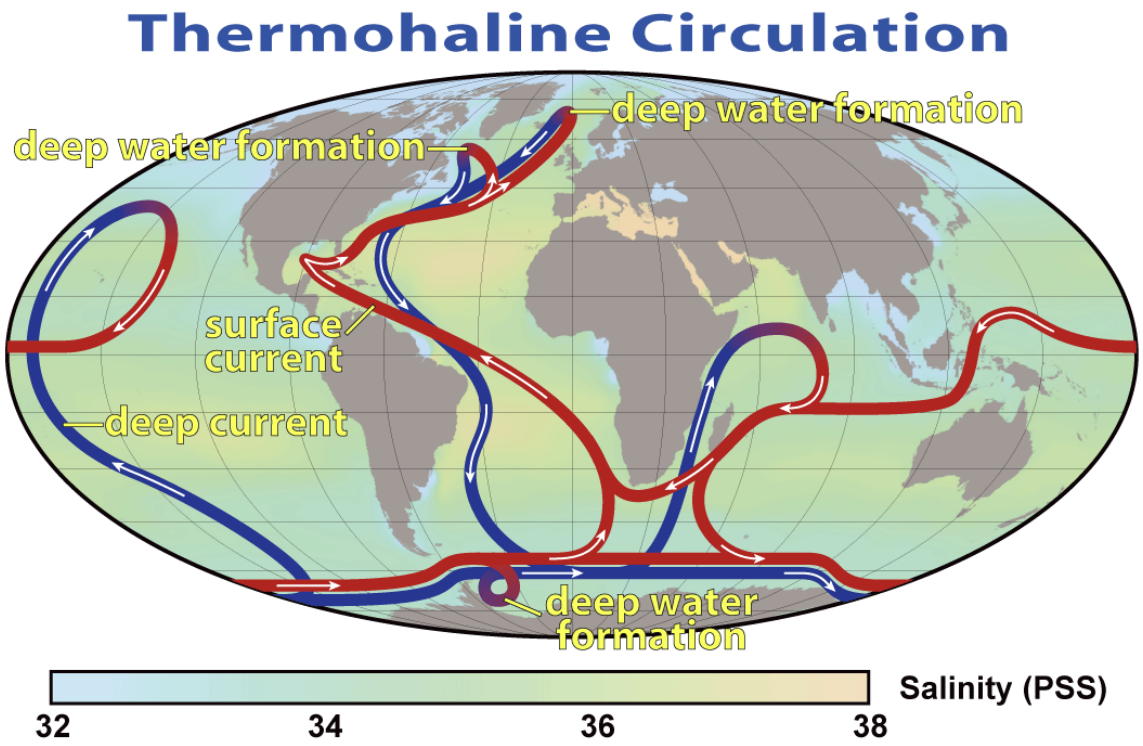

Figure 1.2: Simplified sketch of the thermohaline Circulation or Ocean Conveyor Belt. The three shaded areas are locations where deep convection occurs. Note that deep convection also occurs int he Mediterranean Sea, but is not indicated in the figure. (from `https://en.wikipedia.org/wiki/Shutdown_of_thermohaline_circulation`)

1.2. Deep convection and downwelling

The THC has a few areas where waters mix vertically and sink (see figure 1.2). The process of mixing is called deep convection and the sinking of waters is called downwelling. In the next sections, first deep convection will be explained (section 1.2.1), and thereafter downwelling (section 1.2.2)

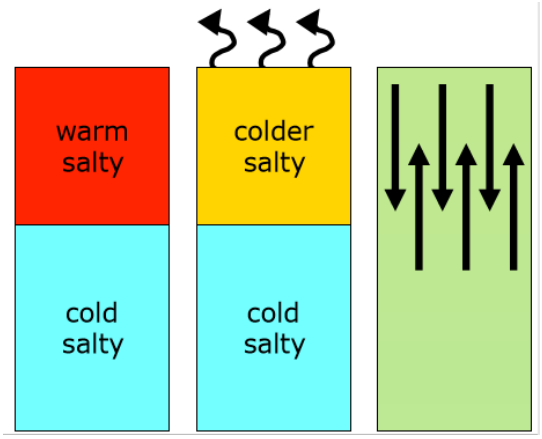

Figure 1.3: Simplified sketch of Deep convection due to temperature differences. The black arrows on top indicate cooling and the black arrows in the figure indicate mixing. Left panel: warm and salty water is on top of cold and salty water. Middle panel: the top layer becomes colder due to surface cooling. Right panel: the top layer has cooled enough for its density to be lower than the bottom layer, and thus they mix as the heavier surface layer starts to sink [5].

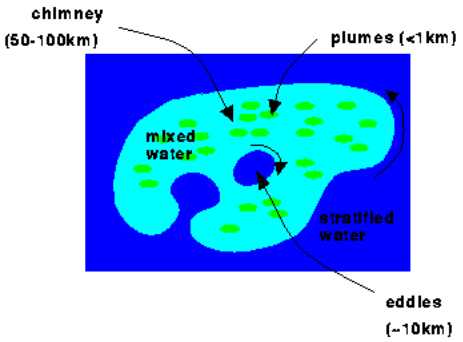

Figure 1.4: Schematic top view of deep convection (from `http://puddle.mit.edu/~helen/oodc.html`). In the plumes vertical mixing occurs with speeds of up to 0.1 m/s. Between the chimney and the stratified waters a horizontal density gradient exists, causing Convective Eddies to be formed due to baroclinic instabilities.

1.2.1. Deep convection

As explained above, the strength of the AMOC depends on vertical mixing. One of the regions where this vertical mixing occurs, is in the Labrador Sea (figure 1.2, located between Canada and Greenland). During winter, the surface waters cool. When the surface waters become so cold that the water column becomes statically unstable, they mix vertically with the waters below, as illustrated in figure 1.3. This is called convection. In the Labrador Sea, convection can reach depths of up to 2.5 km [7], and is therefore also referred to as "deep convection". Furthermore, due to a cyclonic gyre there is Ekman suction in the interior of the Labrador Sea. This causes the isopycnals – contour lines of constant density – in the Labrador Sea interior to dome upward, bringing already denser waters closer to the surface, further enhancing deep convection [8].
In order to further explain deep convection, a distinction between vertical mixing and net vertical volume transport has to be made. Due to convective mixing surface waters can reach great depths. The area in which this happens is referred to as "the chimney" (figure 1.4). In the chimneys there are plumes, which have a radius of about 1 km. Here, waters get convected downward and upwards with velocities larger than 0.1 m/s [9]. It is clear that a region of convection causes vertical mixing. However a region of convection often has no or a very small net vertical volume transport, as the upward and downward flow balance each other out [10].
The strength and depth which deep convection reaches is determined by several factors. The first one is the magnitude of the atmospheric-induced surface cooling. Deep convection usually only occurs in winter time in the Labrador Sea, when the surface cooling is at its maximum. Colder winters cause a larger difference in temperature between the sea surface and the atmosphere. This increases the cooling rate of the ocean and thus increases the density of the oceans top layer. The result is that colder and denser waters are formed during a cold winter as opposed to a mild winter [11]. Secondly, an increase in salinity creates denser waters and thus can facilitate deep convection. This could be due to evaporation of the surface waters or due to brine rejection: when sea ice is formed, the salt does not freeze with it and is thus rejected to the surrounding waters. The third factor is that the thermal expansion coefficient α reduces as water gets colder. This means that when a warm and a cold water are affected by an equal reduction of temperature, already colder waters have a reduced density increase. Thus to achieve the same density increase as the warmer waters, the colder waters will need to be cooled even further [11]. This combined with the first effect causes already cold surface water to loose both less heat and have a reduced thermal expansion coefficient, resulting in a reduced density increase as opposed to warmer waters. The fourth factor at play which can enhance or hinder the formation of deep waters is due to the wind driven gyre. In the case of the Northern Hemisphere the circulation is cyclonic in the subpolar region. This results in Ekman suction which brings the deeper and thus denser waters closer to the surface, making these regions more susceptible to deep convection [5]. In figure 1.2 several areas where deep waters form are shown, the focus of this study lies on the Labrador Sea.

In order to calculate the convection depth, the definition of the Mixed Layer Depth (MLD) is used. The mixed layer is defined as a homogenized layer where the homogenization is caused by turbulence due to surface forcing [12]. Following [1] the MLD is defined as the depth where $\Delta\sigma_\theta$ = 0.005 kg/m^3 or ΔT = 0.025 kg/m^3 with respect to the threshold value at 10 m depth, where $\Delta\sigma_\theta$ is the potential density and T is the temperature (potential temperature).

1.2.2. Downwelling

A net vertical transport is not caused by convection in the interior, as concluded in the previous chapter. But it is known that denser waters return at depth to the equator (see chapter 1.1). This sinking of waters is called downwelling. In order to describe downwelling it is necessary to make a clear distinction between Eulerian and diapycnal downwelling, as there are large differences between these two. Eulerian downwelling is downwelling from depth perspective whereas diapycnal downwelling is downwelling which occurs across isopycnals. This is downwelling from density space instead of depth space [13].

In those regions where deep convection occurs the net Eulerian downwelling is close to zero. This is found in [1] and [13]. The strongest Eulerian downwelling occurs near the west coast of Greenland in the Labrador Sea. Here however, there is almost no diapycnal downwelling in that region. Diapycnal downwelling occurs when isopycnals cross the MLD [13], which occurs in the interior during deep convection.

It is clear that when looking at downwelling from different perspectives, large differences are found in the Labrador Sea basin.

1.3. Labrador Sea hydrography and circulation

The density loss through deep convection in the interior is compensated by lateral advection of warmer and fresher waters from the boundary currents entering the Labrador Sea ([1, 14]: and references therein). Before this process can be explained, first the boundary currents of the Labrador Sea (section 1.3.1) and thereafter the hydrography of the Labrador sea (section 1.3.2) need to be presented. Thereafter, it will be explained how these boundary current waters are laterally advected into the basin (section 1.3.3) and how this connects to downwelling and deep convection. Then, the influence an increased salinity has on this circulation will be outlined (section 1.3.4), which also highlights a recent debate about the importance of the overturning in the Labrador Sea. Lastly, the research questions are presented for this thesis (section 1.4).

1.3.1. Main currents

In the Labrador Sea three different currents can be distinguished (figure 1.5). The upper current contains fresher but cold waters, which contain meltwater of Arctic origin, and is called the West Greenland Current (WGC) when it is in the Labrador Sea. This current follows the bathymetry to the northern edge of the Labrador Sea. There, it splits up into a part that flows westward toward the Canadian coast and a part that continues northward to Davis Strait. Near the Canadian coast, this current is joined by the Baffin Island Current, which in turn is fed by fresh waters from the Canadian Archipelago and Baffin Bay. The current below this is called the Irminger Current, and contains saltier but warmer waters than the WGC. This current is located at a depth of around 500 m. The waters of this current originate from the North Atlantic Current, which is an extension of the Gulf Stream. The final and deepest current is called the Denmark Strait Overflow Water and contains deep waters formed around the Nordic Seas. [14]

1.3.2. Hydrography of the Labrador Sea

The interior is stratified in a similar fashion as the boundary currents (figure 1.6). Here, five water masses can be distinguished. The upper 200 m is fed by the fresh and cold boundary current from the continental shelves. These waters are cold during winter times, but surface warming increases in the summer, such that the waters are on average warmer than those below it, resulting in T = 3.6 °C and S = 34.75 PSU for the interior. The layer between 200 - 800 m is fed by the Irminger current, which is warm and saline and results in T = 3.4 °C and S = 34.84PSU for this layer. Labrador Sea Water is formed when convection penetrates deep enough during winter time (800 - 2000 m). T = 2.8 °C and S = 34.88PSU for this layer. Finally, the the bottom waters of the Labrador Sea are from the North East Atlantic Deep Waters (NEADW) and the Denmark Strait Overflow Waters (DSOW), where T = 1.8 °C and S = 34.90PSU [14].

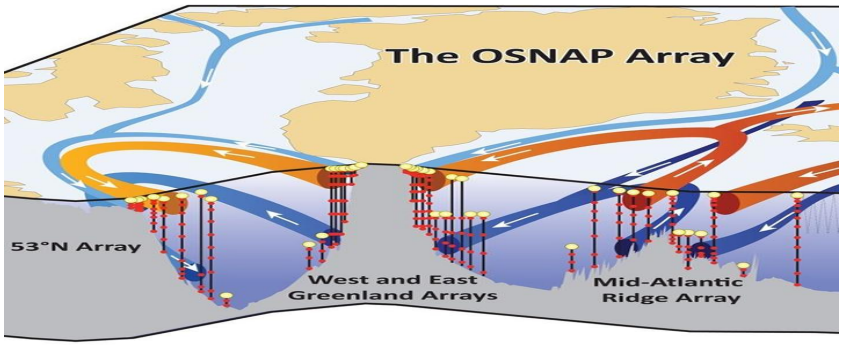

Figure 1.5: 3D view of three currents entering the Labrador Sea. From top to bottom: light blue = West Greenland Current, Orange = Irminger Current, dark blue = Deep Western Boundary Current. (from: `https://www.o-snap.org`)

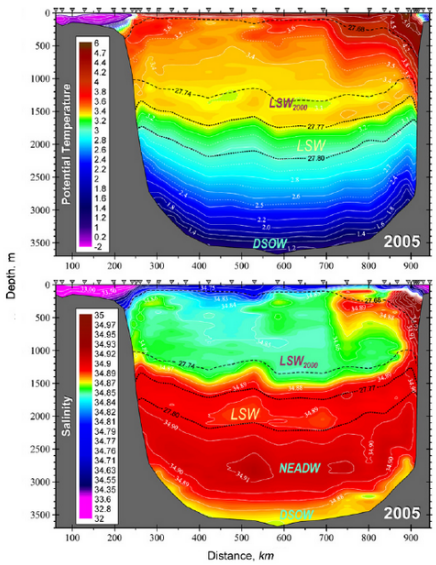

Figure 1.6: Hydrography of the Labrador Sea in the year 2005 along the WOCE AR7W section, from [15]. Potential temperature is shown in the upper panel and salinity is shown in the lower panel. The black dotted lines are isopycnals. LSW = Labrador Sea Water, LSW_{2000} = Labrador Sea Water formed in 2000. NEADW = NortEast Atlantic Deep Water, DSOW = Denmark Strait Overflow Water. the black lines are isopycnals [15].

1.3.3. (Sub)Mesoscale activity (eddies)

Exchange of water masses between the boundary current and the interior happens through eddies. In the Labrador Sea three types of eddies may be formed, namely: Convective Eddies (CE), Boundary Current Eddies (BCE) and Irminger Rings (IR) [16].

CE are formed during and directly after deep convection. When deep convection occurs, a lateral density gradient is formed between the convective area and its surroundings. This density gradient causes a so called rim current to develop as prescribed by the thermal wind balance. As this rim current grows, so do baroclinic instabilities. These baroclinic instabilities cause CE's to be shed off and they mix the waters of the convected area with their surrounding waters [9]. These eddies are relatively small and are in the order of the Rossby radius of deformation (10 km). Such a CE over a chimney is illustrated in figure 1.4.

BCE's are eddies that form from the BC through baroclinic instabilities and mix BC and interior waters. Their size is also in the order of the Rossby radius of deformation. IR's (radius of about 25 km) are formed near the SW coast of Greenland favored by the steepening of the slope there. This steepening of the coast causes the transport to contract, as the transport tends to follow the bathymetry. This effect is called topographic steering [5]. A faster flow means that the current becomes more barotropically unstable, resulting in more eddies.

The IR's in the northern central Labrador Sea and also to lesser extent the BCE's along the Labrador Current are vital components which act against preconditioning for deep convection [17]. They limit the area of deep convection to the southern part of the Labrador Sea. Even when the deep convection is under favourable circumstances, the local buoyancy loss due to air-sea interaction is counteracted by the strongly stratifying effect of the IR and BCE. Also, in years when there is no deep convection, there is still a slow, steady restratification of the interior [18]. This supports the notion that restratification is not associated with the convective processes but with the mean horizontal density gradients. The convective eddies in the central Labrador Sea on the other hand, which are tightly linked to the strength of deep convection, are the main driver of the restratification during springtime [17].

However, the strength of convection does influence the horizontal density gradient [1]. It is expected that with increased buoyancy loss during convection the upper waters will become denser and the mixed layers are likely to deepen. This also causes the horizontal density gradient between the boundary and the interior of the basin to increase. As shown by [1], this again increases the baroclinic instability of the eddies and thus intensify the eddy field and enhance downwelling. However, the increase of the enhanced efficiency of the eddies to restratify the interior imposes a negative feedback on the convection depth.

A schematic overview of how the volume transport, eddies and diapycnal mixing work in a Labrador Sea-like basin is given in figure 1.7. There, it is seen that water masses leave the boundary current, experience diapycnal mixing in the interior (deep convection) and return to the boundary current. Furthermore, it is seen that the waters in the BC close to the surface experience diapycnal mixing [13].

1.3.4. Influence of salinity on the circulation

In this section it will be described how freshwater moves into the interior of the Labrador Sea.

A large inflow of freshwater into the interior could cause deep convection be prevented. Such a freshening occurred in years 1968 - 1971 and is known as the Great Salinity Anomaly (GSA) [19]. During those years the convection layer did not reach beyond the extent of the fresh surface layer. However, the large inflow of fresher waters alone could not cause the GSA. The GSA also coincided with a period of mild winters, which could also contribute to a reduction or prevention of deep convection [11]. In the last decades, one of both factors alone has not been able to reproduce the GSA deep convection shut down. Eventually the harsh winter of 1972 increased the buoyancy loss and, along with increased lateral salinity fluxes, restarted the strong vertical mixing. The source of the higher salinity waters could not be identified from the data in [11].

It was found that most of the freshwater that flows into the interior of the Labrador Sea comes from the Nordic Seas and the East Greenland ice sheet [20, 21]. According to the modelling study done by [21], freshwater, which is close to the coast, needs to be transported by winds further offshore before it can be captured by the eddies and be transported into the interior.

Salinity also has an important effect during deep convection in the Labrador Sea: during deep convection, the temperature and salinity of water masses change. This change results in colder but fresher waters being formed in the Labrador Sea [22, 23]. According to the measurements of [22], this leads to a lot a large transformation of salinity and temperature. This transformation was mainly along isopycnals, and thus the overturning in density space is relatively small. Therefore, the overturning in salinity and in temperature cancel each other out to some extent. This mechanism/process is called "density compensation". Interestingly,

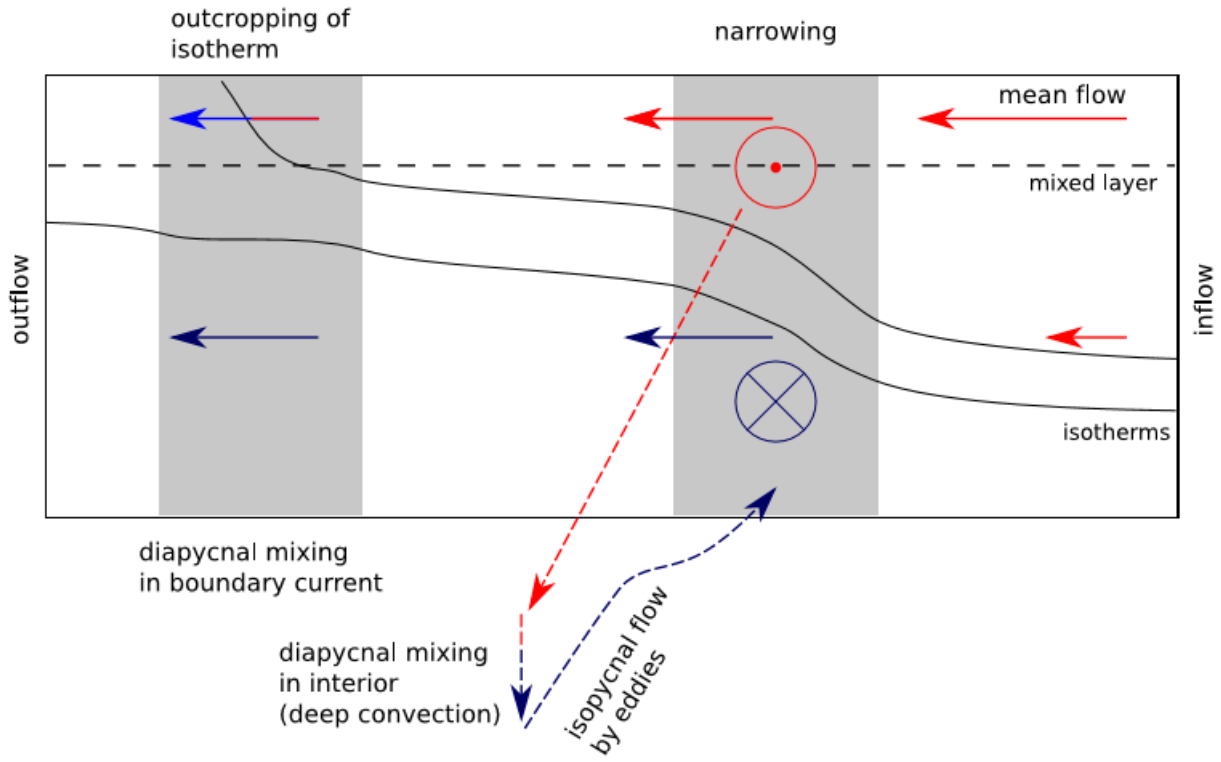

Figure 1.7: A schematic of residual overturning in a marginal sea, where strong eddy activity occurs along the boundary current. In the upper part of the boundary current water mass transformation occurs, where the warmer layers outcrop to the surface. This allows for diapycnal processes to occur at the surface due to a horizontal flow. In the interior water masses are transformed trough deep convection. This is connected to the boundary current by means of eddies which transport waters out of the boundary current. This overturning loop is then closed by an isopycnal eddy flow along tilted isopycnals. [13]

the monthly mean meridional overturning circulation (MOC) does not change much because of this density compensation during their 21 measured months. So that there is no evidence of a direct link between the strength of deep convection and density compensation [22].

1.4. Research questions

Under common circumstances temperature is the dominant driver for the AMOC (see chapter 1.1). Previous research has shown that by neglecting the effects of salinity in the Labrador Sea the circulation can be well represented [1, 16, 24]. In these studies, the density gradients caused by salinity gradients are taken into account by adjusting the temperature gradients accordingly. In those studies salinity was neglected because the effects of temperature were considered dominant as well as to simplify the analysis. However, salinity effects could be important as fresher waters over the interior negatively effect convection [14, 25]. Furthermore, a freshwater lens over the interior reduces the lateral density gradients, which has an impact on the baroclinic instabilities of the BC. Lastly, a model that does not contain salinity cannot have density compensation. The main aim of this thesis is to assess the impact of including salinity in the Labrador Sea circulation. To this end, the model developed by [1] is used in this thesis with the same linear equation of state where the salinity now is no longer a constant. Moreover, another configuration of the model that incorporates the seasonality in the salinity of the boundary current entering the Labrador Sea has been implemented. This will also address the question about the importance of the overturning in the Labrador Sea as recently debated in [26].

Thus the main research question is:

What are the differences in the pathways of watermasses and watermass transformation in the Labrador Sea when the density variations are due to both salinity and temperature variations as opposed to only temperature variations?

To answer this question, several sub-questions have been formulated:

1. How do main features (e.g. EKE, MLD, barotropic streamfunction) of the Labrador Sea circulation change with inclusion of salinity?
2. How does the spatial distribution and magnitude of the overturning transport change with inclusion of salinity in depth and density space?
3. How does a seasonal cycle in salinity affect the outcomes above?

To answer these questions, the model made by [1] was adjusted here to also contain salinity variations, whilst keeping the density variations the same. A model configuration with seasonal cycle in salinity was also made. The output of these three model simulations were then compared to each other.
First, how these models are set up will be explained (chapter 2). Second, a description of Lagrangian particle tracking as well as how these particles will be analyzed is given (chapter 3). Third, the results of main features (e.g., barotropic streamfunction, MLD, EKE and downwelling) and fourth the results of the lagrangian particle tracking are given for each model simulation and are compared to each other (chapter 4 and 5, respectively). Fifth, the conclusion and discussion are presented and sixth, the recommendations are given (chapter 7).

2

Model setup

This chapter gives a description of the model configurations and model output used in this study. First, the general features of each model configuration are shown, as all configurations have the same basis. Thereafter, the differences between the model runs and the reasoning behind these differences are explained.

2.1. General model configuration

The model features that are presented here are the basis of each model configuration and are the same as in [1]. For more details about the model configuration the reader is referred to [1].
The model configurations are created using the MIT General Circulation Model, or in short, MITgcm. It was developed at the Massachusetts Institute of Technology [27]. MITgcm can be used to study both atmospheric and oceanic phenomena. In case of the ocean it solves the hydrostatic primitive equations on a fixed Cartesian, staggered C-grid in the horizontal.
The model domain is 1575 km in the meridional direction and 1215 km in zonal direction. The horizontal resolution is 3.75 km in x and y directions. This is below the internal Rossby radius of deformation as according to [28] this radius is 7.5 km for the first baroclinic mode. The model has 40 levels in the vertical where the resolution increases from 20 m at the top layers to 200 m near the bottom. The maximum depth is 3000 m. Along the boundaries a continental slope is present. Near the west coast of Greenland and to some lesser extent at the eastern side of the Labrador coast a narrowing of the topography is present. The continental slope narrows west of Greenland, and this narrowing is required for the shedding of the IRs from the boundary current [29]. The continental shelves have been omitted in this model.
Two open boundaries exist in the model, one in the east and one in the southwest. In the east, an inflow is prescribed. The analytical expression for the velocity, T and S will be further discussed in sections 2.2.2, 2.2.3 and 2.2.4, as this is different for each model configuration. In the southwest the boundary current leaves the domain. The amount of water that leaves the basin here is set equal to what enters at that time. The other boundaries are closed.
Subgrid-scale mixing has been parameterized with a biharmonic viscosity and diffusivity in the horizontal and a Laplacian viscosity and diffusivity in the vertical direction. The exact values of these parameters are shown in table 2.1, along with other parameters which are used in each model run. Note that the vertical diffusion coefficient is constant over the horizontal but has been prescribed with an exponentially decaying component with depth. This has been done in order to mimic the vertical mixing caused by the wind, as wind forcing is absent in this model. The temperature is advected with a quasi-second order Adams-Bashforth scheme. When statically unstable conditions occur, the convection is then parameterized through enhanced vertical diffusivity ($K_v = 10\ m^2/s$). The $\beta - plane$ approximation is used.
A seasonally and spatially varying heat flux is applied to the model which is an idealized version of the climatology of WHOI OA Flux project [30]. The strongest cooling occurs in the northwest of the basin (figure 2.1a,b). The total annual surface ocean heat loss over the model domain is -18 W/m^2. The heat loss varies in time, where maximum heat loss is in January (-320 W/m^2) and a maximum heat gain in July (140 W/m^2).
Furthermore, to calculate the density, the model uses the linear equation of state:

$$\rho = \rho_0(1 - \alpha(T - T_{ref}) + \beta_S(S - S_0)) \tag{2.1}$$

where $\rho_0 = 1028\ kg/m^3$, α is the thermal expansion coefficient ($1.7 * 10^{-4}\ °C^{-1}$), β_s is the haline contraction

name	symbol	value	unit
Horizontal eddy viscosity	A_h	$0.25e10^9$	m^4/s
Vertical eddy viscosity	A_v	$1,9e10^{-5}$	m^2/s
Horizontal diffusion coefficient	K_h	$0.125e10^9$	m^4/s
Vertical diffusion coefficient	K_v	$K_b + K_0 * e^{(z/z_b)}$	m^2/s
	K_0	10^{-3}	m^2/s
	K_b	10^{-5}	m^2/s
	z_b	100	m
Bottom drag coefficient	-	$2e10^{-4}$	m/s

Table 2.1: Several parameters that are used in each of the model configurations

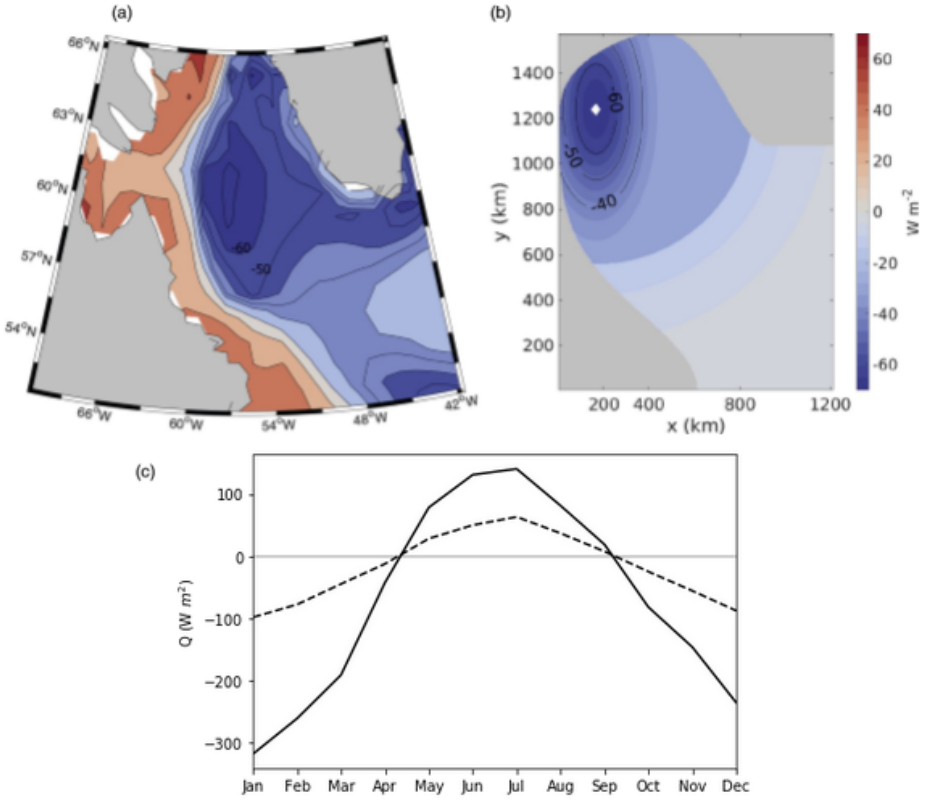

Figure 2.1: (a) Surface mean heat flux of the Labrador Sea, from the climatology of the WHOI AOFlux project [30]. (b) The applied Annual mean surface heat flux in the model configurations (Q < 0 Wm^{-2} means that there is a net surface cooling) (c) Maximum surface heat flux (solid line, occurs at the white marker in b) and average surface heat flux (dashed line) in the model configurations. Adapted from [1].

coefficient ($\beta = 7.5 * 10^{-4}\ PSU^{-1}$) and $Tref$ and $Sref$ are the reference temperature and salinity, respectively ($Tref = 2.62°\ C^{-1}$, $Sref = 34.9\ PSU$).
Each model configuration is run for 20 years where the final 5 years are used for analysis, as the systems require 15 years to stabilize. The variables of each model are u,v,w, T and S and annual and monthly means, as well as every 2-day snapshots are stored.

2.2. Set of model simulations

Three separate model configurations have been designed to address how salinity influences the pathway and water mass transformation in the Labrador Sea. The first model configuration contains only temperature variations; the second model configuration contains both temperature and salinity variations, where the boundary condition gives a constant salinity inflow; the third model configuration is the same as the second one, with the addition of a seasonally varying boundary inflow condition. They are referred to as respectively

Configuration name	**Interior**	**Inflow condition**	**Transport** (Sv)
Reference run	T	seasonal T	19.8
Sconstant	T&S	Seasonal T, fixed S	19.8
Sseasonal	T&S	Seasonal T and S	20.3

Table 2.2: Names of the model configurations, on what the vertical density profile depends for the interior and the inflow conditions (T or S and T), and the transport entering the domain.

the 'reference run', 'Sconstant' and 'Sseasonal' (table 2.2). A first test of the impact of salinity was performed by [25]. There salinity has been added to the model used by [1] in the top layer of the boundary current, which resulted in an increase of the lateral and vertical density gradients. The increase in freshwater in their model also resulted in an increased volume transport. Changes in their model circulation therefore could come from either an increase in volume transport or an increase in lateral and vertical density gradients of the boundary current, or both. Therefore, here it is chosen to keep the density gradients throughout the different model configurations the same as in the reference run.
To achieve this, the initial conditions for the interior and inflow conditions need to be changed. How this is done is shown in the following sections.

2.2.1. Profiles in the interior initial condition

All models are initialized with the same vertical density profile as in [1]. This choice of density profile has also been made so that the data from this report can be compared to that of [1]. Their density profile and temperature profile for the interior are shown in figure 2.2b (red and black solid lines, respectively), which are here used for the reference run. The density profile is shown for the western Labrador Sea in late summer along the WOCE AR7W section [1]. However, the temperature profile depicts a warmer basin than in reality, as density differences due to salinity have been represented as temperature variations.
For Sconstant and Sseasonal, a 36 years (1984-2020) vertically averaged salinity profile was obtained from [31] (blue line in figure 2.2b). This data is directly used for the vertical salinity profile of the model, which can be seen in figure 2.3a, where the blue line represents the 36 years average data and the blue dots is the input data for the model configurations. The salinity profile was obtained from the data within the large square in figure 2.2a. However, in order to keep the density gradient the same as in the reference run, the temperature gradient has to be recalculated. This is done by using the linear equation of state (2.1), where T is the unknown. The result is the black dashed line in figure 2.2b. In reality, the temperature varies differently over the vertical, as can be seen in figure 2.3b. The blue line here represents the 36 years average vertical temperature profile, where the blue dots represent the calculated data at each vertical model layer. The calculated temperature differs about 1 °C, but the shape of the profile is retained. This difference of 1 °C is not deemed significant for the outcome of the results, as this research is mainly about the influence of salinity on the flow patterns.

2.2.2. Inflow conditions of the reference run

The reference run is the same as the model of [1]. This model configuration contains no effects of salinity, and therefore the density differences depend only on variations in temperature.
The circulation in the model is forced by prescribing an inflow at the eastern boundary as in [24]. The meridional temperature ($T_{in}(y,z)$) and the westward flow ($U_{in}(y,z)$) are prescribed and are in geostrophic balance with each other:

$$T_{in}(y,z) = T_{ref}(z) - \frac{\Delta\rho}{2\alpha\rho_0}\left(1-\frac{z}{z_b}\right)\left[1+tanh(\frac{y-y_0}{L_y})\right] \tag{2.2}$$

and

$$U_{in}(y,z) = g\frac{\Delta\rho}{4L_y f\rho_0}\frac{(z-z_b)^2}{z_b}\frac{1}{cosh^2\left(\frac{y-y_0}{L_y}\right)} \tag{2.3}$$

where the density difference across the BC is $\Delta\rho$ = - 0.245 kg/m^3, L_y =22.5 km, which is the width of the inflowing BC, y_0 is the location 22.5 km south of the tip of Greenland, f = 1.26e-04 s^{-1} is the Coriolis parameter, g = 9.81 m/s^2 is the acceleration due to gravity, and z_b is the lowest depth of the model, where $U_{in}(y,z_b)$ = 0. This last condition is required to determine the total transport. T_{ref} is the limit of the offshore temperature profile, which is equal to the interior's profile. The derivation of these equations can be found in Appendix A.

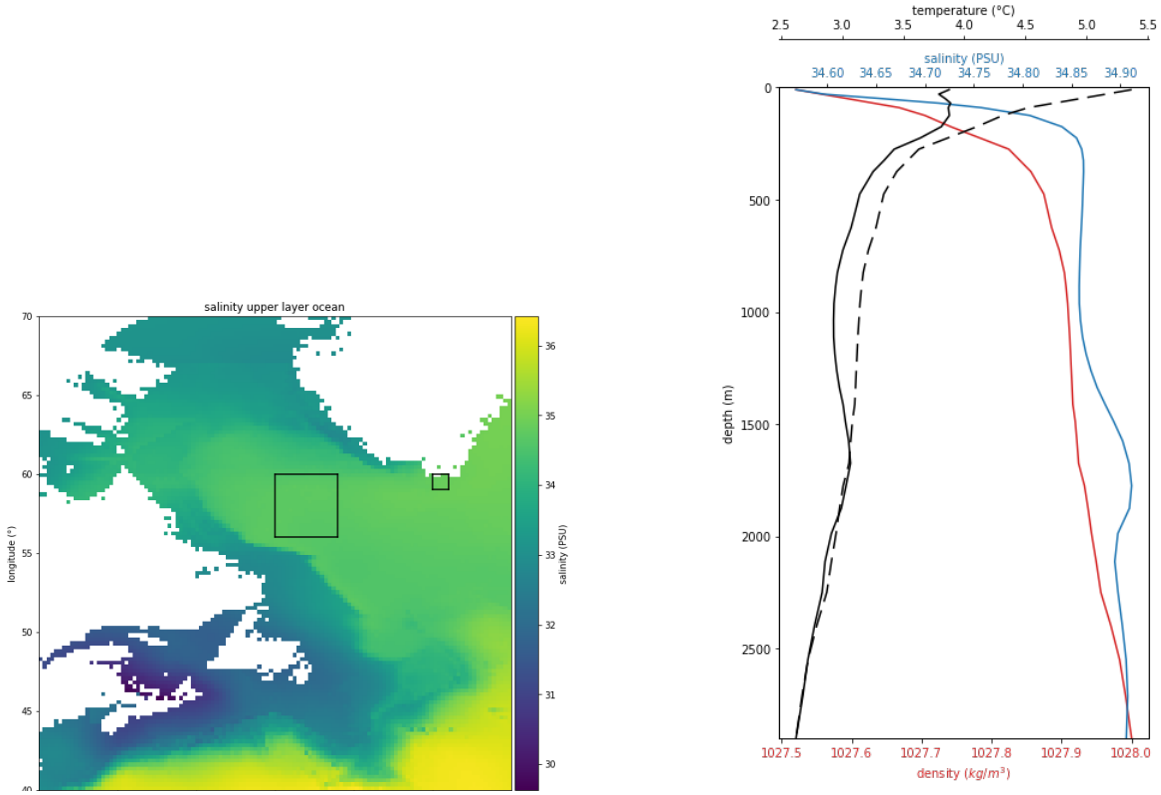

(a) (b)

Figure 2.2: a) 36 Years (1984-2020) average salinity in the top layer in the Labrador Sea. The black boxes indicate which data has been used to construct an average vertical salinity profile. The large square represents the data of the interior and the small square that of the boundary current. Data from [31]. b) The 36 years averaged density, temperature and salinity profiles over the vertical of the interior of the Labrador Sea for the model runs. The red line is the density and is the same in each run. The black solid line is the temperature of the reference run. the black dashed and blue lines are the temperature and salinity of the other runs.

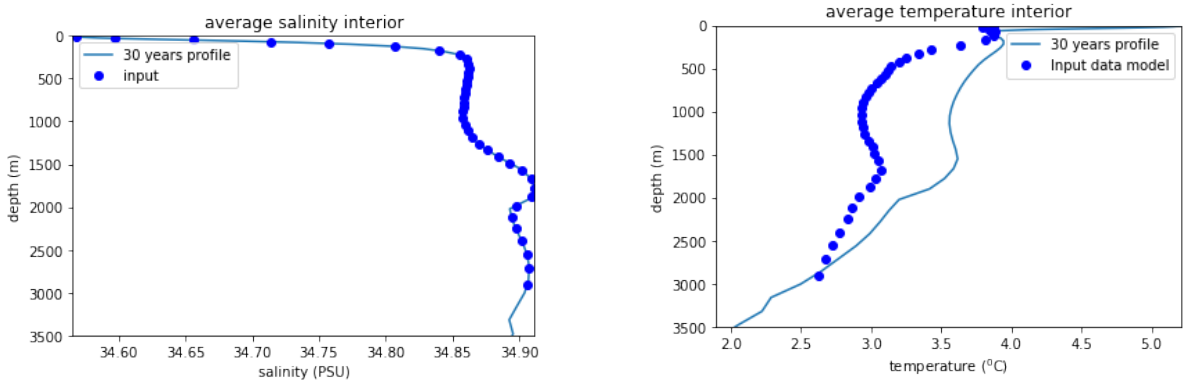

(a) (b)

Figure 2.3: 36 Years (1984-2020) average salinity (a) and temperature (b) for the boundary current, from (line) observations and (dots) as prescribed in the model. Data from: [31]

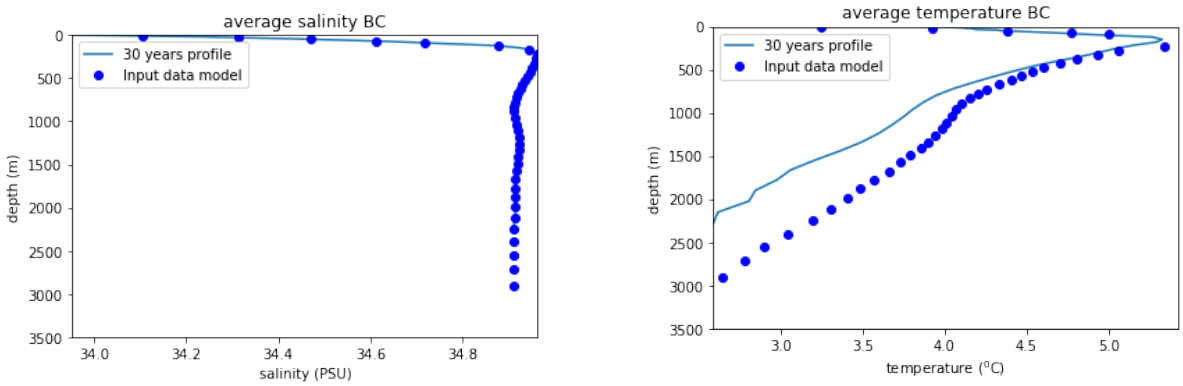

(a) (b)

Figure 2.4: 36 Years (1984-2020) average salinity (a) and temperature (b) for the boundary current, from (line) observations and (dots) as prescribed in the model. Data from [31]

The boundary current also as a seasonal component of temperature (T_{seas}), which is defined the same way as done by [1] (S. Georgiou, personal communication):

$$T_{seas}(t,y,z) = \Delta T_{INT} + 0.5 * (\Delta T_{WGC} - \Delta T_{INT}) * \left[1 + tanh(\frac{y-y_0}{L_y})\right] * e^{z/200} * (1 + sin(2 * \pi * (t-6)/12)) \quad (2.4)$$

Where ΔT_{INT} is the magnitude of the temperature fluctuation of the interior, ΔT_{WGC} is the magnitude of the temperature fluctuation near the Greenland boundary and t is the number of the month, starting from January.
From this equation it can be seen that the boundary current fluctuates sinusoidally over time, completing one cycle in a year. The minimum values occur in March and the maximum values occur in September. Note that the seasonal temperature component will always add warmer (thus lighter) waters to the boundary current. Only in March the seasonal component of equation 2.4 is zero. In equation 2.4 it can also be seen that the seasonal cycle of the boundary current has two components which determine the temperature variation. ΔT_{INT} defines the seasonal cycle of the interior and ΔT_{WGC} defines the seasonal cycle of the WGC. ΔT_{INT} and ΔT_{WGC} are related to each other with a tanh relationship in y direction. The seasonal component decays exponentially in the vertical over 200 m.

2.2.3. Inflow conditions of Sconstant

To calculate the salinity conditions at the inflow of the model, it has been chosen to apply a similar relationship as in equation 2.2 for the inflow condition for salinity:

$$S_{BC,constant}(y,z) = S_{interior}(z) + 0.5 * \left(S_{BC(max)}(z) - S_{interior}(z)\right)\left[1 + tanh(\frac{y-y_0}{L_y})\right] \quad (2.5)$$

where $S_{BC,constant}$ is the salinity in the boundary current, $S_{interior}$ is the salinity of the interior, $S_{BC(max)}$ is the maximum occurring salinity, here assumed to be equal to the salinity profile in figure 2.4a. This vertical salinity gradient of the BC is obtained by using the 36 years average data in the small square under the tip of Greenland in figure 2.2a [31]. The difference between equations 2.2 and 2.5 is that the salinity at each depth is given by data, and thus no vertical relationship $(1 - z/z_b)$ is required in equation 2.5.
With the density and salinity profiles of the inflow known, the temperature profile at the inflow can be calculated through the linear equation of state in the following way:

$$\Delta\rho_S(y,z) = \beta\rho_0(S_{BC,constant}(y,z) - S_{interior}(z)) \quad (2.6)$$

which gives the horizontal and vertical density differences due to salinity. Differences in the density profiles due to variations in temperature are then calculated as:

$$\Delta\rho_T(y,z) = \Delta\rho_{reference\ run}(y,z) - \Delta\rho_S(y,z) \quad (2.7)$$

where $\Delta\rho_{reference\ run}$ is the density inflow condition of the reference run, without the seasonally varying part due to temperature. Lastly, this density profile due to temperature differences can be translated to a temperature profile:

$$\Delta T(y,z) = -\frac{\Delta\rho_T(y,z)}{\alpha\rho_0} \tag{2.8}$$

The resulting temperature profile is shown in 2.4b (blue dots). This profile deviates from the 36 years annual average (blue line), since the density gradient at the inflow is not based on the 36 years annual average but on the same gradient as [1]. The shape of the calculated temperature profile now is much more similar to reality, showing a cooler waters near the surface, with the warmest waters at around 250 m depth.
The velocity profile only depends on density variations. Since the density profile is the same as in the reference run, the velocity profile is the same in this model configuration. Thus the velocity of Sconstant is also prescribed by equation 2.3.

2.2.4. Inflow conditions of Sseasonal

In the seasonal salinity run, Sseasonal, the inflow at the boundary current also has a seasonal cycle in salinity. This represents meltwater coming from Greenland or the Arctic [32]. The seasonal signal of the boundary current was observed to occur mainly in the top levels of the boundary current [31]. Therefore it was chosen to approach the seasonality of the salinity with an exponential function over the vertical, with respect to the mean salinity. It is furthermore assumed that the salinity in the top layer of the model equals the 36 years monthly average salinity at the surface, where possible (small square figure 2.2a). In meridional direction a tanh function has been assumed, in line with the inflow condition for the reference run and Sconstant. The seasonal salinity component of the boundary current can then be described as follows:

$$S_{seas}(t,y,z) = (S_{BC(month,top)}(t,z=0) - S_{BC(top)}(z=0)) * 0.5 * \left[1 + tanh(\frac{y-y_0}{L_y})\right] * e^{z/42} \tag{2.9}$$

where S_{seas} is the seasonal component of the boundary current, $S_{BC(month,top)}$ is the salinity of the top layer during a given month and $S_{BC(max)}$ is the 36 years mean salinity of the top layer. The best fit for the vertical decay scale was found to be 42 m^{-1}.
However, for 5 months the application of this procedure resulted in an unstable stratification at the boundary condition. During the winter months, the boundary current brings in more saline water. This, in combination with the chosen temperature profile - which is not from the same data set as the salinity - gives the unstable stratification (figure 2.5).
In order to re-obtain a stable stratification, the monthly mean salinity of the surface ($S_{BC(month,top)}$) has been adjusted to fresher values. One example of this can be seen in figure 2.6. In this figure the vertical density gradient ($z_{n+1} - z_n$, where n is a given model layer. n = 0 at the top) has been plotted for the total density, and density changes due to temperature and salinity. The solid red line is the original vertical density gradient. This is negative at the top layers (above 80 m depth), which means that the stratification is unstable. The vertical density gradient due to salinity has been adjusted (blue line to blue dotted line). This results in a stable stratification (red dotted line). The density gradient due to vertical temperature differences is the same for the new situation (black line).
The disadvantage of this method however is that the average inflow of salinity is slightly fresher, see the red dots in figure 2.5. This will likely induce a more stable stratification over the entire basin. Also, because the waters at the inflow are on average fresher, $\Delta\rho$ is not exactly the same as in the other configurations, which results in more water to flow into the basin further enhancing this stable stratification. The increase in freshwater inflow follows from equation 2.3, as $\Delta\rho$ has been increased.
The complete inflow boundary condition for salinity then becomes:

$$S_{BC}(t,y,z) = S_{seas}(t,y,z) + S_{BC,constant}(y,z) \tag{2.10}$$

Next, an overview of each inflow condition for each model configuration is given.

2.2.5. Summary of inflow conditions for each model configuration

The inflow conditions for each model configuration are shown in figure 2.7. Each column specifies a different model configuration and each row is from top to bottom the annually averaged inflow condition for the velocity, temperature, salinity and horizontal density gradient with respect to the initial interior's density.

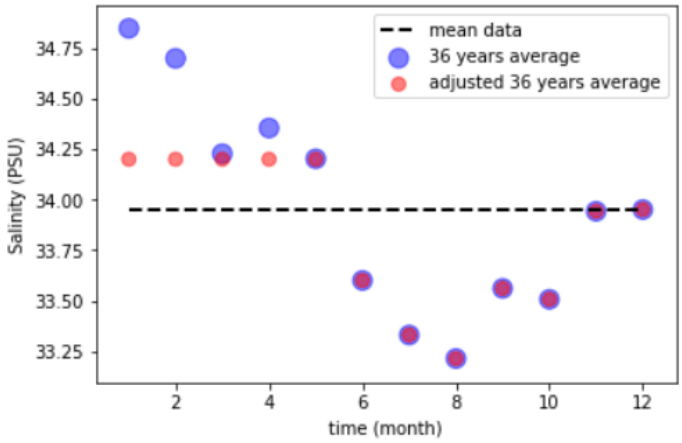

Figure 2.5: Blue dots: 36-years average monthly climatology of salinity in the top layer of the boundary current (data from [31]). Red dots: adjusted value such that a stable stratification at the inflow is achieved, which are used for the Sseasonal configuration. Black dotted line: mean of the monthly values.

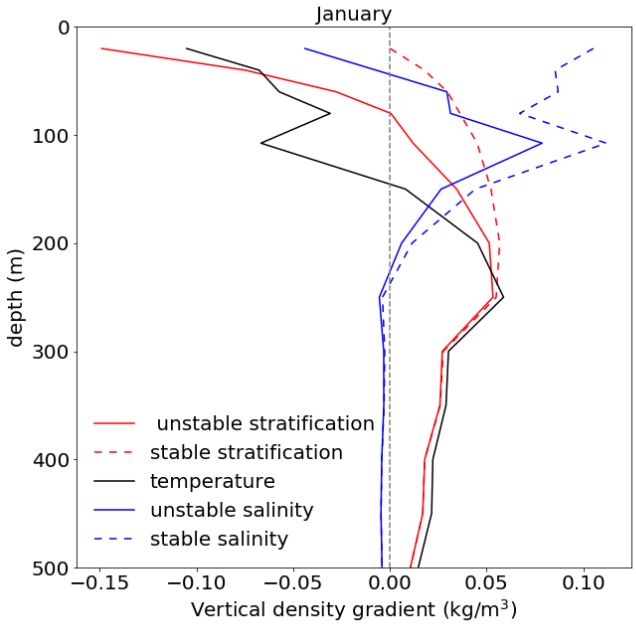

Figure 2.6: Vertical density difference (red), adjusted density (red dotted), density difference due to salinity (blue) adjusted density difference due to salinity (blue dotted) and density difference due to temperature (black)

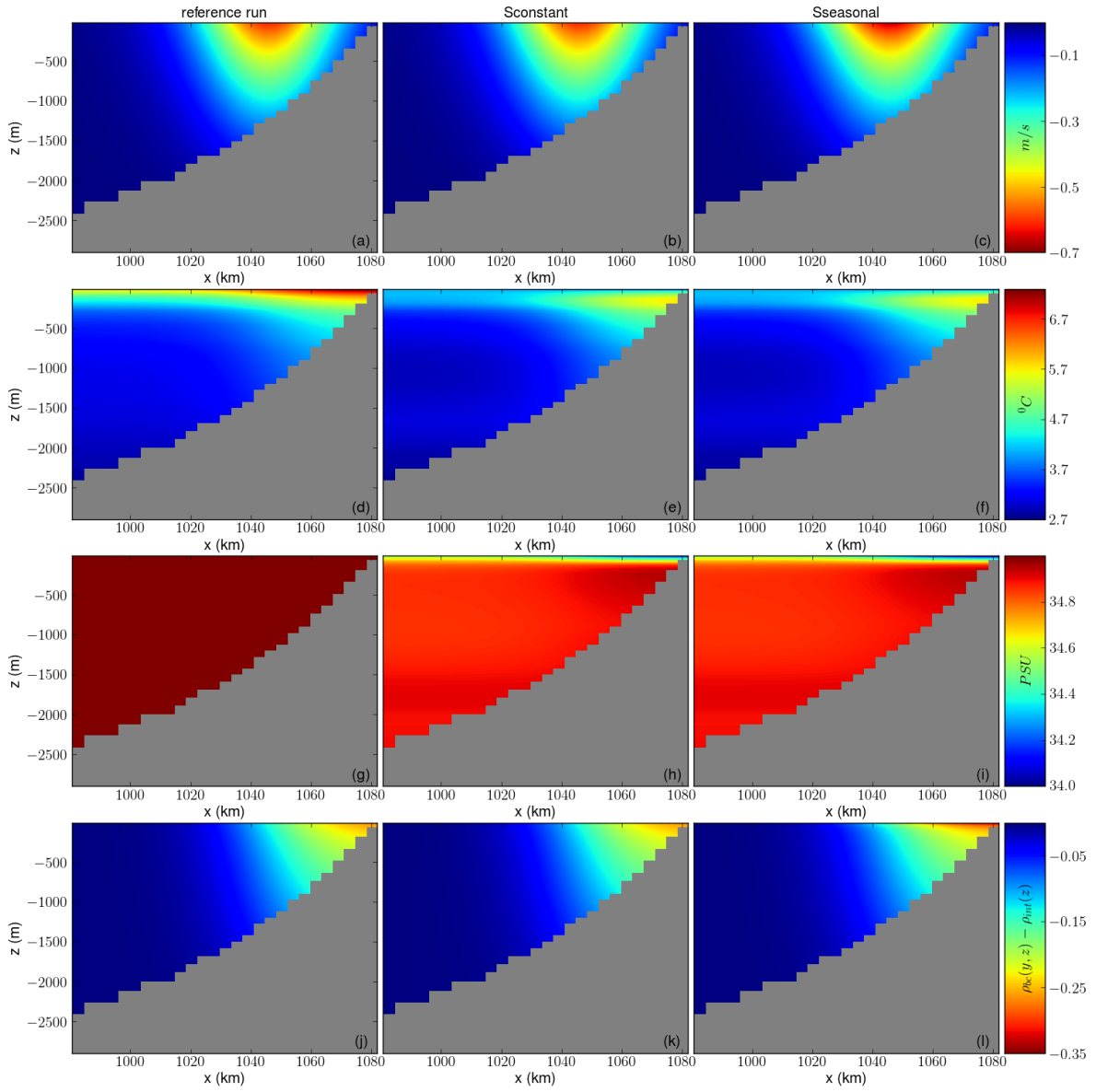

Figure 2.7: The prescribed annually averaged inflow conditions for all three runs. Top to bottom: zonal velocity, temperature, salinity and horizontal density difference with respect to the initial interior density

The zonal velocity (figures 2.7a,b,c) is directly related to the horizontal density gradient (figures 2.7j,k,l) following equation 2.3. The figures for the reference run and Sconstant are exactly the same, as prescribed by the equations's in the sections above. Sseasonal shows an increase in horizontal density gradient (figure 2.7l) with respect to the other two configurations (figure 2.7j,k), as additional fresher waters enter due to the addition of the seasonal salinity cycle. This results in an increased zonal velocity, but can barely be seen in figure 2.7c. The temperature (figures 2.7d,e,f) is significantly different between the reference run and the salinity runs. With the reference run the temperature increases from the bottom till the top of the inflow, whereas the seasonal runs show warmer waters at around 100-500 m depths, and a cooler surface layer. Overall, the salinity runs are cooler. Figures 2.7g,h,i show the salinity inflow condition. For the reference run, this is equal to 35 PSU everywhere, as there are no salinity variations in this model. The salinity runs show an increased freshness at the surface to around 100m depth. The seasonal runs represent the real inflow of the Labrador Sea better, as in reality a colder but fresher surface current with below warmer but more saline enters the Labrador Sea [14] (see also chapter 1.3.1). The next chapter describes how these inflowing water masses and their properties that enter the basin are tracked throughout the basin.

3

Lagrangian particle tracking

This chapter describes how the pathways of water masses are tracked by using the Connectivity Modelling System (CMS). CMS is a probabilistic multi-scale model, which allows for Lagrangian tracking of particles [33]. The setup of CMS will be outlined in this chapter.

3.1. CMS description

CMS can be used to study the pathways of different water masses through the model domain. Properties such as temperature, salinity and density are determined along the path of each particle released.
CMS requires an input file which tells where particles are released in this model. CMS furthermore requires the u, v and w to calculate the pathway of the particles. The movement of the particles is calculated as described by [33]: a Runga-Kutta 4th order stepping scheme in space and time. The particles are almost never on the gridpoints of the model domain, thus a tricubic interpolation over the three dimensions is applied. If one of these 64 gridpoints is in land, a trilinear interpolation is applied instead, requiring only 8 gridpoints. Also, T,S are required as input files to assess the water mass properties where the particle passes. Lastly, The MLD is required to represent vertical motions in convection areas. In these areas, water plumes in the order of 100 m radius sink with a velocity larger than 0.1 m/s and upwell around these areas at lower velocities [9] (see also chapter 1.2.1). However, the MITgcm model is hydrostatic, which means that large vertical velocities are not present in the model. The mixing in convective areas is represented by a large K_v value (see chapter 2.1). To mimic the vertical velocities that occur during deep convection, a random kick of up to 0.1 m/s is applied to particles within the mixed layer in CMS. This value is based on [9] (see also chapter 1.2.1).

3.2. CMS input

For all three model runs, particles are released at the inflow of the model domain with a horizontal separation of 1100 m. The vertical resolution is 20 m from 10 - 250 m and 50 m from 250 - 2250 m depth (see figure 3.1a). Particles are released every two days for a year, and are tracked for 4 years, resulting in 5 years of required input data. These particles are advected forward in time with a time step of one hour. Two day snapshot files for 5 years of u, v, w, T, S and the MLD are used in the simulation. In this study, we choose to release the particles between 0 and 19.7 Sv at the inflow for the reference run and Sconstant and between 0 and 20 Sv at the inflow for Sseasonal. This location is chosen as it represents almost all transport that enters in each model configuration. flowing into each model configuration. Each particle can be given a volume transport, as the velocity of the water mass that enters at the inflow is always known. This transport is determined by multiplying the velocity of the particle by the area it represents. For each model configuration, 465120 particles are released at the inflow over the course of a year.

3.3. CMS output

Not all particles that enter the model domain at the inflow produce sensible or usable data. Therefore, a selection is made of particles which will be analyzed further in this study. Particles that are filtered out are listed below:

1. Some particles were for too close to land, and got stuck before reaching the outflow or the end of the simulation (example figure 3.1b, blue line).
2. Particles that gave as error that they missed data files (not shown).

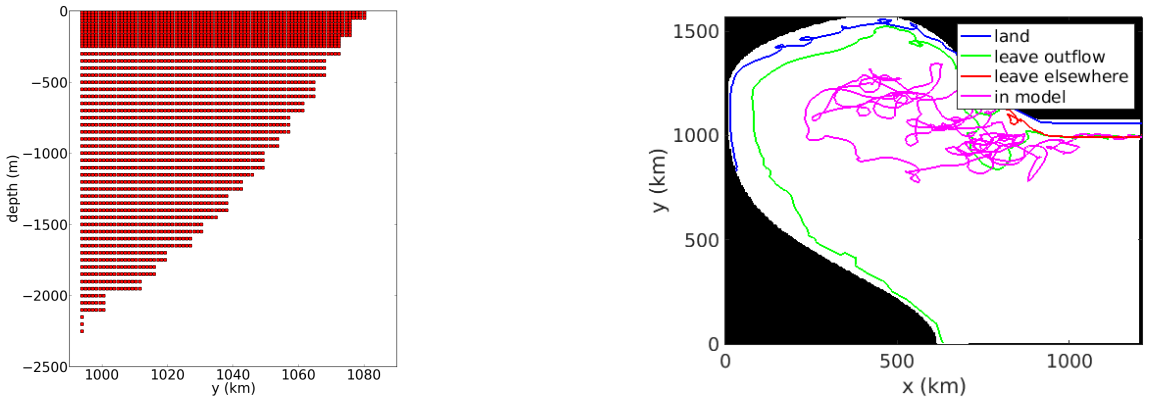

(a) (b)

Figure 3.1: a) Release location at the inflow of the particles in meridional direction over the depth b) pathway of particles for a particle that is too close to land (blue line), leaves through the interior (red line), leaves the model domain at the outflow (green line) or stays in the model after 5 years of running time (pink line)

3. Particles that left the model domain, but not near the outflow (example figure 3.1b, red line). The criteria for particles to be removed is when they left the model at a distance of 2000 m or farther away from the outflow. Setting this criterion to 20000 m did not result in more particles being removed.

These criteria resulted however in the calculated volume transport by CMS being 6-9% lower than 19.6 Sv for the reference run and Sconstant and 20.1 Sv for Sseasonal. The lost volume transport and particles can be seen in table 3.1 and 3.2 respectively for each run.
The particles that are used for analysis are particles that either left the model through the outflow (example figure 3.1b, green line) or resided in the basin after 5 years of simulation (example figure 3.1b, pink line).
Before these particles will be analyzed in chapter 5, Main features (e.g. barotropic streamfuncion, MLD, EKE and downwelling) of these model configurations will be presented first.

Sv	**Reference run**	**Sconstant**	**Sseasonal**
released	18,75	18,75	19,23
after criteria 1&2	18,09	18,1	18,56
after criterion 3	17,66	17,13	17,82

Table 3.1: Lost volume transport for different criteria. Criteria 1 removes particles that are too close to land. Criteria 2 removes particles which have no data files. Criteria 3 removes particles that left the model but not at the outflow

particles	**Reference run**	**Sconstant**	**Sseasonal**
released	465120	465120	465120
after criteria 1&2	445536	445841	445871
after criteria 3	435424	409698	415910

Table 3.2: Lost particles after applying the same criteria as in table 3.1

4

Main features of idealized Labrador Sea circulation

In this chapter the effects of salinity on deep convection are studied by analyzing the Mixed Layer Depth (MLD) and the eddy field in the different model simulations presented in Chapter 2. First, the barotropic streamfunctions are shown, as later analyses are based upon this. Thereafter the MLD is is compared between the different model simulations. Thirdly, the eddies are analyzed by means of the EKE. Lastly, the downwelling in depth space is analyzed by separating the basin in four different areas.

4.1. Mean barotropic streamfunction

The 5-year mean barotropic streamfunction (Ψ_b) for each model configuration is shown in figure 4.1. Here it can be seen that the contour lines of the BC follow the bathymetry, with little to no differences between the model simulations. Furthermore, the contour lines narrow at the narrowing of the bathymetry (x = 800 km, y = 1100 km). This is also seen in [1, 16, 24]. This means that the boundary current flows faster in this area, increasing the barotropic instabilities of the BC. Some small differences can be seen in the interior between the model simulations. Sconstant and Sseasonal reach lower streamfunction values as opposed to the reference run in the interior, but also reach higher values near the boundary current. The total transport that enters the basin per model configuration is 19.8 Sv for the reference run and Sconstant and 20.3 Sv for Sseasonal (see table 4.1). The maximum barotropic streamfunction increases between each model configuration and is 27.3, 28.7 and 30.1 Sv for the reference run, Sconstant and Sseasonal respectively. The black dashed line in figure 4.1 represents the 19.6 Sv line for the reference run and Sconstant and the 20.1 Sv line for Sseasonal. These values are used in later analyses and are chosen at these contour lines because: 1. this is the closest value to the total incoming transport where this streamline follows the boundary current or bathymetry. 2. the transport that enters the basin but is offshore of this line and the land is the same for each run (=0.2 Sv, table 4.1).

4.2. Mixed layer depth

The MLD can be viewed as the thickness of a statically unstable water column over which vertical mixing of the water masses takes place. The MLD can be defined as the depth at which the density exceeds the surface density by a value of $5 * 10^{-3} kg/\mathrm{m}^3$ [34]. The mean winter (February and March) MLD over the last 5 simulation years is shown for each model configuration in figure 4.2. The maximum MLD of the reference run, Sconstant and Sseasonal are respectively 1712, 1803 and 1649 m. Figure 4.2 shows that there is little difference in the mixed layer depth when the density is determined by salinity as well (compare figure 4.2a

	reference run	**Sconstant**	**Sseasonal**
transport entering (Sv)	19,8	19,8	20,3
contour cutoff (Sv)	19,6	19,6	20,1
maximum barotropic streamfunction (Sv)	27,3	28,7	30,1

Table 4.1: Sv entering the basin, the chosen contour line and the maximum barotropic streamfunction in the basin for the model simulations.

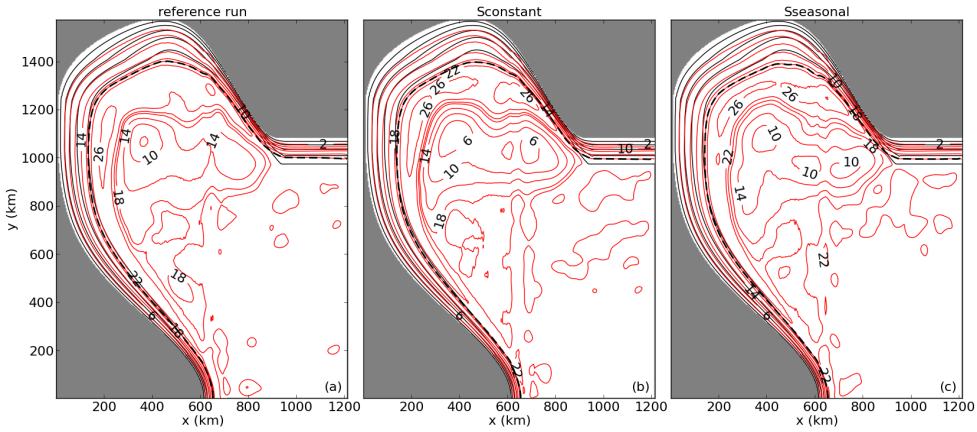

Figure 4.1: 5-Year mean barotropic streamfunction (ψ_B, contour interval is 4 Sv) of each model configuration. The black dashed line is the 19.6 (20.1) Sv contour line for the reference run and Sconstant (Sseasonal). The dark grey lines outline the bathymetry (interval 500 m).

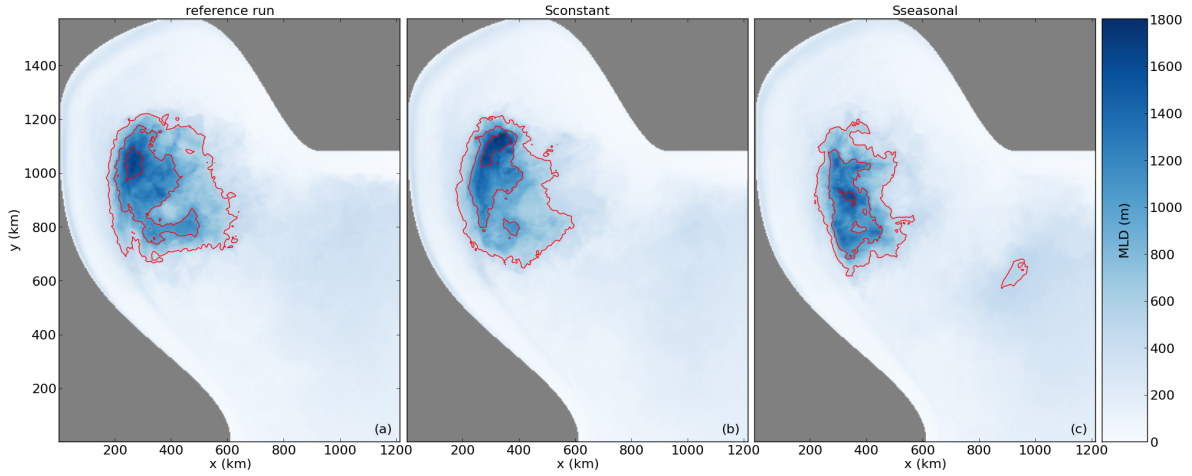

Figure 4.2: The 5-year mean Mixed Layer Depth (MLD) of February and March of each model configuration (contour interval is 500 m)

and 4.2b). In figure 4.2c the area of the MLD is smaller and centered more towards the west. This is likely because eddies from the boundary current bring more buoyant waters towards the interior, which prohibit deep convection [1].

The upper panel of figure 4.3 shows that over the last 5 years of the model simulations each model simulation has reached equilibrium; the sea surface temperature and sea surface salinity (SST and SSS respectively) only have an annual cycle. Notably, in the run Sconstant (4.3b) there is a seasonal cycle of the SSS which is in anti-phase with the temperature. The seasonal cycle in salinity exists because during summer time, more warm surface waters enter at the inflow. This increase in transport at the surface also increases the transport of freshest waters – which are close to the surface – during summer time. This is what is reflected in figure 4.3b and why the SST and SSS are exactly in anti-phase. This anti-phase is also seen in (figure 4.3c), but the maximum SSS now occurs roughly a month later, and is larger in amplitude. This is because the inflow condition now also contains a seasonal cycle in salinity, which enhances the annual SSS variations even further. The bottom panel in figure 4.3 shows the maximum MLD per month. The runs that contain salinity clearly have a higher maximum MLD during winter convection. Whilst the reference run has MLDs of about 2 km, Sconstant and Sseasonal have MLDs of up to 3 km, which is the ocean's floor in these model configuration.

To investigate the difference in maximum MLD depth further, figure 4.4 shows the 5 years average contour lines (thick lines) of the MLD during February and March, where figure 4.4 a, b and c show respectively the 500 m, 1000 m, and 1500 m contour line for the MLD. The contour of the 500 m MLD encompasses a wider

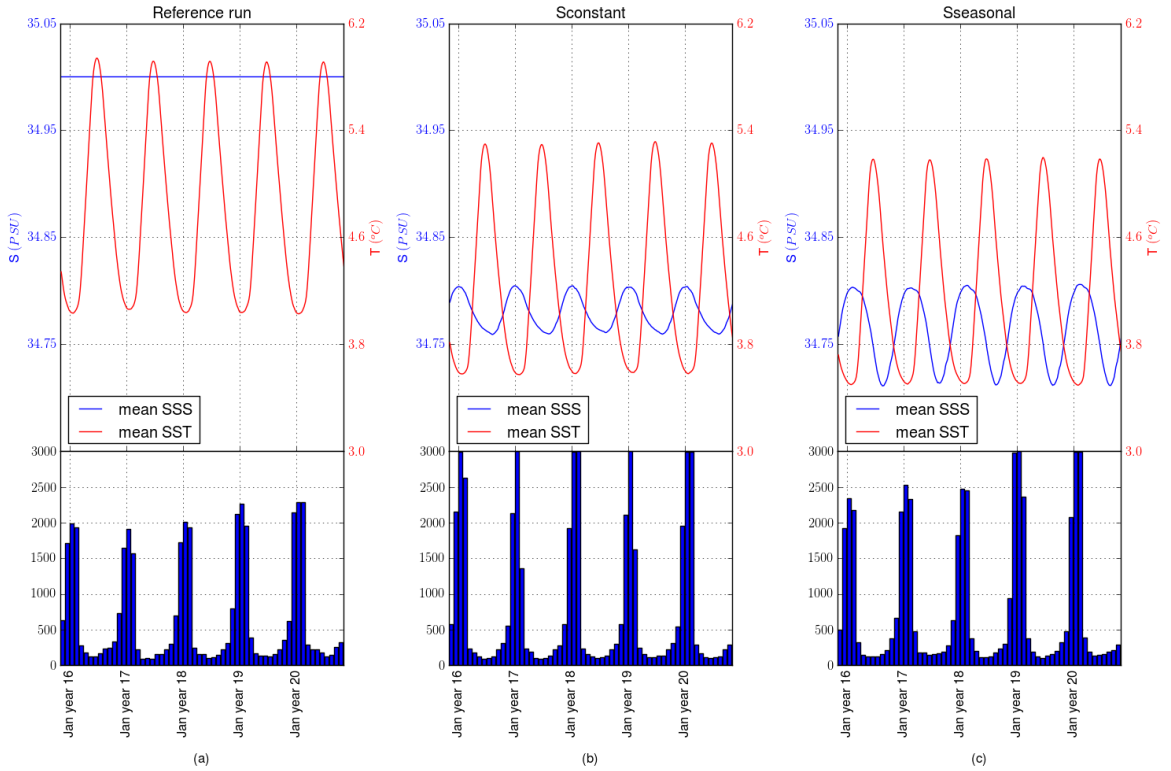

Figure 4.3: Top panel: 5-year average sea surface temperature and salinity (SST and SSS) of the simulations; bottom panel: the maximum mixed layer depth over the last 5 years of the simulations.

area for the reference run than for the salinity runs, but only by a small margin. This is also true for the 1000 m contour line. At 1500m, the contour lines of the reference run and Sconstant are of the same order, but the MLD contour of Sconstant lies slightly more northeastward than the reference run. Sseasonal encompasses a smaller area at a depth of 1500 m. This is in line with expectations, as the inflow conditions represent more buoyant waters entering the basin. Figure 4.4 also shows the MLD contour per year (thin lines). From these it can be seen that the MLD contour for each year separately concentrates around the average MLD contour for each model simulation. This means that the 5-year average MLD gives a good picture of the average MLD, and thus the differences spotted between the model simulations are not due to large annual variations in the MLD.

4.3. Eddy kinetic energy

To calculate the intensity of the eddy field the following measure is used: the Eddy Kinetic Energy (EKE). In equation form this is:

$$EKE = \frac{1}{2}(\overline{u'^2 + v'^2}) \tag{4.1}$$

with $u = \overline{u} + u'$ and $v = \overline{v} + v'$, where $\overline{u}$ and $\overline{v}$ are the 5 year mean velocities and u' and v' are the anomaly velocities to this mean value, based on two day snapshots. Lastly, the 5 years average is taken over the squared anomaly velocities, which results in figure 4.5 for the surface EKE. Large values of EKE mean that there is much variance in the flow field. This can only be caused by the eddies, as they mostly represent the fluctuating (turbulent) component of the flow [1]. The maximum EKE of the reference run, Sconstant and Sseasonal are respectively 530, 750 and 820 cm^2/s^2.

In this figure, it can be seen that the EKE is the largest near the narrowing of the bathymetry at the west coast of Greenland. Because of this narrowing, the current narrows as well and becomes barotropically unstable. This causes eddies to be shed off in this area, which is reflected as an increase in EKE [35].

Between figure 4.5a and 4.5b the surface EKE increases significantly after the narrowing at the west coast of Greenland, where the maximum surface EKE increases by 41.5%. This increase occurs even though the initial vertical and lateral density profile, and the density profile at the inflow is the same in these simulations. No

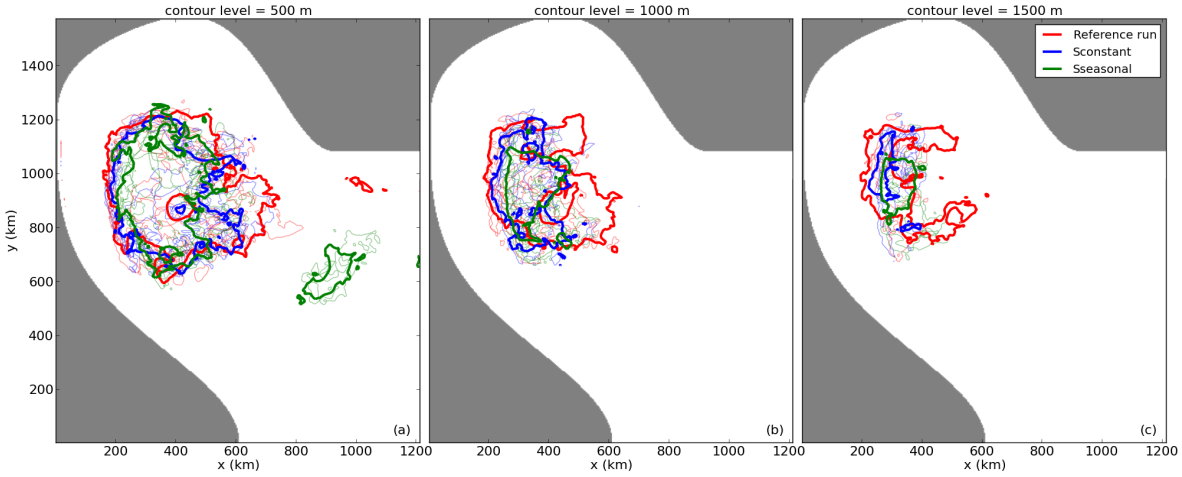

Figure 4.4: Average contour (thick lines) of the winter MLD over the last 5 years of the model simulations (red = reference run, blue = Sconstant, green = Sseasonal). a) MLD level = 500 m. b) MLD level = 1000 m. c) MLD level = 1500 m. The thinner, transparent lines are the MLD per year for five years for each of the model simulations.

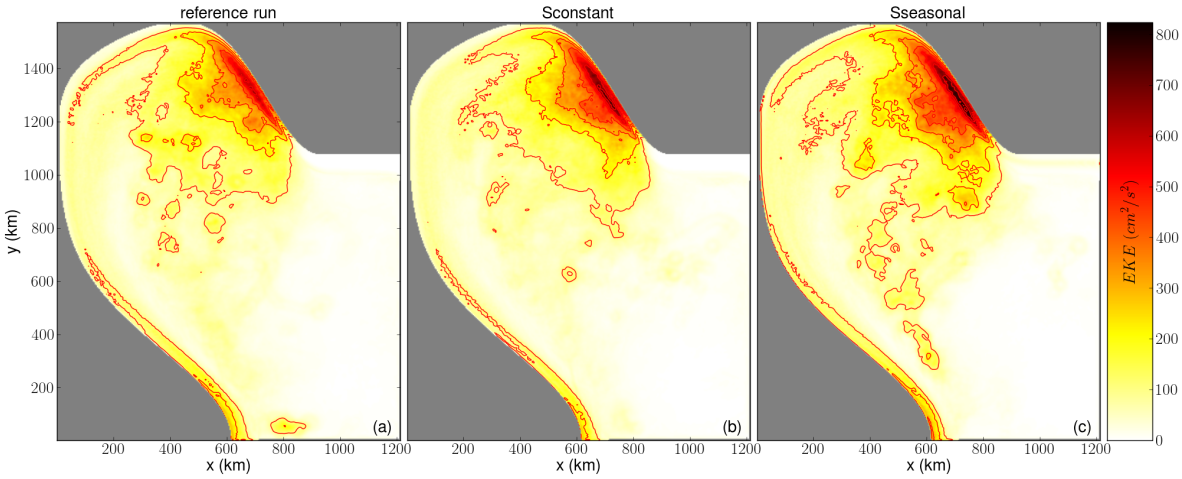

Figure 4.5: Surface Eddy Kinetic Energy (EKE) of for a) reference run b) Sconstant c) Sseasonal (contour interval is 100 cm^2/s^2)

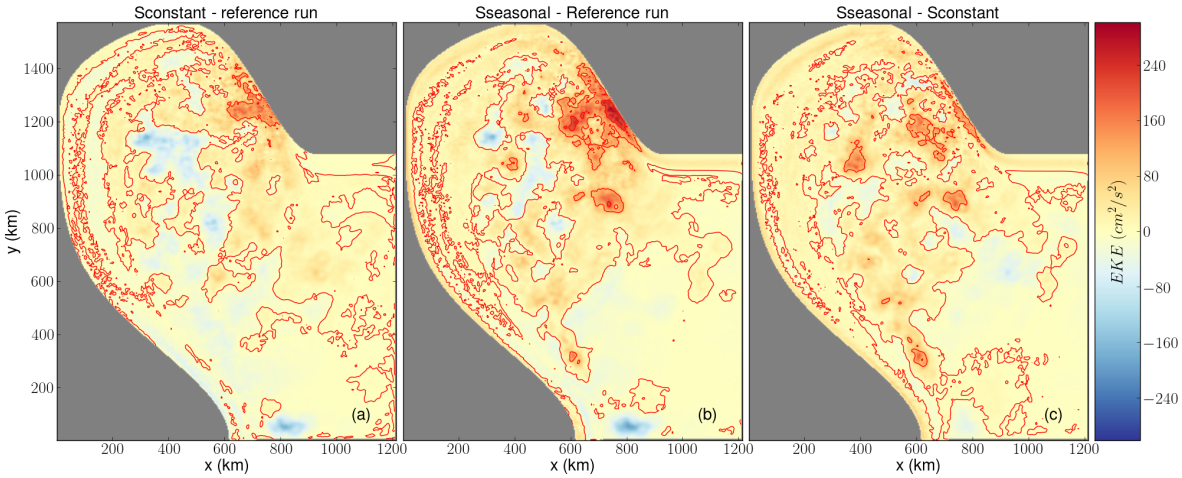

Figure 4.6: Surface Eddy Kinetic Energy (EKE) comparisons between the model simulations. a) The reference run is compared to Sconstant b) the reference run is compared to Sseasonal. c) Sseasonal is compared to Sconstant. (contour interval is 100 cm^2/s^2)s

clear answer to why this increase happens between these model simulations was found. The increase in maximum surface EKE does however coincide with an increase in maximum monthly MLD, and coincides with a small increase in the 5-year average MLD.

Between figure 4.5b and 4.5c an increase of the EKE is also visible at this location, where the maximum EKE between these runs increases by 9.3%. This can be explained as follows: because the boundary current is fresher in Sseasonal than in Sconstant, the horizontal density gradient increases. An increase in horizontal density gradient is associated with more baroclinic instabilities, and thus a higher EKE [8].

The differences between the model runs in EKE are more clearly shown in figure 4.6. Here, in figure 4.6a it can be seen that overall the EKE increase between the reference run and Sconstant is mainly at the area of the maximum EKE, just after the tip of Greenland. The same is reflected in 4.6b, but more strongly, as Sseasonal's maximum EKE is higher. Also, both figures show a negative anomaly in the center of the Labrador Sea, which is the area where the MLD has its maximum for each run (figure 4.2). The decrease in EKE here indicates that less eddies bring buoyant waters here, explaining the increase found in the average and monthly maximum MLD.

Figure 4.6c shows the difference between Sseasonal and Sconstant. From this figure also the increase in EKE is located at the EKE's maximum for each run, but since the maximum EKE increase is relatively small between these runs, this is less apparent here.

In figure 4.7 the properties of eddies are tracked by following a sea surface temperature anomaly of the 2-day snapshots over time. Three snapshots of eddy cross-sections are shown at different time intervals for each model simulation. In each simulation, eddies bring more buoyant waters to the interior. As an example, in the reference run (figure 4.7a-c) warmer boundary current waters are transported towards the interior. Over time (b-c) the eddy looses buoyancy due to the air-surface heat-flux, and eventually dissipates (not shown here). A similar process happens in Sconstant (figure 4.7d-f) and Sseasonal (figure 4.7g-i): here eddies bring warmer and fresher waters towards the interior (figure 4.7a-c) d and g). The eddies eventually loose buoyancy due the surface heat flux, and the horizontal and vertical gradient in salinity reduces as well (figure 4.7 e, f, h and i). The difference between Sconstant and Sseasonal is that the latter carries more fresh water, and as can be seen in the last panels of either run (figure 4.7f-i) the eddy is more distinct in figure 4.7i, as the boundary current is fresher. This suggests that with a freshening of the boundary current, eddies live longer [25]. Furthermore, in the runs Sconstant and Sseasonal it can be seen that in figures 4.7f and i the warmer water is below colder waters at a depth of about 300 m. In reality, also fresher, colder waters are on top of the warmer, more saline waters within the eddies [36].

Thus, when salinity is added to the model simulations, a large, yet unexplainable peak in the maximum EKE can be seen. Furthermore, the 5-year average and monthly maximum MLD increases for model simulations that contain salinity. The increase in MLD can be explained due to a reduction in EKE over the convection area.

4.4. Downwelling

The downwelling is analyzed by separating the basin into four areas, based on the 19.6 (20.1) Sv streamline for the reference run and Sconstant (Sseasonal) as defined in chapter 4.1. These four areas can be seen in figure 4.8 and are based on [1]. Area 1 is the area where the highest eddy activity is. In Area 2 the most intense cooling occurs. Area 3 is defined as another area with a small EKE peak (e.g. figure 4.5a, along the coast near the outflow). Area 4 is the interior of the basin. Even though the streamlines for each model configuration are not the same, no visible differences were found between these 4 areas for the different model simulations and therefore only one figure is shown for all model simulations. The vertical transport for each model configuration is shown in figure 4.9. The black line, which shows the net vertical transport, does not show much variation between the model simulations, with a maximum downwelling of 2.95 Sv. Only a small reduction in this value is seen in the run Sseasonal, but here more and fresher waters enter the basin at the inflow (see figure 2.7). This suggests that salinity has no influence on the net vertical transport in the basin. The differences between the model simulations are mainly seen in the increase in downwelling in area 1 and the increase in upwelling in area 4. The downwelling in area 1 increases for the Sconstant with respect to the reference run and increases even further for Sseasonal. Similarly an increase in upwelling is seen in area 4. This increase in up and downwelling coincides with a similar increase in EKE in area 1, meaning that the upwelling and downwelling of area 4 and area 1 could be linked to the EKE. The same result is found in [1].

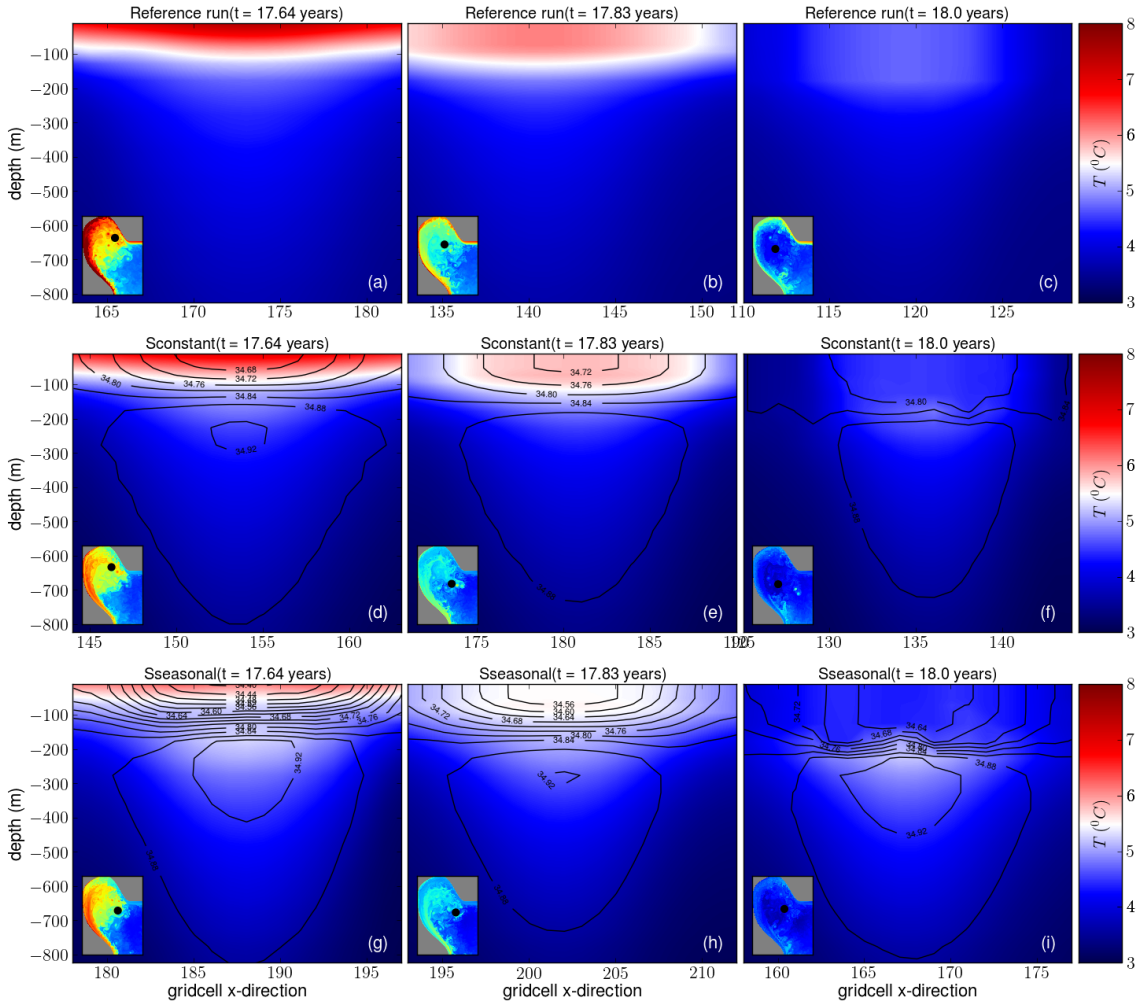

Figure 4.7: Cross section of several eddies that are shed from the boundary current. The colours indicate the temperature and the contour lines the salinity. The map on the bottom left shows the SST and the position of the eddy (green dot). (4.7a-c): an eddy of the reference run in August (a), October (b) and January (c). (4.7d-f) eddy in Sconstant, (4.7g-i) eddy in Sseasonal.

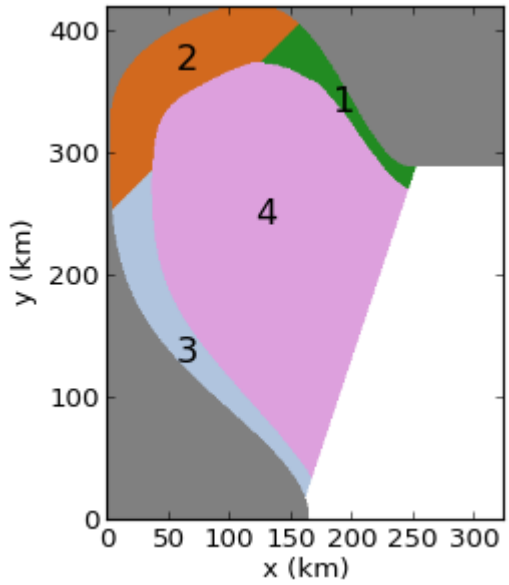

Figure 4.8: Separation of 4 areas in the basin for all model simulations. Area 1 is the area with the highest EKE. Area 2 is the area with the highest cooling. Area 3 is the area with another smaller EKE peak. Area 4 is the interior of the basin.

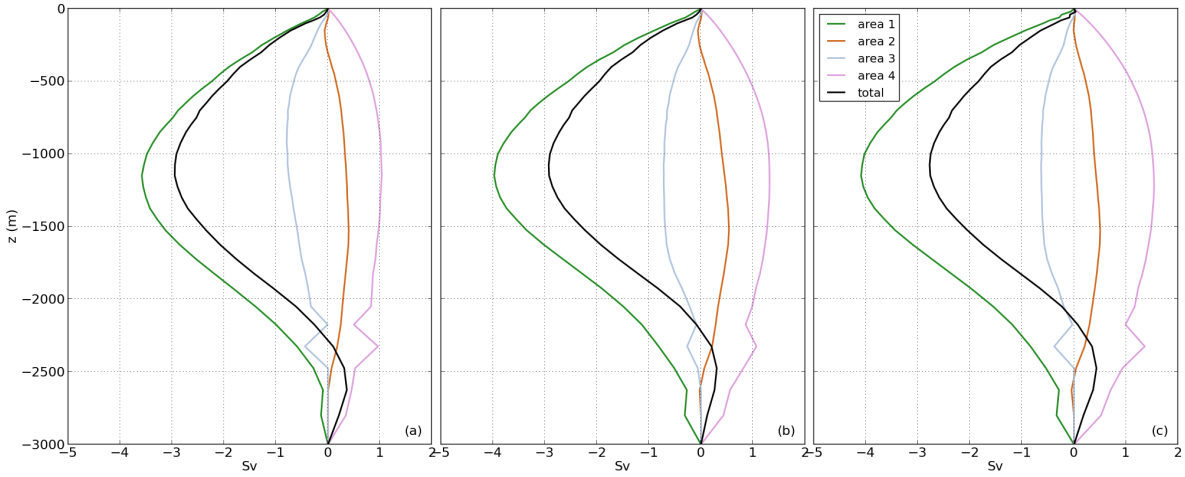

Figure 4.9: Vertical volume transport in Sv for each model simulations. The transport is separated per area as defined in figure 4.8. (a) is the reference run, (b) is Sconstant, (c) is Sseasonal

This chapter gave an overview of the main features of the Labrador Sea circulation in the idealized model used for this study. An unexpected large increase in maximum EKE is found when salinity was added to the idealized model (41.5%). It could not be explained why the EKE increased, since it is expected that with the same density gradients between the reference run and Sconstant no increase in instabilities would occur. The 5-year average MLD also increased slightly with the addition of salinity, whereas the monthly maximum MLD showed a significant increase. This can be attributed to the fact that there is a reduction in EKE over the convection area when salinity is added to the model: less eddies transport buoyant waters to this area, thus increasing the MLD. No changes were found in net maximum downwelling when salinity was added. This was expected, as no buoyancy is added or lost between the reference run and Sconstant, and the net loss in buoyancy is the same in all model simulations. Differences in up and downwelling are found however when looking at different areas of the domain for each model simulation.
The data presented in this chapter is not able to show the pathways the water masses take in the Labrador Sea basin. The next chapter will track the pathways of these water masses by means of Lagrangian particle tracking. There, separations of which pathway the water masses take will be made, and it will be shown how these waters transform along these pathways.

5

Lagrangian pathways and volume transport

In this chapter the volume transport throughout the basin is calculated by a Lagrangian tool (CMS, already presented in Chapter 4). First, two methods for classifying particles through the basin are compared, and based on these methods a new method has been developed. Secondly, a comparison between the pathways of the transport between the model simulations are made. Thirdly, the overturning in depth space for these model simulations is given where thereafter the overturning in temperature, salinity and density space are analyzed. Here, a closer look is also taken at particles that travel through the BC and through the interior. Lastly, the top 110 m of the BC are analyzed in more detail, as this is the location of the freshest waters in the model.

5.1. Separating boundary current and interior pathways

To analyze processes that happen in the boundary current and in the interior of the model simulations a distinction has been made between particles that travel only through the boundary current during their lifetime and particles that leave the boundary current and enter the interior at some point (during their lifetime). Two separate ways of determining whether particles flow only through the boundary current or also enter the interior have been investigated here, and based on the outcome of these results a criterion is chosen.
Particles that flow through the boundary current only are labelled as 'withinBC'. For the interior particles, a distinction is made between particles that enter the interior and leave model during their lifetime (InteriorShort) and particles that enter the interior and stay in the model at the end of the model run (InteriorLong) (all names are chosen after [37]). Similarly, this can be done for the boundary current particles, but a negligible amount of particles (little over 200 particles, table 5.2, labelled as 'BClong') resided in the BC for longer than 5 years. As their magnitude is negligible compared to the other particles, they will not be taken into account, and are only shown here for completeness.
The first method is based on [38]. There, particles have to be at least 50 km away from the 2500 m isobath towards the interior to be labelled as interior particles. At these locations, the velocity in the basin is roughly equal everywhere, meaning that these locations are part of the interior of the Labrador Sea.
Method 2 is based on [1]. There, the boundary current is defined as the particles that travel between the land and the 18 Sv contour line during their time in the model domain. Additionally, particles have to be out of the boundary current for 20 days total to be labelled as interior particles. This has been slightly adapted here to that the particles have to be 20 consecutive days out of the boundary current. In our case the boundary current is defined as the 19.7 Sv contour for the reference run and Sconstant and 20 Sv contour for Sseasonal. The robustness of these two methods has been analyzed by adjusting the distance for the first method with respect to the 2500 m isobath to 10 km and 30 km. For the second method the robustness is tested by adjusting the total consecutive days that a particle has to be away from the 19.7 or 20 Sv contour to either 10 or 30 days. The results for the reference run are presented in tables 5.1 and 5.2. The results for Sconstant and Sseasonal yield similar outcomes, and are therefore not presented here. First, the impact of changing the travel distance is analyzed (method 1). In table 5.1, large differences can be seen between the number of particles and volume transport that are defined as withinBC or InteriorShort particles. About 50% of the particles that are withinBC with the 50 km restriction are labelled as InteriorShort when this criterion is only 10 km. The BClong and InteriorLong particles do not vary much with difference in criterion. This is probably

Reference run	**withinBC**	**BClong**	**InteriorShort**	**InteriorLong**
50 km				
Particles	97283	242	130527	168717
Transport (Sv)	7,45	0,01	5,62	4,33
30 km				
Particles	70682	223	157128	168736
Transport (Sv)	5,83	0,01	7,26	4,33
10 km				
Particles	46627	221	181183	168738
Transport (Sv)	3,64	0,01	9,44	4,33

Table 5.1: Method 1: particles and transport for BC, BClong, InteriorShort and InteriorLong particles for the criterion 50, 30 and 10 km offshore from the 2500 m bathymetry line. A total of 396769 particles are calculated carrying 17.42 Sv.

Reference run	**withinBC**	**BClong**	**InteriorShort**	**InteriorLong**
30 days				
Particles	127917	155	149993	157248
Transport (Sv)	7,75	0,01	5,59	4,32
20 days				
Particles	114171	155	163739	157248
Transport (Sv)	7,02	0,01	6,32	4,32
10 days				
Particles	96405	155	181505	157248
Transport (Sv)	5,97	0,01	7,37	4,32

Table 5.2: Method 2: particles and transport for BC, BClong, InteriorShort and InteriorLong particles for the criterion 30, 20 and 10 consecutive days offshore of the 19.7 Sv line (20 Sv for Sseasonal). A total of 435313 particles are calculated carrying 17.67 Sv.

due to the fact that when a particle remains in the basin for at least 4 years, it is very likely to be in the interior, as otherwise the boundary current would have moved this particle outside of the domain. The same can be said for the InteriorLong particles derived from method 2 (table 5.2). The change in the number of withinBC particles to InteriorShort particles however seems to be less sensitive to a change in the number of consecutive days the particles have to be out of the BC to be labelled as InteriorShort. The decrease between 30 days and 10 days represents only a loss of about 25% of the particles and a similar loss in volume transport. Thus, this method is sensitive to the choice of consecutive days. Note that the total tracked particles between table 5.1 and table 5.2 is not equal, as the criterion based on the bathymetry has been done with a different, earlier CMS configuration, with the only difference being the number of particles released in both simulations.

In this study it is chosen to use method 2; where the particles have to be out of the boundary current for 20 consecutive days to be labelled as interior particles. The reasons for this are: one, this criterion is based on the streamline of the flow rather than the bathymetry, and the streamline defines better where the BC is. Two: for a particle to be considered as an interior particle it has to be in the interior and away from the BC for some time. Method 2 bases interior particles both on time and distance, whereas method 1 only defines interior particles on distance. Example pathways for this method of withinBC, InteriorShort and Interiorlong particles can be seen in figure 5.1.

The following section shows the results for those particles classified according to the method 2, and compares them for the three model configurations.

5.2. Comparison pathway transport

In this section the transport through the model domain will be tracked for each different model simulation and will be compared to each other. The distribution of particles into the above-defined pathways classes is summarized in Table 5.3. These comparisons are made with respect to the reference run, unless stated otherwise. It is seen here that the sum of the particles and total volume transport differs between each model simulation, even though the same number of particles is released. Lower numbers in the salinity simulations are likely due to the MLD reaching to the bottom during winter times. Particles in these simulations are more likely to get advected out of the model through the bottom due to how CMS handles particles in the MLD.

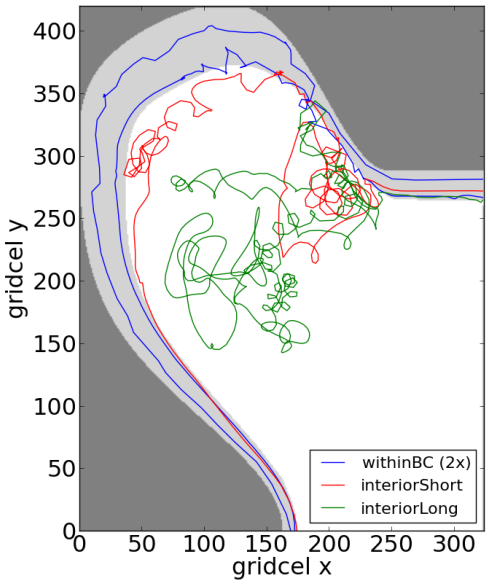

Figure 5.1: Example pathways for particles that are defined as withinBC, InteriorShort or Interiorlong, based on method 2 (see text for description of this method). Darkgray is the landmass; lightgray is the BC; white is the interior. Note that one of the withinBC particles sometimes is in the defined interior but is still classified as withinBC

This results in 25735 (6.1%) particles less being analyzed in Sconstant as opposed to the reference run and similarly a loss of 19531 (4.1%) particles for Sseasonal. For the volume transport this results in a loss of 0.55 Sv for Sconstant and an increase of 0.14 Sv for Sseasonal as opposed to the reference run. While in both runs that include salinity there is more water transported into the BC than in the reference run (Table 5.3), the larger increase in Sseasonal is due to its smaller MLDs with respect the Sconstant simulation, which allows CMS to handle better Lagrangian particles located at the bottom.

A clear difference is seen in the BC particles: more water mass is transported in the BC in Sconstant and Sseasonal. For Sconstant, this is even so despite the fact that there is less overall tracked water volume transport. The transport increases from 7.02 to 8.22 Sv for Sconstant and to 8.15 Sv for Sseasonal. Likewise, a reduction in transport for the interior particles is seen in these simulations: for InteriorShort the transport reduces from 6.32 to 5.02 or 5.68 Sv for Sconstant and Sseasonal respectively, and for InteriorLong this is from 4.32 to 3.87 or 3.98 Sv. This finding is not in line with the earlier found increased EKE near the west coast of Greenland for Sconstant (chapter 4.3). a higher EKE means that the BC is more unstable, and thus sheds off more eddies,

	BC	**BClong**	**Intshort**	**Intlong**	**sum**
Reference run					
particles	114171	155	163739	157248	435313
transport (Sv)	7,02	0,01	6,32	4,32	17,67
%	39,7	0,1	35,8	24,4	100
Sconstant					
particles	131497	165	133894	144022	409578
transport (Sv)	8,22	0,01	5,02	3,87	17,12
%	48	0,1	29,3	22,6	100
Sseasonal					
particles	127563	109	147533	140577	415782
transport (Sv)	8,15	0	5,68	3,98	17,81
%	45,8	0	31,9	22,3	100

Table 5.3: Number of particles and transport that occurs for withinBC, BClong, InteriorShort and InteriorLong particles for the reference run, Sconstant and Sseasonal

which results in more transport into the interior. Surprisingly, here the opposite is found: with a higher EKE less waters are transported into the interior.

The differences between Sconstant and Sseasonal can be explained as follows: due to an increase in horizontal density gradients, which is larger in Sseasonal. Due to the thermal wind balance, the boundary current becomes more unstable, causing more water mass to be transported from the boundary current due to baroclinic instabilities. This is also reflected in the data between Sconstant and Sseasonal: less water is transported through the BC and more waters are transported through the interior. Both InteriorShort and InteriorLong transport increase in the Sseasonal run opposed to Sconstant. This means that lateral exchanges induced by a stronger EKE field in Sseasonal are reflected in the interior pathways.

5.3. Overturning depth space based on Lagrangian particles

To analyze how salinity influences the pathways of transport in the Labrador Sea, first we look at the overturning in depth space for each model simulation. The transport has been calculated as follows: the assigned volume transport (explained in chapter 3) of each particle is summed between bin sizes of 100 m at the inflow and at the outflow. The transport which enters and leaves the basin can be seen in figure 5.2 for each of the model simulations. Between the model simulations no large differences are found; so the following therefore applies to all model simulations. More than 95% of the particles that are labelled as 'withinBC' enter the basin in the top 1000 m, where the largest inflow is at the surface (blue bars, panels a,d and g). These withinBC waters are to a minor extent transformed to deeper water masses when they reach the outflow (green bars, figure a, d or g), where 95% of the of the water is transported out of the model above 1500 m. For the InteriorShort particles, more than 95% of the water mass is transported above 1400 m, where the distribution is more uniform over the vertical, with only decrease at the lower depths (blue bars, b, e and h). Similar to the withinBC particles, these water masses are more spread over the vertical at the outflow, with 95% of the particles exiting above 1800 m. The InteriorLong particles show similar behaviour to that of the InteriorShort particles at the inflow (blue bars c,f and i). It is clear from the difference in inflow and outflow depths that a net downward transporting overturning circulation exists in each of the models, with their magnitude being (almost) the same.

This net downward transport becomes also apparent when looking at a and e of figures B.3, 5.3 and B.4 (B indicates that the figure can be found in appendix B). There, the net vertical transport is shown binned every 100 m when calculated at the location (Eulerian, green line), for the withinBC particles (black line), InteriorShort particles (red line), their sum (Lagrangian, purple line) and for the InteriorLong particles. In these figures the Eulerian transport is the same where more waters flow into the basin above 1000 m, and leave below this depth. The net maximum downwelling amounts to a little over 4 Sv located at 1000 m depth (figures B.3e, 5.3e and B.4e). This net maximum downwelling is however not reflected in the Lagrangian particles: the maximum downwelling for each model run is little over 1 Sv, but does still occur at 1000 m depth. This could be explained by the large amount of InteriorLong particles (± 4 Sv for each model simulation) that are still existent in the model at the end of their simulation duration: these particles are likely responsible for the waters that leave at a lower depth. As [37], who did a similar analysis backwards in time, releasing particles at the outflow, found that the InteriorLong particles consisted of the deepest formed waters at the outflow in their model. This assumption is strengthened further by figure B.5b, figures B.6b and B.7b. They show similar results and are for Sconstant and Sseasonal, respectively): the yellow line here is the total Lagrangian transport at the inflow. This line coincides almost with the Eulerian calculations. At the outflow (figure B.5), no InteriorLong particles exist. The difference between the Lagrangian and Eulerian calculations is thus likely due to the InteriorLong particles.

5.4. Overturning density space based on Lagrangian particles

To analyze how salinity influences the pathway of water volume transport in the Labrador Sea, the transport of each model simulations has also been analyzed in temperature, salinity and density spaces. Transport in temperature space is calculated across isotherms, for salinity this is across isohalines and in density space this is across isopycnals. The inflow and outflow are analyzed by separating the particles similarly to the previous chapter. In this section, Sconstant is analyzed first, whose results are very similar to Sseasonal. Thereafter, these results are compared to the reference run.

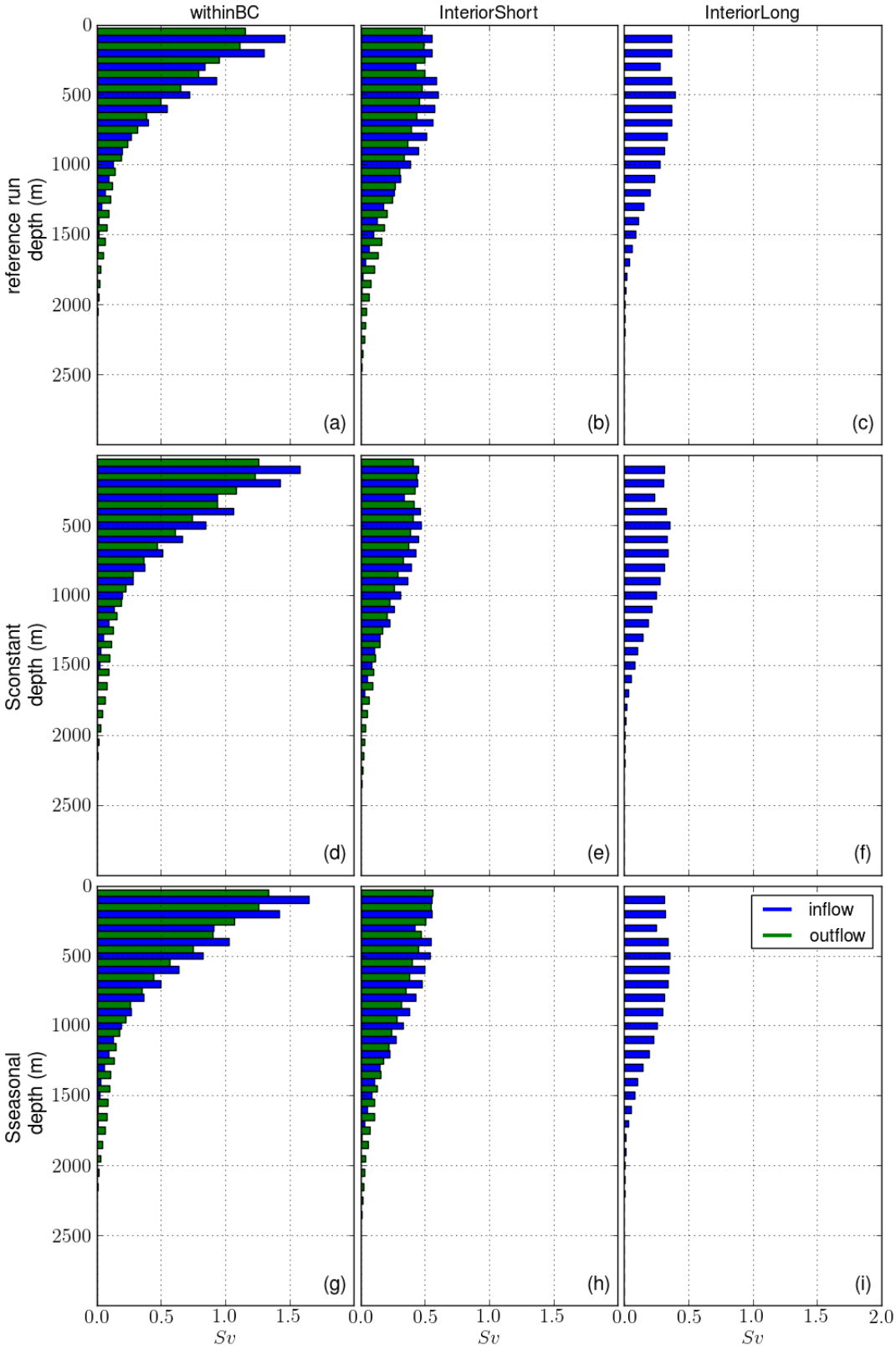

Figure 5.2: Bar plots of transport of the inflow (blue bars) and outflow (green bars) in depth space binned every 100 m. Figures a-c show the reference run, d-f show Sconstant and g-i show Sseasonal. From top to bottom separations have been made for particles that flow only through the boundary current (a,d,g), InteriorShort particles (b,e,h) and InteriorLong particles (c,f,i).

5.4.1. Overturning density space for Sconstant and Sseasonal

Although the bar plots are only displayed for Sconstant, conclusions are similar to Sseasonal since plots depict a similar behaviour. A similar plot of Sseasonal is shown in appendix B, figure B.2. Before figures 5.3b-d and f-h are explained, first a look will be taken at bar plots of the in and outflow in density space (figure 5.4) in similar fashion to figure 5.2

Figure 5.4a shows the overturning in temperature space for the BC water masses; the waters above 4.8 °C at the inflow (blue bars) for the withinBC and InteriorShort trajectories are all transformed to waters colder than 4.8 °C when they leave the domain (green bars). Two peaks in temperature can be distinguished at the outflow; one at 4.5 °C and a flatter one at around 3 °C. Similarly, an overturning in the InteriorShort particles can be seen (figure 5.4b).

In salinity space (figures 5.4d-f) the freshest waters (below 34.6 PSU) become more saline in the BC. Also, the most saline waters (above 34.9 PSU) experience a freshening from inflow (blue bars) to outflow (green bars). Again, two peaks can be seen again at the outflow (green bars) in figure 5.4d, one at 34.75 PSU and one at 34.9 PSU. In the interior (figure 5.4e) this change is less obvious: most of the particles that take this pathway are already relatively saline with an average of 34.86 PSU (blue bars). The most saline waters (above 34.9 PSU) here also experience an overall freshening. The fresher particles (here below 34.7 PSU) also experience overturning in salinity space and become more saline. The result is that on average no overturning occurs in the basin in salinity space, where the average of these particles is still 34.86 PSU. In density space (figure 5.4g-i) BC particles (figure 5.4g) clearly show an overturning. Waters get converted during their pathway from inflow to outflow to heavier waters, from 27.64 to 27.72 kg/m^3 (blue to green bars). Two peaks in the outflow (green bars) are also seen again at 27.6 and 27.9 kg/m^3. For the interior short particles this change is less obvious. The lightest waters (below 27.6 kg/m^3) get converted to heavier waters (from 27.77 to 27.8 kg/m^3). The InteriorLong particles consist of the most dense waters at the inflow, with an average of 27.78 kg/m^3.

The net transport in temperature, salinity and density space for Sconstant is given in figure 5.3b,c and d and are given cumulative in f, g and h respectively. First, we look at the overturning in temperature space (figure 5.3b and f). In this figure, two peaks can be distinguished, one at 4.5 °C and another one at 3 °C. The first peak is mostly caused by the withinBC particles and is not at all reflected in the Eulerian transport. The second peak is from both the withinBC and InteriorShort particles. This peak is also calculated in the Eulerian transport, but is much larger here. This difference is again likely due to the lack of InteriorLong particles which contribute significantly to this overturning: as with the analysis done in depth space, the total transport of all particles at the inflow is shown in figure B.6f (yellow line). This again coincides with the Eulerian calculations. At the outflow however, only the Lagrangian particles (purple line) reach the outflow. These particles show less overturning at the peak of 3 °C compared to the Eulerian data. From [37] it is known that the InteriorLong particles are represented by the coldest, densest water masses (also reflected in the reference run here, which is the same). Thus it is strongly suggested that significant overturning occurs with the InteriorLong particles. This means that the resulting Lagrangian calculations show significantly less overturning for each space (depth, density, temperature and salinity).

For salinity (figure 5.3c and g) first, a negative peak and then a positive peak at 34.9 and 34.85 PSU is seen respectively. This means that the most saline waters (34.9 PSU) from the inflow are transformed to slightly less saline waters (34.85 PSU) at the outflow. Furthermore, waters with salinity below 34.8 PSU are converted to more saline waters, which is seen in the positive signal of the cumulative transport (figure 5.3f). In this figure, it can be seen that most of the conversion of salinity occurs in the withinBC particles (black line), as the peak is much larger than the InteriorShort particles (purple line). Some conversion does occur in the interior at 34.8 PSU. Again, there is a large difference between the Eulerian and Lagrangian calculations, which can be attributed to the InteriorLong particles not reaching the outflow again (yellow line B.6h versus purple line B.6i).

Lastly, the overturning in density space is analyzed (5.3d and h). Two peaks are seen in the Lagrangian tracking of particles, the first one at 27.5 kg/m^3, consisting mainly of withinBC particles, and the second one is at 27.9 kg/m^3, consisting of both withinBC and InteriorShort particles. The deficiency between Eulerian and Lagrangian calculations is also seen here in the second, denser peak likely caused by the InteriorLong particles (yellow line B.6k versus purple line B.6l). The shape of the vertical cumulative transport in density space (5.3h) is almost a reflection of that of the temperature space cumulative transport (5.3f), suggesting that salinity plays a minor role in the total overturning occurring in the basin. However, the maximum cumulative transport in density space, 4.8 Sv, is smaller than that of temperature space, 5.3 Sv, which means that salinity reduces the overturning by 10 % in density space.

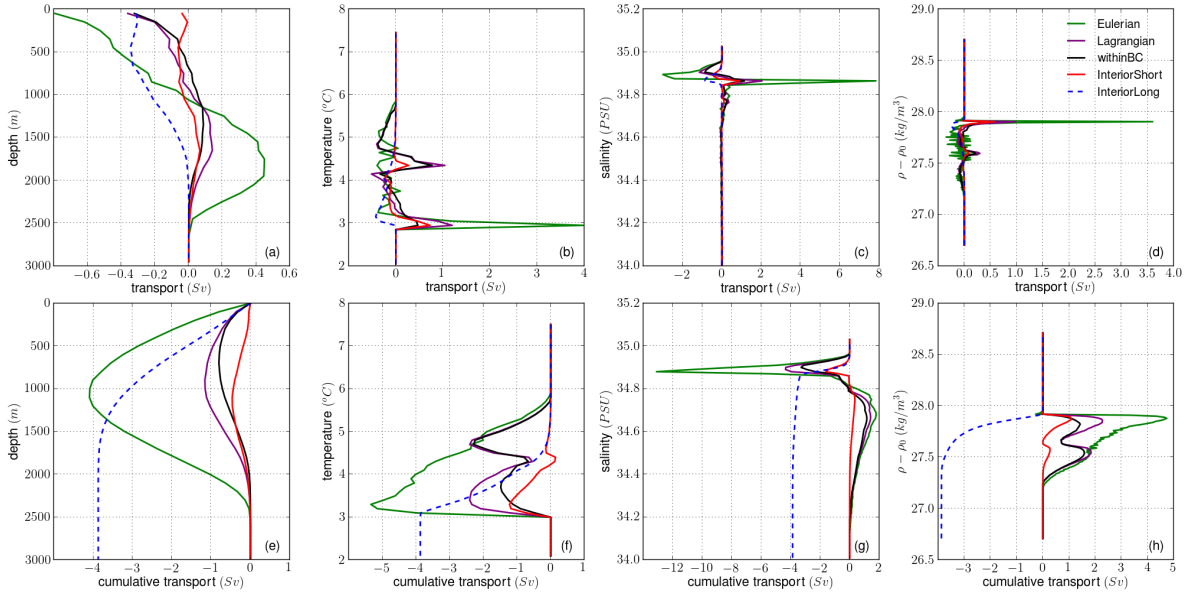

Figure 5.3: Net volume transport (out - in, top panels) and cumulative transport (bottom panels) for Sconstant binned every 100 m for depth space (a,e), 0,1 ^0C for temperature space (b,f) 0.01 PSU for salinity space (c,g) and 0.01 kg/m^3 for density space (d,h). Eulerian is the total calculated net transport (green line), withinBC particles are black, InteriorShort particles are red, their sum is the Lagrangian calculated flow (purple). The transport of the InteriorLong particles is also shown (blue dashed line).

5.4.2. Overturning density space for the reference run

The differences of Sconstant (and Sseasonal) with respect to the reference run are presented here.
The two peaks in temperature can also be distinguished at the outflow for the reference run, where one peak is at 5.2 °C and a flatter peak is around 4 °C. Similarly, an overturning in the InteriorShort particles can be seen (figure B.1b), where a small peak is at 5.2 °C and a larger one at 3.5 °C. Compared to Sseasonal, the two peaks in temperature are also seen here, but are located at higher values, because of how the inflow here is defined. In this figure it is also clear that already colder particles traverse through the interior as opposed to the withinBC particles (4.8 and 4 °C on average, respectively). The InteriorLong particles (B.1c) consist mainly of the coldest waters at the inflow, similar to Sconstant, where these particles are also the coldest waters. Figure B.1d-f show no changes in salinity, as this run has no variation in this. This means that figures B.1g-i depend only on the temperature and thus the same conclusions can be drawn here.
From figure 5.3, similar conclusions can be drawn for the reference run as for Sconstant (figures B.3, B.4), apart for salinity space. The main difference between figure B.3 of the reference run and that of Sconstant (figure 5.3) is that the maximum overturning equals 3.9 Sv in both temperature and density space for the reference run while it equals 5.3 and 4.8 Sv for Sconstant. The overturning in temperature and density space is thus significantly larger for the runs that contain salinity, even with the reducing effect of density compensation.

5.4.3. Closer look at the withinBC particles

Overturning occurs in the boundary current as well, although not through deep convection [13]. Therefore, a closer look is taken at the BC particles by means of a TS-diagram for Sconstant. This can be seen in figure 5.5. The overturning in density space is here illustrated by a TS diagram for Sconstant (figure 5.5a) at the inflow of the model. Figure 5.5 b-g shows the TS diagrams of intermediate sections along the boundary current, while Figure 5.5h shows the TS diagram at the outflow. The inset figure at the bottom right in each figure is where the TS diagram is located. It is evident that warmer and fresher waters (figure 5.5a) get transformed to more saline and colder waters at the outflow (figure 5.5). Also, it can be seen in figure 5.5a that most of the waters have a salinity of around 34.9 PSU and are in between 3 and 5 °C. The fresher and cooler surface waters range from 34.2 to 34.8 PSU with an average temperature of 4.5 °C. These waters will be referred to as the 'fan'. Temperature and salinity first cool and become more saline gradually when the boundary current enters area 1 (see figure 4.8) and progresses along this area (figure 5.5b-d). These changes are mostly reflected in the 'fan', which becomes smaller and more saline. After the boundary current progresses to the area in figure 5.5e a second peak appears around 34.6 PSU and 4.5 °C and the fan now ranges in salinity between 34.55 and

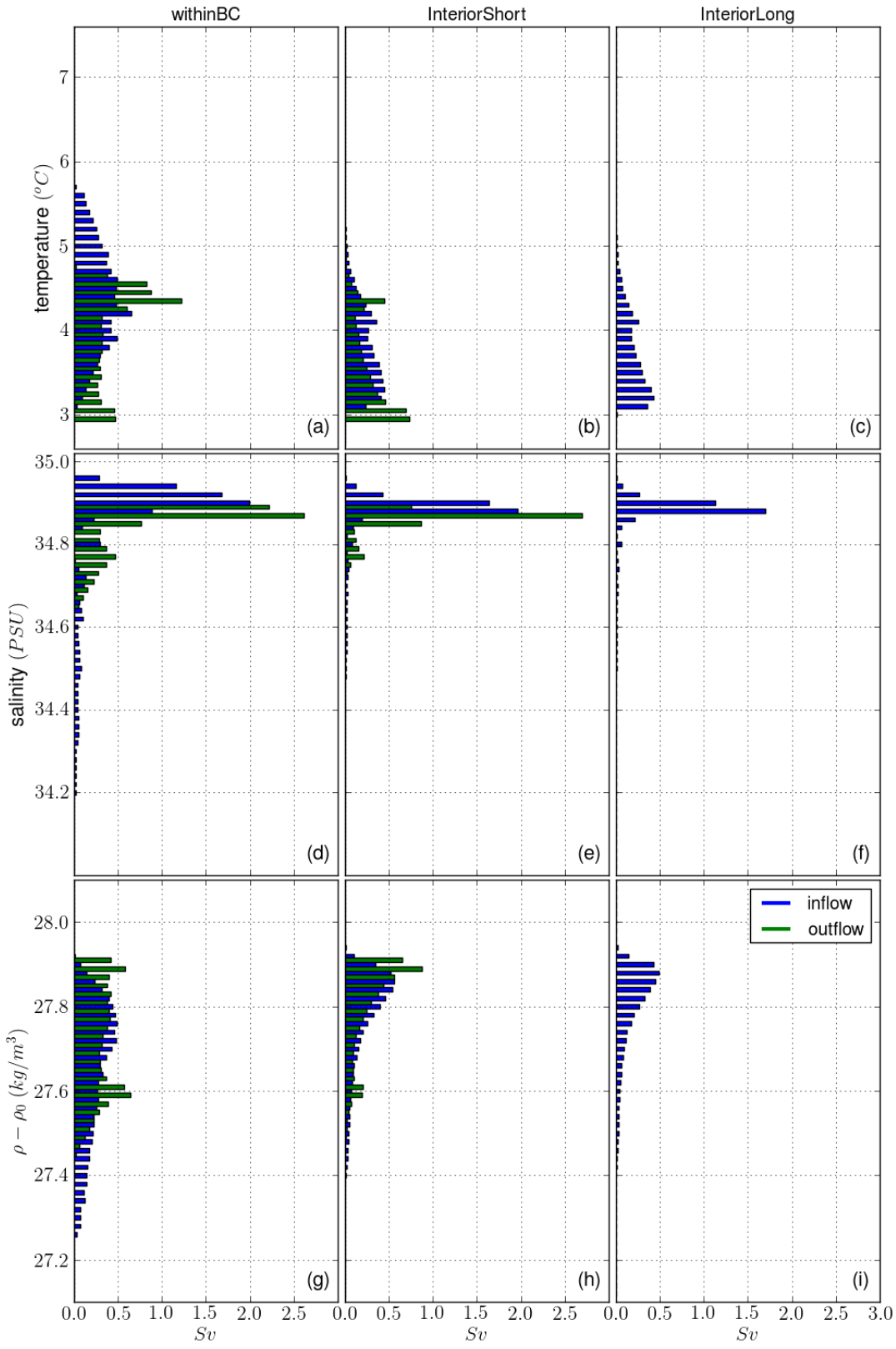

Figure 5.4: Bar plots of transport of the inflow (blue bars) and outflow (green bars) for Sconstant. Figures a-c show temperature space, binned every 0.1 °C, d-f show salinity space binned every 0.01 PSU and g-i density space binned every 0.01kg/m^3. From top to bottom separations have been made for particles that flow only through the boundary current (a,d,g), InteriorShort particles (b,e,h) and InteriorLong particles (c,f,i).

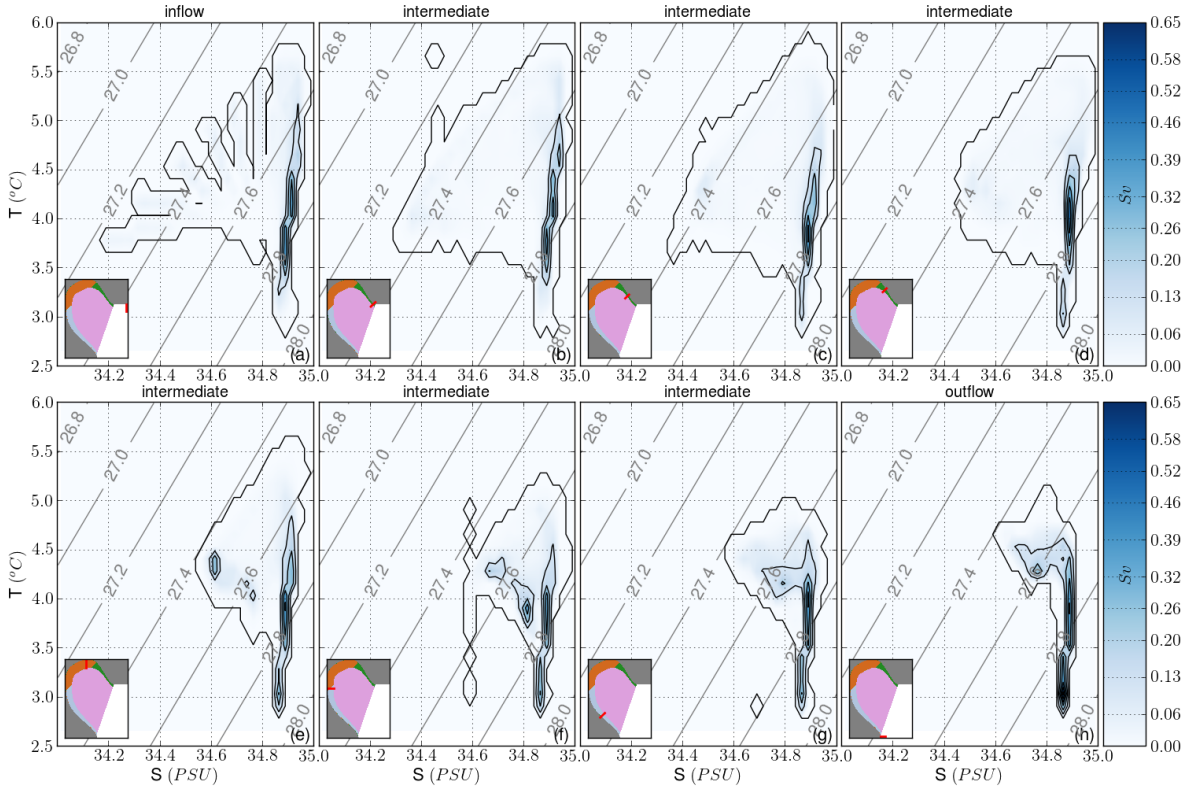

Figure 5.5: TS diagrams for withinBC particles along their trajectory for the run Sconstant. The small figure in each plot indicates where data for the TS-diagram is obtained. a) TS-diagram boundary current. b-d) TS-diagram area 1, e,f) TS-diagram area 2, g) TS-diagram area 3, h) TS-diagram at the outflow. The grey lines are the specific density contours

34.95PSU. Two peaks appear in figure 5.5f, at 34.7 and 34.8 *PSU* and with 4.2 or 3.8 °C respectively. Almost all of the surface waters have been transformed here as can be seen by the shape of the 'fan' - it's almost gone. Figure 5.5g shows one peak again, at 34.8 *PSU* and 4 °C. The fan here only surrounds the tops of both peaks. Finally, at the outflow (figure 5.5h) Almost all waters in the fan have been converted to the peak located at 34.7 *PSU* and 4.3 °C. These peaks are also seen in the green bars of figure 5.4, which means that the first peak is caused by conversion which happens in the withinBC particles.

Thus, it is evident that significant overturning occurs in the BC, for both temperature and salinity, even though there is only a surface forcing. both ranges in temperature and salinity reduce, which means that significant mixing occurs in the BC.

5.4.4. Closer look at the InteriorShort particles

In the previous section it was found that less volume transport leaves the BC. To investigate where this reduction volume transport occurs and where the particles re-enter the BC, a closer look is taken at the InteriorShort particles.

It is not possible to analyze the InteriorShort particles along their trajectory by means of TS-diagrams, as the InteriorShort particles take many different pathways. Therefore, only the TS-diagrams of the in- and outflow are shown in figure 5.6. Similarly to that TS-diagrams for the BC, fresher and warmer waters get converted to more saline and colder waters. The difference is however that no secondary peak occurs for these InteriorShort particles; most of the waters are thus converted to the peak at 34.9 *PSU* and between 3-4 °C (figure 5.6b). It is also evident from these figures that the inflow condition for the InteriorShort particles has a smaller range in temperature compared to that of the withinBC particles (figure 5.5a), ranging from 3-4 °C rather than 3-5 °C, at 34.9 *PSU*. Similarly, the outflow also shows a narrower, and colder range from 3-4 °C at 34.9 *PSU* for the InteriorShort particles (figure 5.6b) and 3-4.5 °C at 34.9 *PSU* for the withinBC particles (figure 5.5h).

The InteriorShort particles are analyzed by looking at where they leave and re-enter the BC. This is analyzed this way to find out whether the reduction in volume transport for the model configurations with salinity is

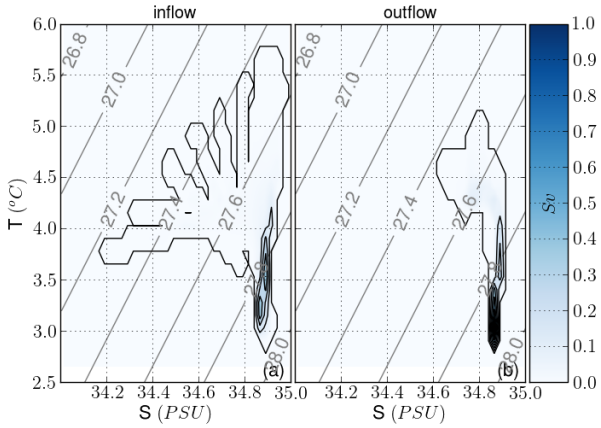

Figure 5.6: TS diagrams for the InteriorShort particles at the inflow (a) and outflow (b) for the run Sconstant. The grey lines are the specific density contours

near the EKE maximum or elsewhere. The leave and re-entry locations of the particles has been separated into five areas, where three of these areas are previously defined in chapter 4.4 (see also figure 4.8). This separation is made this way to determine whether the volume transport changes near the main EKE peak (area 1), the area of highest cooling (area 2) or the area with the secondary EKE peak (area 3). Particles could also leave and re-enter in between the inflow and area 1 (inflow) or between area 3 and the outflow (outflow). The last re-entering condition of the particles is based analogously on the criteria for InteriorShort particles: the last re-entry point of a particle is if the particle re-enters the boundary current after having been out of the boundary current for at least 20 consecutive days for the last time. The results are shown in table 5.4. Most of the InteriorShort particles leave the domain either close to the inflow or at area 1 for each model configuration. Close to the inflow the volume transport however is very low. At area 1, most of the volume transport occurs: 4.71, 3.86 and 4.4 Sv for the reference run, Sconstant and Sseasonal respectively. This coincides with the area of the highest EKE (figure 4.5). At areas 2 and 3 InteriorShort particles also leave the BC, but to a lesser extent compared to area 1. Near the outflow almost no particles leave the BC. from table 5.3 it was already known that for Sconstant and Sseasonal less particles travel through the interior. In Sconstant, every area experiences a reduction in particles leaving the BC. This reduction is largest in area 1 (0.85 Sv). With the run Sseasonal the particles that leave the BC increases slightly and most of this increase is seen in area 1 and to less extent in area 3 with respect to Sconstant. This means that the reduction in particles leaving the BC when salinity is included into the model cannot be explained by a reduction in particles leaving the BC elsewhere than near the EKE peak.

Particles re-enter the BC more evenly distributed, with peaks in area 1 and area 3 for the reference run and almost no re-entry at the inflow. At Sconstant, more waters re-enter the BC at area 1, even though less waters leave the BC overall. The reduction in re-entering water masses is seen most significantly in area 3, and to some less extent in area 2 and at the outflow. This reduction in waters re-entering in area 3 is 1,09 Sv. in Sseasonal, more water masses re-enter mostly in area 1 and at the outflow compared to Sconstant.

A closer look is taken at area 1, where most particles leave and re-enter the BC. In figure 5.7 it is shown where particles leave (a) the BC, re-enter (b) and the net transport of these two (c) for Sconstant. The horizontal axis is the zonal location of the 19.7 Sv line and the vertical scale is the depth. The contour lines indicate the EKE at an interval of 100 cm^2/s^2. The horizontal and vertical bin resolutions are respectively 18750 and 250 m. Similar figures for the reference run and Sseasonal are seen in figures B.8 and B.9. Figure 5.7a and b shows that most of the waters leave and re-enter the BC in the top 1000 m. For the inflow waters leave the BC below 1000 m as well, but less than in the top 1000 m. One (widespread) peak can be seen in figure 5.7a, where the peak is slightly upstream of the EKE max but spreads out to slightly downstream of the EKE peak. The re-entering particles (figure 5.7b) have one peak which coincides with the EKE max. The net transport at the BC is seen in figure 5.7c. Particles on average leave area 1, and mostly do so where the bathymetry narrows at x = 800 km, slightly before the EKE max. Most of the net transport also happens in the top 1000 m, with some outflow below this depth. Similar results are seen for the reference run and Sseasonal (figure B.8 and B.9). The only difference are the magnitudes of the particles that leave and re-enter.

In summary, the main result here is that the reduction in particles leaving the BC when salinity is incorporated into the model cannot be attributed to a reduction in particles that leave elsewhere than near the EKE

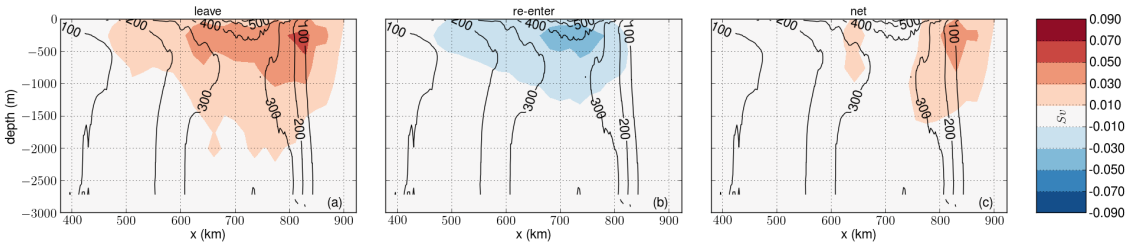

Figure 5.7: Concentration of where volume transport leaves the BC (a), re-enters the BC (b) and net transport (c) of InteriorShort particles in area1 for the Sconstant. The contour lines show the EKE.

	inflow	**area 1**	**area 2**	**area 3**	**outflow**	**sum**
Reference run						
particles leave	28658	113401	11062	9753	976	163850
transport leave (Sv)	0,16	4,71	0,72	0,67	0,07	6,33
particles re-enter	1050	61511	21962	54695	24632	163850
transport re-enter (Sv)	0,01	2,1	0,9	2,26	1,05	6,32
Sconstant						
particles leave	26088	92290	9173	5680	783	134014
transport leave (Sv)	0,17	3,86	0,57	0,37	0,05	5,02
particles re-enter	3140	64252	19316	28172	19134	134014
transport re-enter (Sv)	0,02	2,22	0,78	1,17	0,83	5,02
Sseasonal						
particles leave	35537	96260	7807	7537	520	147661
transport leave (Sv)	0,23	4,4	0,51	0,51	0,04	5,69
particles re-enter	3598	69599	19212	28799	26453	147661
transport re-enter (Sv)	0,02	2,53	0,82	1,17	1,14	5,68

Table 5.4: Total transport and particles for where they leave and re-enter the boundary current, binned per area, as in figure 4.8, where 'inflow' is between the inflow and area1 and 'outflow' is between area 3 and the outflow.

peak. However, more volume transport does re-enter the BC near the EKE peak in Sconstant and Sseasonal. This increase in volume transport that enters the BC coincides with the maximum EKE. This increase occurs even though there is less transport of the InteriorShort particles in Sconstant and Sseasonal. Thus, salinity variations have an impact on the magnitude and distribution of where waters leave and re-enter the model, even tough the density gradient remains the same with respect to the reference run. The magnitude is still in the same order as the reference run, implying that a model without salinity variations still captures the major processes in a idealized model of the Labrador Sea.

5.4.5. Closer look at particles released in the top 110 m.

Here, the top 110 m of the water column will be analyzed for the different runs, as these are the waters representing the most fresh inflow for the runs Sconstant and Sseasonal (see figure 2.7 h and i). The aim of this analysis is to investigate the overturning in the freshest waters, and compare these surface waters to that of the reference run. The overturning in depth, temperature, salinity and density space are given in figure 5.8 for Sseasonal. Similar calculations are also seen in the reference run and Sconstant (apart for salinity with respect to the reference run) and are therefore shown in appendix B (figures B.10 and B.11). In depth space (figure 5.8 a and e) it can be seen that the these top waters are converted to deeper waters up to a depth of 1500 m. In temperature space, figure 5.3b showed two large positive peaks, whereas only one positive peak is shown in figure 5.8. This peak consists mainly of the withinBC particles and has a maximum of 0.4 Sv. This means that the top waters of the boundary current are partly responsible for the first peak in figure 5.3 b, where the maximum of this peak is at 1 Sv. One significant difference between the reference run and Sconstant is that the maximum overturning in temperature space differs significantly: this is -1.8 and -0.5 Sv for the reference run and Sconstant, respectively.
In salinity space (figure 5.8c and g) The overturning exists only for Sconstant (and Sseasonal) and is more

significant compared to the overturning in temperature, up to 1.5 Sv at 34.6 PSU. Here it is clearly seen that the most fresh waters (>34.6 PSU) are converted to more saline waters, with peaks at 34.7 and 34.85 PSU. In density space all the model simulations show the (almost) the same overturning, with a maximum of 1.8 Sv. In summary, the overturning for any of the model configurations remains (almost) the same in density space for the top 110 m of the inflowing waters. The major difference is that in the model configurations that contain salinity, most of this overturning is governed by a overturning in salinity space, whereas for the reference run this can only be due to overturning in temperature space. Thus, a model that contains only temperature variations represents the overturning in density space very well for the top 110 m inflowing waters in a idealized model of the Labrador Sea, but of course cannot separate this overturning signal due to overturning in temperature or salinity space.

5.5. Summary

This chapter presented the transport in the Labrador Sea by means of Lagrangian particle tracking. It was found that between the reference run and Sconstant no changes can be found in overturning in depth space. For density space significant differences are found: the maximum overturning in density space increases from 3.9 to 4.8 Sv. The run with salinity did contain an effect called 'density compensation', reducing the maximum found overturning in temperature space (5.3 Sv) by 10%. Furthermore, two peaks were found in temperature and salinity at the outflow of each model. These are attributed to overturning that occurs in the BC and overturning that occurs in the interior, respectively.
It is also found that a significant discrepancy exist between Eulerian and Lagrangian perspective. These are explained by the high volume transport of Interiorlong particles: these particles consist of the deepest, densest waters found by [37]. At the outflow, whereas here they represent somewhat colder and saline waters in the inflow. This already strongly suggests that these particles are important for a large part of the overturning to deeper, denser waters. This notion is further supported by the fact that at the inflow the transport of all Lagrangian particles (withinBC, Interiorshort and Interiorlong) are almost equal to the overturning in all spaces (depth, temperature, salintiy and density) from Eulerian perspective. At the outflow however, the most dense, cold, saline and deepest waters show a large discrepancy between Eulerian and Lagrangian perspective, due to the lack of Interiorlong particles which do not reach the outflow by definition. This strongly suggests that the residence time of water masses in the Labrador Sea plays a critical role in the overturning signal: Water masses that take longer than four year to leave the basin are responsible for a significant amount of overturning in any of the spaces.
An attempt has been made to explain why with increasing EKE for Sconstant less transport is through the interior as opposed to the reference run. It was found that the volume transport mainly reduces near the EKE peak; exactly the opposite of what would be expected. However, an increase of waters that re-enter is found in this area, which also coincides with the EKE peak. This suggests that the EKE maximum is linked to waters that re-enter the BC, but is less so linked to waters that leave the BC there.
Lastly, the surface waters, which are the freshest waters in Sconsant and Sseasonal, have been analyzed in order to compare the overturning between the model configurations. It was found that the overturning in density and depth space remained the same, but consists mostly of overturning in salinity space for Sconstant and Sseasonal. Thus the overturning for the (near) surface waters is well presented in a model that contains only temperature variations but cannot make a distinction between overturning in salinity or temperature space.

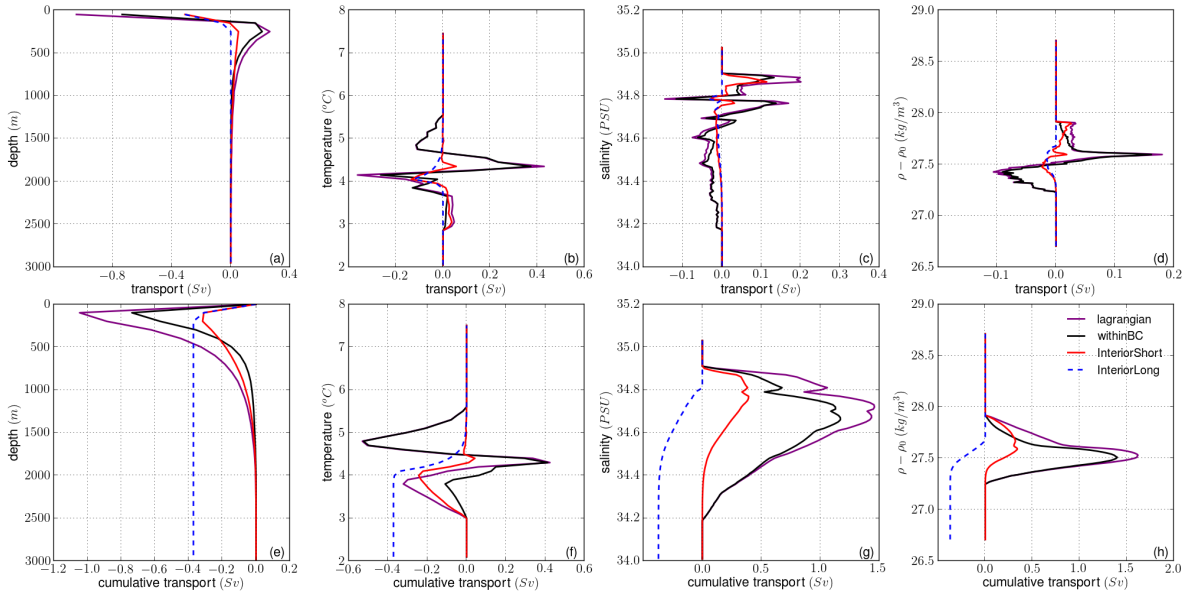

Figure 5.8: Net overturning (top panels) and cumulative overturning (bottom panels) for particles starting in the top 110 m at the inflow for Sconstant binned every 100 m for depth space (a,e), 0,1 ^0C for temperature space (b,f) 0.01 PSU for salinity space (c,g) and 0.01 kg/m^3 for density space (d,h). The withinBC particles are black, InteriorShort particles are red, their sum is the calculated Lagrangian flow (purple). The transport of the InteriorLong particles is also shown (blue dashed line).

6

Discussion and Conclusion

This study investigated whether the volume transport and water mass transformation changes in an idealized simulation of the Labrador Sea when the density variations consist of both salinity and temperature variations as opposed to only a temperature variations. The model that incorporates temperature variations is called the 'reference run' and the models that also incorporates salinity variations is called Sconstant. The resulting density variations are constructed to be equal in the reference run and Sconstant. Also a model configuration which contains a seasonal cycle in salinity has been made (Sseasonal), but most conclusions drawn for Sconstant are the same for Sseasonal. Unless differences are mentioned, Sconstant and Sseasonal show similar results and therefore conclusions below are based on the reference run and Sconstant only.
The main research question of this thesis is repeated here:

What are the differences in the pathways of watermasses and watermass transformation in the Labrador Sea when the density variations are due to both salinity and temperature variations as opposed to only temperature variations?

As are the sub-questions:

1. How do main features (e.g. EKE, MLD, barotropic streamfunction) of the Labrador Sea circulation change with inclusion of salinity?
2. How does the spatial distribution and magnitude of the overturning transport change with inclusion of salinity in depth and density space?
3. How does a seasonal cycle in salinity affect the outcomes above?

First, the sub-questions will be answered in order, and thereafter the main question is answered.
Also, The simulations here analyzed are a highly idealized version of the Labrador Sea, and therefore the results need to be seen in the light of this. For example, the horizontal resolution of the model is 3.75 km, which is too coarse to resolve convective eddies. Convection has been parameterized by enhancing the vertical diffusivity. Furthermore, no wind forcing is present in the model. The mixing caused by wind is parameterized by a vertical decaying diffusion coefficient. Yet, these idealized model simulations are able to capture the boundary current entering the model domain, captures the baroclinic instabilities at the tip of Greenland, resulting in Irminger Rings as well as the overturning in depth space in the basin which is of the same order of magnitude as in reality. Here the overturning is about 4 Sv downwards, whereas in reality this is estimated and measured to be around 1 Sv [39, 40].

How do main features (e.g. EKE, MLD, barotropic streamfunction) of the Labrador Sea circulation change with inclusion of salinity?

No significant differences between the model simulations are found in the pathway of the boundary current. The contour lines of the streamfunction follow the bathymetry as expected for each model run, independent of whether the model contains spatial and lateral salinity variations or not.
The 5-year average mixed layer depth (MLD) for the winter months of February and March shows no significant changes in any of the model runs. The maximum depth for the reference run is 1712 m and 1803 m for Sconstant. With Sseasonal, the location of the deepest average MLD is slightly northeast of that of the reference run. Thus the effects of salinity are not significantly influencing the depth of the average MLD. However,

when looking at the maximum MLD of each month, large differences are seen when salinity is included in the model: depths of 3000 m are reached during the winter months as opposed to depths of about 2000 m for the reference run.
The eddy kinetic energy (EKE) increases significantly for Sconstant. The maximum goes from 530 to 750 cm^2/s^2, and occurs just after the narrowing of the bathymetry at Greenland. Between the runs, this increase in EKE is mainly found in this area.
The total net downwelling stays the same in the basin, which is 3 Sv at a depth of 1000 m for both model configurations. However, the net maximum downwelling increases in area 1 (see figure 4.8), which is the area with the maximum EKE. This increase in downwelling is cancelled out by the combined increased upwelling of areas 2 (area of maximum surface cooling) and area 4 (interior). Thus adding salinity to the model does not increase the net total downwelling, but does increase the up- or downwelling in different regions of the Labrador Sea.

How does the spatial distribution and magnitude of the overturning transport change with inclusion of salinity in depth and density space?

Preferred pathways and associated transport have been investigated by releasing passive particles for a year. Then particles were tracked for a total time of 4 years. The total calculated transport was 17.67 and 17.12 Sv for the reference run and Sconstant respectively. A separation between particles that flow only through the boundary current (withinBC), particles that cross the interior before exiting the model (InteriorShort) and particles that reside in the basin after their lifetime of 4 years (InteriorLong) is made. Even though less transport overall is calculated for Sconstant, more particles flow through the boundary current (from 7.02 to 8.22 Sv). About an equal reduction is seen in the InteriorShort particles, from 6.32 to 5.02 Sv.
A larger outflow out of the boundary current is usually associated with a higher EKE as it is related with more baroclinic instabilities thus favoring lateral advection of particles from the boundary current to the interior. Thus a higher EKE would translate here in less withinBC particles. The opposite is true however: the EKE westward of Greenland is higher for Sconstant but the withinBC particles is also higher. The reduction in InteriorShort particles has been investigated further by investigating where particles leave along the boundary current. It was found that the largest reduction is indeed where the EKE is the largest, which is when particles cross from area 1 to area 4 in figure 4.8, going from 4.71 to 3.86 Sv. In the other areas a reduction of flow into the interior was also found, but less significant as area 1. The inflow into these areas has also been calculated. Between the reference run and Sconstant overall a reduction of waters re-entering the boundary current was found. Only in area 1 the re-entering water volume increased slightly, from 2.1 to 2.22 Sv. Thus, adding salinity to the model actually reduces the volume that is transported through the interior and likewise increases the water mass that is transported through the boundary current. Furthermore, the Sconstant run contains less InteriorLong transport (from 4.32 to 3.87 Sv). This however is likely attributed to the overall reduction in volume transport: it was found that particles leave the model area through the ocean floor more often in the Sconstant. This is likely due to how CMS defines the particles vertical movement in the MLD and the fact that the MLD reaches the bottom of the model in the winter months. CMS assigned a random vertical velocity of up to 0.1 m/s above the MLD. This causes particles to more often leave the basin through the bottom for Sconstant. These particles are thus not represented as InteriorLong or InteriorShort particles, explaining the reduction in InteriorLong and InteriorShort particles between the reference run and Sconstant.
For the overturning in depth space, the vertical profile is very similar for each run. Surface waters are converted to deeper waters and the profile is more barotropic at the outflow for each model simulation. Salinity does thus not influence the overturning in depth space. This was expected, as the density variations throughout the model configurations remained the same, as well as the surface forcing. This means that the waters that enter in each model configuration and leave should have a similar reduction in density, resulting in waters sinking to the same depths.
The overturning in temperature space also shows a similar pattern for both runs, two peaks in temperature distinguishable at the outflow at 5.2 and 4 °C for the reference run and 4.5 and 3 °C for Sconstant. This difference in peak is due to the temperature compensation required in the vertical density profile for the reference run, causing the peaks to shift towards higher temperatures. Furthermore, the maximum transport across the isotherms for the Sconstant is higher than for the reference run (5.3 and 3.9 Sv, respectively). For the reference run, this overturning in density space is the same, as no salinity effects play a role here. But for Sconstant, the overturning reduces to 4.8 Sv in density space, meaning that about 10% density compensation occurs for the Sconstant run. In reality, density compensation can be much higher [22]. But also, in reality other freshwater fluxes exist in the model, such as freshwater entering from Davis St. [41], or surface salinity

fluxes due to precipitation or evaporation for example. These fluxes could contribute to a larger density compensation, but has not been investigated here.
The warmer peak in temperature for both runs is mainly from the withinBC particles. This means that the warmer, surface waters of the boundary current are converted to colder waters along their trajectory. The second peak occurs in both the withinBC particles and the InteriorShort particles.
When comparing the Eulerian measurements to the Lagrangian measurements (figure 5.3) for each space (depth, temperature, salinity and density) it is seen that a significant amount of the transport is missing with the Lagrangian measurements. These transports should be almost the same, as the Lagrangian particles should eventually all pass the Eulerian measurement locations with the same change in properties. Some small differences could occur because the Eulerian measurements are the average of 1 year, while the Lagrangian measurements are the measurements of particles released at this 1 year, and could take longer to reach the outflow. However, there is a large difference between Eulerian and Lagrangian measurements. This is due to the fact that there are many InteriorLong particles in each model simulation (about 4 Sv for each model configuration), which are likely responsible for the reduced signature in overturning. Also, these water masses are likely the most dense water masses at the outflow, following from [37]. At the inflow here, they do not differ much from the InteriorShort particles in their T and S properties. Also, when adding the transport of all released particles at the inflow, the transport (almost) overlaps with the Eulerian measurements (see figure B.6b, for example). At the outflow (figure B.6c) the Lagrangian measurements show reduced transport at the deeper depths flowing out the model domain compared to Eulerian transport, suggesting further that the Interiorlong particles are responsible for a significant overturning signal. The conclusion here is thus that the overturning in depth and density space (also in temperature and salinity space) is mainly reflected in water masses that have resided in the basin for longer than 4 years. Even though the largest contribution in overturning is likely due to the InteriorLong particles, the Lagrangian volume transport (= withinBC and InteriorShort) is also important, as can be seen in figure 5.3e for example: in depth space the maximum Eulerian transport is 4 Sv whereas the Lagrangian transport is 1 Sv, which is 25 % of the maximum Eulerian transport. However, different results are found in [37]: here the Lagrangian and Eulerian transport are almost equal to each other. The difference is that their model did measure for one extra year, traced the particles backwards in time and took less water masses into account at the outflow. This resulted in a reduced amount of InteriorLong particles measured.
The transformation of the withinBC particles has also been investigated by means of a TS diagram for Sconstant. It is found that the withinBC transport shows a gradual overturning signal gradually along the boundary current, where the warmest and freshest waters become colder and more saline along the way. Most of the waters are converted to 37.7 PSU and 4.3 °C. The latter coincides with the peak of figure 5.3 and the first coincides with the first peak in salinity of figure 5.4d (green bars). Thus it can be concluded that the warmer peak in temperature and the fresher peak in salinity of figure 5.4 are at least due to transformations occurring in the boundary current.
Also the top 110 m of the boundary current have been investigated specifically, as these waters contain the bulk of the freshwater inflow. These waters are mainly captured by withinBC particles. It becomes evident that the top waters are partly responsible for the warmer peak in temperature of each model run. For example in figure 5.3b the peak is at 4.5 °C and has a maximum of 1 S and the top 110 m have a maximum of 0.4 Sv at this location. However, the maximum overturning in temperature and salinity space is significantly different between the reference run and Sconstant: the maximum overturning in temperature space is -1.8 and -0.5 Sv respectively, and for salinity the overturning is 1.5 Sv for Sconstant. However, the overturning in density space shows almost no differences between the runs, with a maximum of 1.8 Sv. This means that in the top 110 m waters significant overturning occurs in salinity space, but that the results in density space are not influenced by adding salinity to the model. The results presented here do not suggest that density compensation occurs in the top 110 m. The overturning in salinity and temperature space even strengthen each other.

How does a seasonal cycle in salinity affect the outcomes above?

As mentioned, all conclusions above for Sconstant also apply to Sseasonal, with only small differences. Thus seasonality has no large influence on the annual volume transport in the Labrador Sea in this model simulation. Because of how Sseasonal is constructed, more and fresher waters are added into the basin, increasing the vertical and lateral annually averaged density gradient. A higher lateral density gradient results in an increased EKE, which is also seen here, the maximum EKE for Sconstant is 750 cm^2/s^2 and is 820 cm^2/s^2 for Sseasonal. The increased vertical density gradient results in the maximum MLD being lower for Sseasonal: it goes from 1803 to 1649 m with respect to Sconstant. The reduction in MLD can be explained by the fact that

the vertical density gradient is larger for Sseasonal, meaning that the surface needs to cool for a longer period in order to overcome this increased density gradient. As the cooling periods are equally long in each model, the resulting MLD will be lower for Sseasonal. Due to the same reasoning, the net vertical downwelling over the 4 areas is also lower for Sseasonal, with a maximum of 2.8 Sv (see figure 4.9c). from this figure in area 1 and the upwelling in area 4 does increase, suggesting that these patterns are linked to the increase in EKE over area 1.
With respect to the Lagrangian measurements more water is tracked for Sseasonal than for Sconstant (17.81 Sv as opposed to 17.12 Sv). This is most likely due to more transport flowing into the model, but similar conclusions are still drawn when comparing Sseasonal to the reference run as opposed to comparing with Sconstant to the reference run for all Lagrangian measurements.

Main research question: what are the differences in the pathways of watermasses and watermass transformation in the Labrador Sea when the density variations are due to both salinity and temperature variations as opposed to only temperature variations?

The overturning in the Labrador Sea is of the same magnitude in depth and density space when the density consist of either only temperature gradients or also has salinity gradients. However, significant differences are seen in the freshest waters in the overturning signal (top 110 m waters), where most of the overturning in density space is from overturning in salinity space. The transport re-entering near this EKE peak did increase when salinity variations were added. Also, an increase in EKE is found near the west coast of Greenland when salinity variations exist. Strangely, this coincided with a reduced transport of particles leaving the boundary current overall and near this area. Lastly, a model that contains salinity variations can contain the phenomena called density compensation, which is significant in the Labrador Sea [22].

7

Recommendations

This chapter will give the recommendations for future work. First, suggestions are made based on physical processes which could be investigated. Second, suggestions are made about technical aspects of this thesis could be improved.

The first recommendation is about the fact that the model contains a vertical salinity gradient now in the inflow and the interior, but that there is no salinity flux is applied at the surface yet due to precipitation or evaporation. Furthermore, a freshwater inflow also exist at Davis Strait [41]. The maximum overturning in each model in depth space is about 4 Sv, whereas in reality the downwelling is in the order of 0.9 ± 0.5 Sv [40]. The fresh water from Davis Strait could likely reduce the overturning in density space: the increase in freshness of the model could result in waters becoming less dense. Therefore, it is recommended to further investigate the influence of salinity fluxes by adding the freshwater flux from Davis Strait

The second recommendation is to investigate further the great salinity anomaly. [25], Who used a similar model like the one used in this thesis already made a study on this, but their model only contained salinity variations in the surface layer. Since one of the model configurations here contains a seasonal variation in salinity as well (Sseasonal), this idealized model could be used to investigate the influence of seasonal cycles in salinity further. Known is that large fluctuations in salinity combined with a reduced surface heat loss result in a great salinity anomaly (i.e. the temporal shutdown of deep convection) [14]. This model could be used to study the effects of the great salinity anomaly more precisely, as it is an idealized model. First, it can be investigated whether deep convection has stopped by analyzing the mixed layer depth. Second, it can be investigated how long deep convection is prohibited with a realistic forcing that occurred during the GSA. Lastly, it can be tested whether deep convection restarts with increasing the forcing. Note that an important factor for preventing deep convection for consecutive years is that the thermal expansion coefficient α normally reduces when waters cool. This model contains a linear equation of state, thus it is not able to reproduce this effect. The first suggestion could give insight in how important this α is. A second suggestion would then be to apply a non-linear equation of state, to investigate how α influences the prevention of deep convection to restart.

The third recommendation is to explore the importance of wind forcing on transport in the Labrador Sea. The wind forcing affects at least two processes: the first one is the doming upwards of the isopycnals in the interior [8] and the second one is the transport of fresh waters from the shelf towards the interior [21]. The upward doming of the isopycnals could reduce the threshold for deep convection to start in the current model configuration. Increasing the transport of fresh waters from the shelf – or in these model configurations fresh waters close to the shelf – due to wind forcing however could again reduce the net downwelling. Ideally these two effects of the wind forcing should be separated, if possible.

The last and fourth recommendation is about a technical aspect of the Sseasonal model configuration presented here, which can be improved. This configuration was implemented in order to have inflow conditions and density gradients similar to those in the reference run. However, in this case it was not possible since the seasonal cycle induced a vertically unstable water column during winter months. One solution for future studies in to start the model configuration with the 30-year mean conditions of salinity and temperature. Now, this is only the case for the salinity profile. The temperature profile represents the western Labrador Sea in late summer along the WOCE AR7W section [1]. Also, it is recommended to have the seasonal cycle for temperature changed to the 36 years average as well. With all profiles based on the same data set, the vertical stability will be preserved and the transport and density gradient of each model configuration can be set

equal. It was chosen not to do this here, in order to compare the results better to those of [1], as the density gradients are equal for the reference run and Sconstant.

Bibliography

[1] S. Georgiou, C. van der Boog, N. Brüggemann, S. Ypma, J. Pietrzak, and C. Katsman. On the interplay between downwelling, deep convection and mesoscale eddies in the Labrador Sea. *Ocean Modelling*, 135, 02 2019. doi: 10.1016/j.ocemod.2019.02.004.

[2] T. Kuhlbrodt, A. Griesel, M. Montoya, A. Levermann, M. Hofmann, and S. Rahmstorf. On the driving processes of the Atlantic meridional overturning circulation. *Reviews of Geophysics - REV GEOPHYS*, 45, 04 2007. doi: 10.1029/2004RG000166.

[3] S. Rahmstorf. edited by S. A. Elias. Thermohaline Ocean Circulation. *In: Encyclopedia of Quaternary Sciences*, 2006.

[4] J. W. Sandström. Dynamische Versuche mit Meerwasser. *Ann. Hydrogr. Marit. Meteorol.*, 36:6–23, 1908.

[5] J. Pietrzak and C. Katsman. *An Introduction to Oceanography for Civil and Offshore Engineers*. Delft University of Technology, Delft University of Technology, 2017.

[6] H. Stommel. Thermohaline Convection with Two Stable Regimes of Flow. *Tellus*, 13(2):224–230, 1961. doi: 10.1111/j.2153-3490.1961.tb00079.x.

[7] I. Yashayaev and J. Loder. Further intensification of deep convection in the Labrador Sea in 2016. *Geophysical Research Letters*, 44(3):1429–1438, 2017. doi: 10.1002/2016GL071668. URL `https://agupubs.onlinelibrary.wiley.com/doi/abs/10.1002/2016GL071668`.

[8] J. Marshall and R. A. Plumb. *Atmosphere, Ocean, and Climate Dynamics: An Introductory Text*, volume 93. Elsevier Academic Press., Amsterdam, 2008. ISBN 13: 978-0-12-558691-7.

[9] J. Marshall and F. Schott. Open-ocean convection: Observations, theory, and models. *Reviews of Geophysics*, 37(1):1–64, 1999. doi: 10.1029/98RG02739. URL `https://agupubs.onlinelibrary.wiley.com/doi/abs/10.1029/98RG02739`.

[10] B. Klinger and T. Haine. *Ocean Circulation in Three Dimensions*. Cambridge University Press, 2019. doi: 10.1017/9781139015721.

[11] R. Gelderloos, F. Straneo, and C. Katsman. Mechanisms behind the Temporary Shutdown of Deep Convection in the Labrador Sea: Lessons from the Great Salinity Anomaly Years 1968-71. *Journal of Climate*, 25:6743–6755, 10 2012. doi: 10.1175/JCLI-D-11-00549.1.

[12] C. de Boyer Montégut, G. Madec, A. Fischer, A. Lazar, and D. Iudicone. Mixed layer depth over the global ocean: An examination of profile data and a profile-based climatology. *Journal of Geophysical Research*, 109, 01 2004.

[13] N. Brüggemann and C. Katsman. Dynamics of downwelling in an eddying marginal sea: contrasting the Eulerian and the isopycnal perspective. *Journal of Physical Oceanography*, 09 2019. doi: 10.1175/JPO-D-19-0090.1.

[14] R. Gelderloos. *Variability in Labrador Sea Water formation*. PhD thesis, Utrecht University, 2012.

[15] I. Yashayaev. Hydrographic changes in the Labrador Sea, 1960–2005. *Progress in Oceanography*, 73(3): 242 – 276, 2007. ISSN 0079-6611. doi: https://doi.org/10.1016/j.pocean.2007.04.015. URL `http://www.sciencedirect.com/science/article/pii/S0079661107000857`. Observing and Modelling Ocean Heat and Freshwater Budgets and Transports.

[16] R. Gelderloos, C. A. Katsman, and S. Drijfhout. Assessing the Roles of Three Eddy Types in Restratifying the Labrador Sea after Deep Convection. *Journal of Physical Oceanography*, 41(11):2102–2119, 2011. doi: 10.1175/JPO-D-11-054.1. URL `https://doi.org/10.1175/JPO-D-11-054.1`.

[17] J. Rieck, C. Böning, and K. Getzlaff. The Nature of Eddy Kinetic Energy in the Labrador Sea: Different Types of Mesoscale Eddies, Their Temporal Variability, and Impact on Deep Convection. *Journal of Physical Oceanography*, 49(8):2075–2094, 2019. doi: 10.1175/JPO-D-18-0243.1.

[18] F. Straneo. Heat and Freshwater Transport through the Central Labrador Sea*. *Journal of Physical Oceanography*, 36, 04 2006. doi: 10.1175/JPO2875.1.

[19] R. Dickson, J. Meincke, S. Malmberg, and A. Lee. he "great salinity anomaly" in the Northern North Atlantic 1968–1982. *Progress in Oceanography*, 20(2):103 – 151, 1988. ISSN 0079-6611. doi: https://doi.org/10.1016/0079-6611(88)90049-3. URL http://www.sciencedirect.com/science/article/pii/0079661188900493.

[20] J. Cuny, P. Rhines, P. Niiler, and S. Bacon. Labrador Sea Boundary Currents and the Fate of the Irminger Sea Water. *Journal of Physical Oceanography - J PHYS OCEANOGR*, 32:627–647, 02 2002. doi: 10.1175/1520-0485(2002)032<0627:LSBCAT>2.0.CO;2.

[21] R. Castelao, H. Luo, H. Oliver, A. Rennermalm, M. Tedesco, A. Bracco, P. Yager, T. Mote, and P. Medeiros. Controls on the Transport of Meltwater From the Southern Greenland Ice Sheet in the Labrador Sea. *Journal of Geophysical Research: Oceans*, 05 2019. doi: 10.1029/2019JC015159.

[22] S. Zou, M. Lozier, F. Li, R. Abernathey, and L. Jackson. Density-compensated overturning in the Labrador Sea. *Nature Geoscience*, 13:1–6, 02 2020. doi: 10.1038/s41561-019-0517-1.

[23] R. Pickart and M. Spall. Impact of Labrador Sea Convection on the North Atlantic Meridional Overturning Circulation. *Journal of Physical Oceanography*, 37(9):2207–2227, 2007. doi: 10.1175/JPO3178.1. URL https://doi.org/10.1175/JPO3178.1.

[24] C. Katsman, M. Spall, and R. Pickart. Boundary Current Eddies and Their Role in the Restratification of the Labrador Sea. *Journal of Physical Oceanography*, 34, 09 2004. doi: 10.1175/1520-0485(2004)034<1967:BCEATR>2.0.CO;2.

[25] T. van Dam. Effects of a Freshening Boundary Current on Deep Convection and Eddy Activity in the Labrador Sea. Additional Thesis, TU Delft, 2018.

[26] M. Lozier, F. Li, S. Bacon, F. Bahr, A. Bower, S. Cunningham, M. De Jong, L. de Steur, B. Deyoung, J. Fischer, S. Gary, B. Greenan, N. Holliday, A. Houk, L. Houpert, M. Inall, W. Johns, H. Johnson, C. Johnson, and J. Zhao. A sea change in our view of overturning in the subpolar North Atlantic. *Science*, 363:516–521, 02 2019. doi: 10.1126/science.aau6592.

[27] J. Marshall, A. Adcroft, C. Hill, L. Perelman, and C. Heisey. A finite-volume, incompressible Navier Stokes model for studies of the ocean on parallel computers. *Journal of Geophysical Research*, 102:5753–5766, 10 1997. doi: 10.1029/96JC02775.

[28] J. Gascard and A. Clarke. The Formation of Labrador Sea Water. Part II. Mesoscale and Smaller-Scale Processes. *Journal of Physical Oceanography*, 13(10):1779–1797, 1983. doi: 10.1175/1520-0485(1983)013<1779:TFOLSW>2.0.CO;2. URL https://doi.org/10.1175/1520-0485(1983)013<1779:TFOLSW>2.0.CO;2.

[29] A. Bracco, J. Pedlosky, and R. Pickart. Eddy Formation near the West Coast of Greenland. *Journal of Physical Oceanography*, 38(9):1992–2002, 2008. doi: 10.1175/2008JPO3669.1. URL https://doi.org/10.1175/2008JPO3669.1.

[30] L. Yu, X. Jin, and R. Weller. Multidecade Global Flux Datasets from the Objectively Analyzed Air-sea Fluxes (OAFlux) Project: Latent and Sensible Heat Fluxes, Ocean Evaporation, and Related Surface Meteorological Variables. *OAFlux Project Tech. Rep. OA-2008-01*, 01 2008.

[31] V. Gouretski. WOCE-Argo Global Hydrographic Climatology (WAGHC Version 1.0), 2018. URL https://doi.org/10.1594/WDCC/WAGHC_V1.0.

[32] Y. Qian, T. Dixon, P. Myers, J. Bonin, D. Chambers, M. Van den Broeke, M. Ribergaard, and J. Mortensen. Recent increases in Arctic freshwater flux affects Labrador Sea convection and Atlantic overturning circulation. *Nature Communications*, 7, 01 2016. doi: 10.1038/ncomms10525.

[33] C. Paris, J. Helgers, E. Sebille, and A. Srinivasan. Connectivity Modeling System: A probabilistic modeling tool for the multi-scale tracking of biotic and abiotic variability in the ocean. *Environmental Modelling and Software*, 42, 04 2013. doi: 10.1016/j.envsoft.2012.12.006.

[34] R. Pickart, D. Torres, and R. Clarke. Hydrography of the Labrador Sea during Active Convection. *Journal of Physical Oceanography - J PHYS OCEANOGR*, 32:428–457, 02 2002. doi: 10.1175/1520-0485(2002)032<0428:HOTLSD>2.0.CO;2.

[35] C. Eden and C. Böning. Sources of Eddy Kinetic Energy in the Labrador Sea. *Journal of Physical Oceanography*, 32(12):3346–3363, 2002. doi: 10.1175/1520-0485(2002)032<3346:SOEKEI>2.0.CO;2. URL https://doi.org/10.1175/1520-0485(2002)032<3346:SOEKEI>2.0.CO;2.

[36] H. Hátún, C. Eriksen, and P. Rhines. Buoyant Eddies Entering the Labrador Sea Observed with Gliders and Altimetry. *Journal of Physical Oceanography - J PHYS OCEANOGR*, 37, 12 2007. doi: 10.1175/2007JPO3567.1.

[37] S. Georgiou, S. Ypma, N. Brüggemann, J. Sayol, J. Pietrzak, and C. Katsman. Pathways of the water masses exiting the Labrador Sea: The importance of boundary–interior exchanges. *Ocean Modelling*, 150:101623, 2020. ISSN 1463-5003. doi: https://doi.org/10.1016/j.ocemod.2020.101623. URL http://www.sciencedirect.com/science/article/pii/S1463500319303385.

[38] L. Schulze and E. Frajka-Williams. Wind-driven transport of fresh shelf water into the Labrador Sea Basin. *Ocean Science Discussions*, pages 1–30, 03 2018. doi: 10.5194/os-2018-18.

[39] M. Spall and R. Pickart. Where Does Dense Water Sink? A Subpolar Gyre Example. *Journal of Physical Oceanography*, 31(3):810–826, 2001. doi: 10.1175/1520-0485(2001)031<0810:WDDWSA>2.0.CO;2. URL https://doi.org/10.1175/1520-0485(2001)031<0810:WDDWSA>2.0.CO;2.

[40] J. Holte and F. Straneo. Seasonal Overturning of the Labrador Sea as Observed by Argo Floats. *Journal of Physical Oceanography*, 47(10):2531–2543, 2017. doi: 10.1175/JPO-D-17-0051.1. URL https://doi.org/10.1175/JPO-D-17-0051.1.

[41] P. Myers. Impact of freshwater from the Canadian Arctic Archipelago on Labrador Sea Water formation. *Geophysical Research Letters*, 32(6), 2005. doi: 10.1029/2004GL022082. URL https://agupubs.onlinelibrary.wiley.com/doi/abs/10.1029/2004GL022082.

A

Appendix A - Derivation inflow conditions for the reference run

Here, the derivation of the formula's given in chapter 2.2.2 is shown, which are from [24]. First, the thermal wind balance itself is derived from the geostrophic balance and hydrostatic pressure. Thereafter combining the thermal wind with the linear equation of state along with mathematical profiles in y and z direction result in the found relationships for U and T at the inflow. Geostrophic balance for zonal velocity:

$$u = \frac{-1}{f\rho_0}\frac{\partial P}{\partial y} \tag{A.1}$$

Hydrostatic pressure:

$$-\rho g = \frac{\partial P}{\partial z} \tag{A.2}$$

Take z derivative of (A.1):

$$\frac{\partial u}{\partial z} = \frac{-1}{f\rho_0}\frac{\partial P}{\partial y \partial z} \tag{A.3}$$

Substitute (A.2) into (A.3):

$$\frac{\partial u}{\partial z} = \frac{g}{f\rho_0}\frac{\partial \rho}{\partial y} \tag{A.4}$$

Which is also known as the 'thermal wind balance'.
Next the linear equation of state is defined:

$$\rho = \rho_0(1 - \alpha(T - T_{ref})) \tag{A.5}$$

Combine (A.4) with (A.5) and apply 'sum rule':

$$\frac{\partial \rho}{\partial y} = \frac{\partial \rho_0(1 - \alpha(T - T_{ref}))}{\partial y} = -\rho_0 \alpha \frac{\partial T}{\partial y} \tag{A.6}$$

Hence

$$\frac{\partial u}{\partial z} = \frac{-g\alpha}{f}\frac{\partial T}{\partial y} \tag{A.7}$$

The temperature profile in y and z direction has then been prescribed with a hyperbolic tangent relationship in y direction and a linear relationship in z direction as in [24]:

$$T_{in}(y,z) = T_{ref}(z) - \frac{\Delta\rho}{2\alpha\rho_0}\left(1 - \frac{z}{z_b}\right)\left[1 + tanh\left(\frac{y - y_0}{L_y}\right)\right] \tag{A.8}$$

The factor $\frac{\Delta\rho}{\alpha\rho_0}$ comes from equation (A.5)

$$\Delta T = \frac{1}{\alpha} - \frac{\rho}{\alpha\rho_0} = \frac{\alpha\rho_0 - \alpha\rho}{\alpha^2\rho_0} = \frac{-\Delta\rho}{\alpha\rho_0} \tag{A.9}$$

where ΔT = T - T_{ref} and Δ ρ = ρ - ρ_0 And the factor 1/2 comes from the choice of the profile in y direction [24].

Lastly, combining equation (A.8) and (A.4) by taking the derivative of T with respect to y and integrating over z where at z_b u=0 will give:

$$U_{in}(y,z) = g\frac{\Delta\rho}{4L_y f\rho_0}\frac{(z-z_b)^2}{z_b}\frac{1}{cosh^2\left(\frac{y-y_0}{L_y}\right)} \tag{A.10}$$

B

Appendix B - Supplementary figures

This appendix contains supplementary figures of the model configurations. Most of the figures are from the reference run and Sseasonal.

B.1. Bar plots of volume transport at the inflow and outflow

Here the bar plots in temperature, salinity and density space of the reference run (figure B.1) and Sseasonal (figure B.2) are shown. These are constructed similarly as the bar plot for Sconstant (figure 5.4).

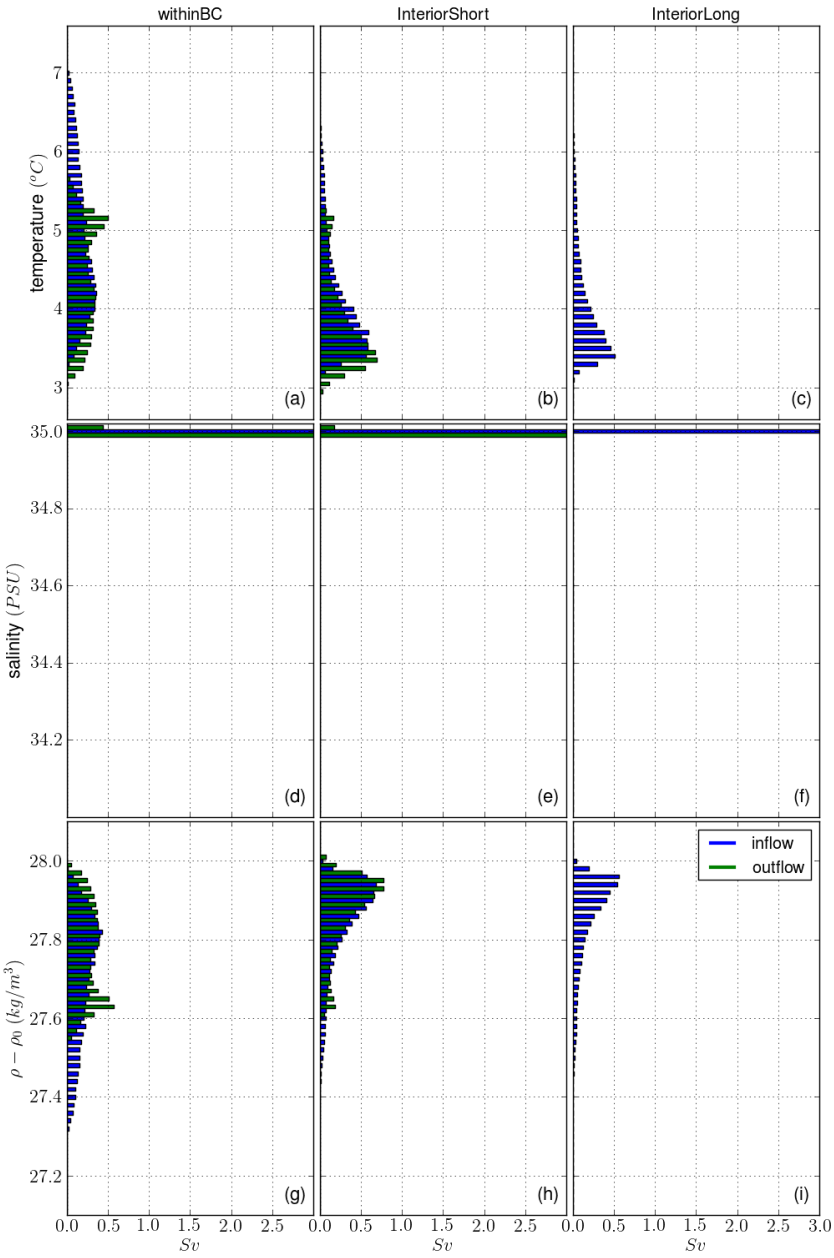

Figure B.1: Bar plots of transport of the inflow (blue bars) and outflow (green bars) for the reference run in. Figures a-c show temperature space, binned every 0.1 ^0C, d-f show salinity space binned every 0.01 PSU and g-i density space binned every $0.01 kg/m^3$. From top to bottom separations have been made for particles that flow only through the boundary current (a,d,g), InteriorShort particles (b,e,h) and InteriorLong particles (c,f,i).

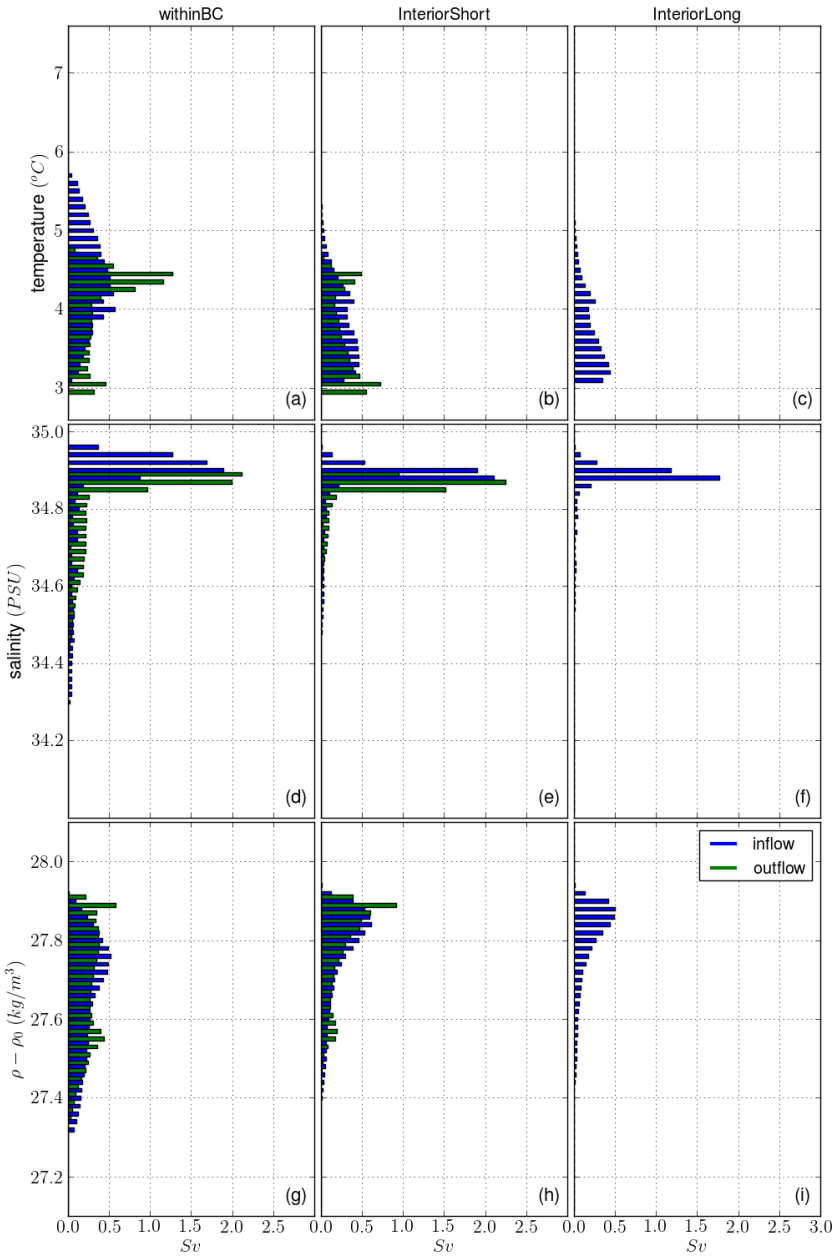

Figure B.2: Bar plots of transport of the inflow (blue bars) and outflow (green bars) for Sseasonal in. Figures a-c show temperature space, binned every 0.1 ^0C, d-f show salinity space binned every 0.01 PSU and g-i density space binned every 0.01kg/m^3. From top to bottom separations have been made for particles that flow only through the boundary current (a,d,g), InteriorShort particles (b,e,h) and InteriorLong particles (c,f,i).

B.2. Net and cumulative volume transport

Here the net and cumulative overturning in depth, temperature, salinity and density space is shown for the reference run (figure B.3) and Sseasonal (figure B.4).

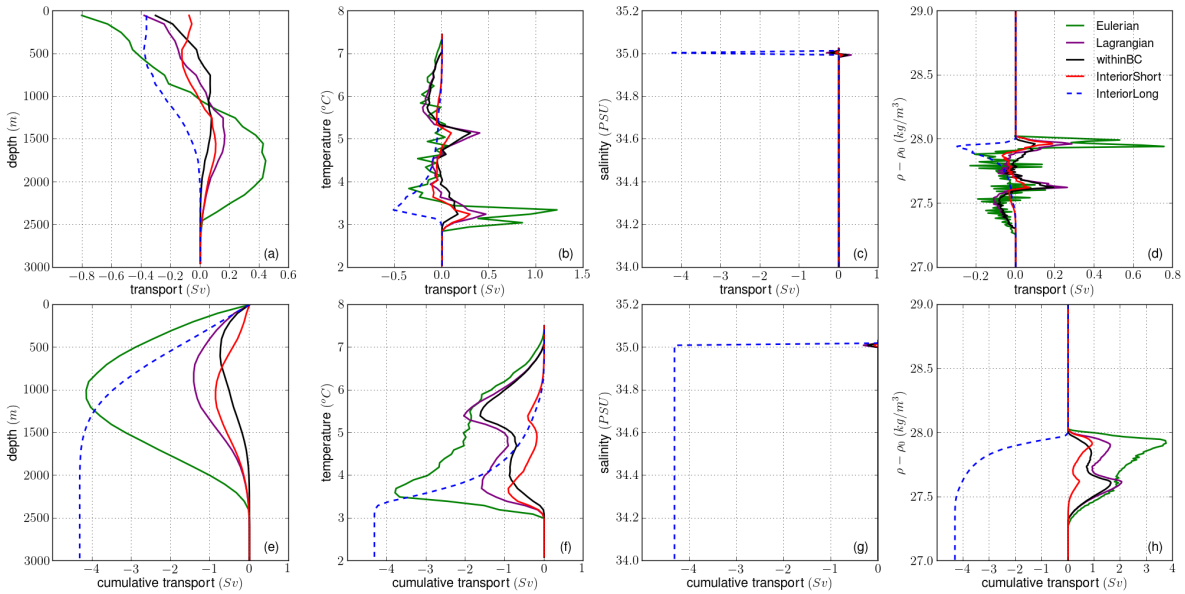

Figure B.3: Net volume transport (out - in, top panels) and cumulative transport (bottom panels) for the reference run binned every 100m for depth space (a,e), 0,1 ^0C for temperature space (b,f) 0.01 PSU for salinity space (c,g) and 0.01 kg/m^3 for density space (d,h). Eulerian is the total calculated net transport (green line), withinBC particles are black, InteriorShort particles are red, their sum is the calculated Lagrangian flow (purple). The transport of the InteriorLong particles is also shown (blue dashed line).

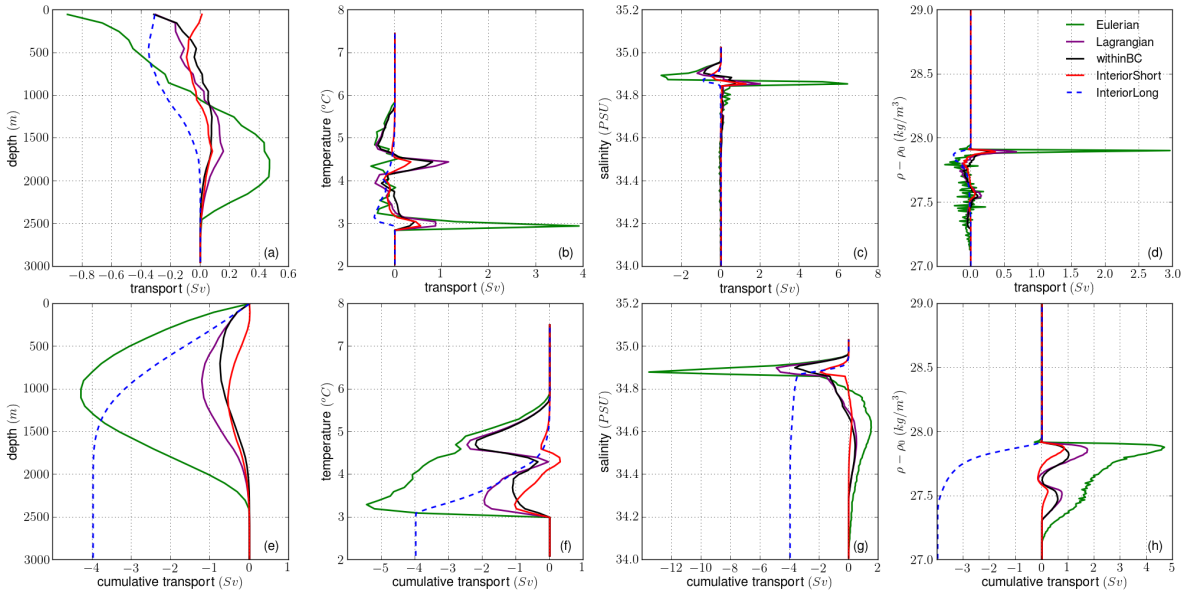

Figure B.4: Net volume transport (out - in, top panels) and cumulative transport (bottom panels) for Sseasonal binned every 100m for depth space (a,e), 0,1 ^0C for temperature space (b,f) 0.01 PSU for salinity space (c,g) and 0.01 kg/m^3 for density space (d,h). Eulerian is the total calculated net transport (green line), withinBC particles are black, InteriorShort particles are red, their sum is the calculated Lagrangian flow (purple). The transport of the InteriorLong particles is also shown (blue dashed line).

B.3. Volume transport separated into inflow and outflow, and net volume transport

This section shows the net volume transport in depth, temperature, salinity and density space (a,d,g and j of figures B.5, B.6 and B.7. These columns are the same as for example for the reference run figure B.3a-d. Next, the volume transport is separated into inflow (b,e,h and k) and outflow (c,f,i and l) of figures B.5, B.6 and B.7.

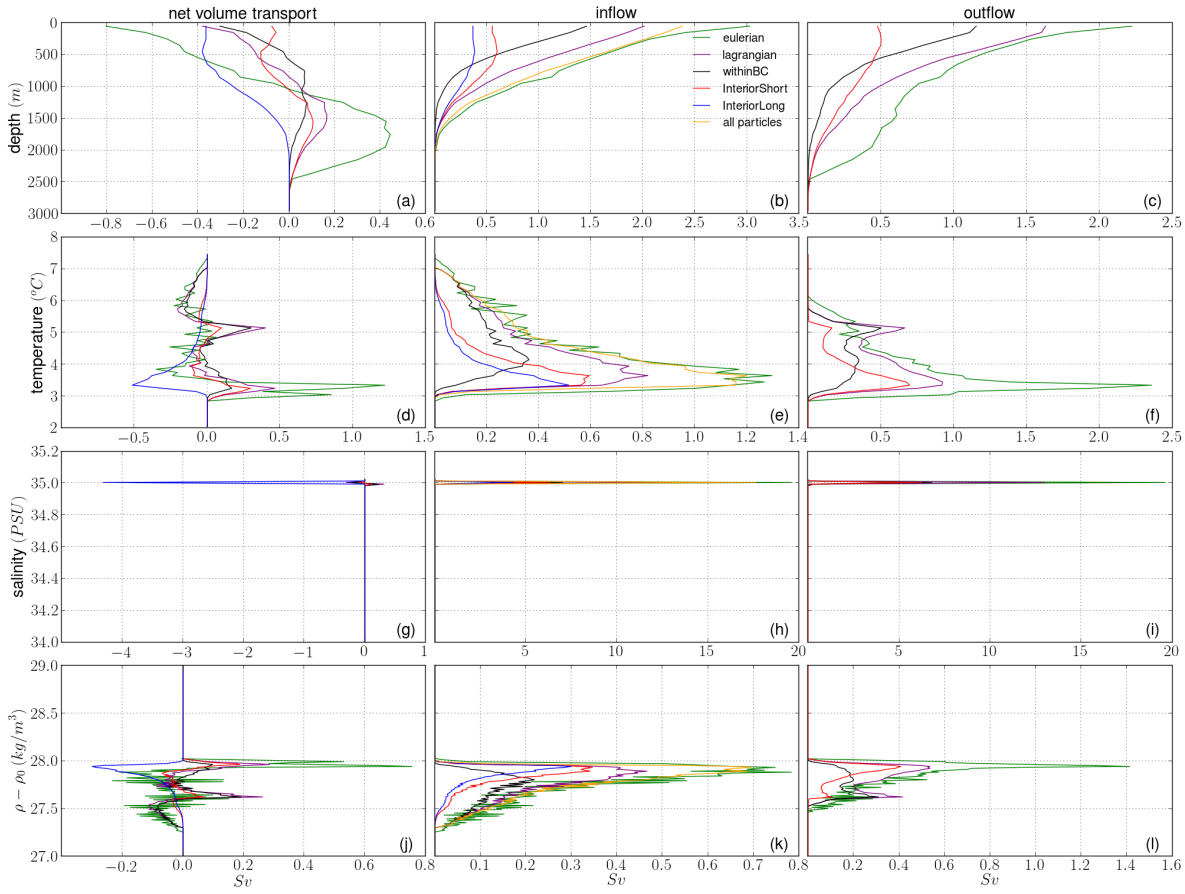

Figure B.5: Net overturning (left column), total inflow (middle column) and total outflow (right column) for the reference run binned every 100m for depth space (a,b,c), 0,1 ^0C for temperature space (d,e,f) 0.01 PSU for salinity space (g,h,i) and 0.01 kg/m^3 for density space (j,k,l). Eulerian is the total calculated net transport (green line), withinBC particles are black, InteriorShort particles are red, their sum is the calculated Lagrangian flow (purple). The transport of the InteriorLong particles is also shown (blue dashed line). The yellow line at the inflow is Lagrangian + InteriorLong.

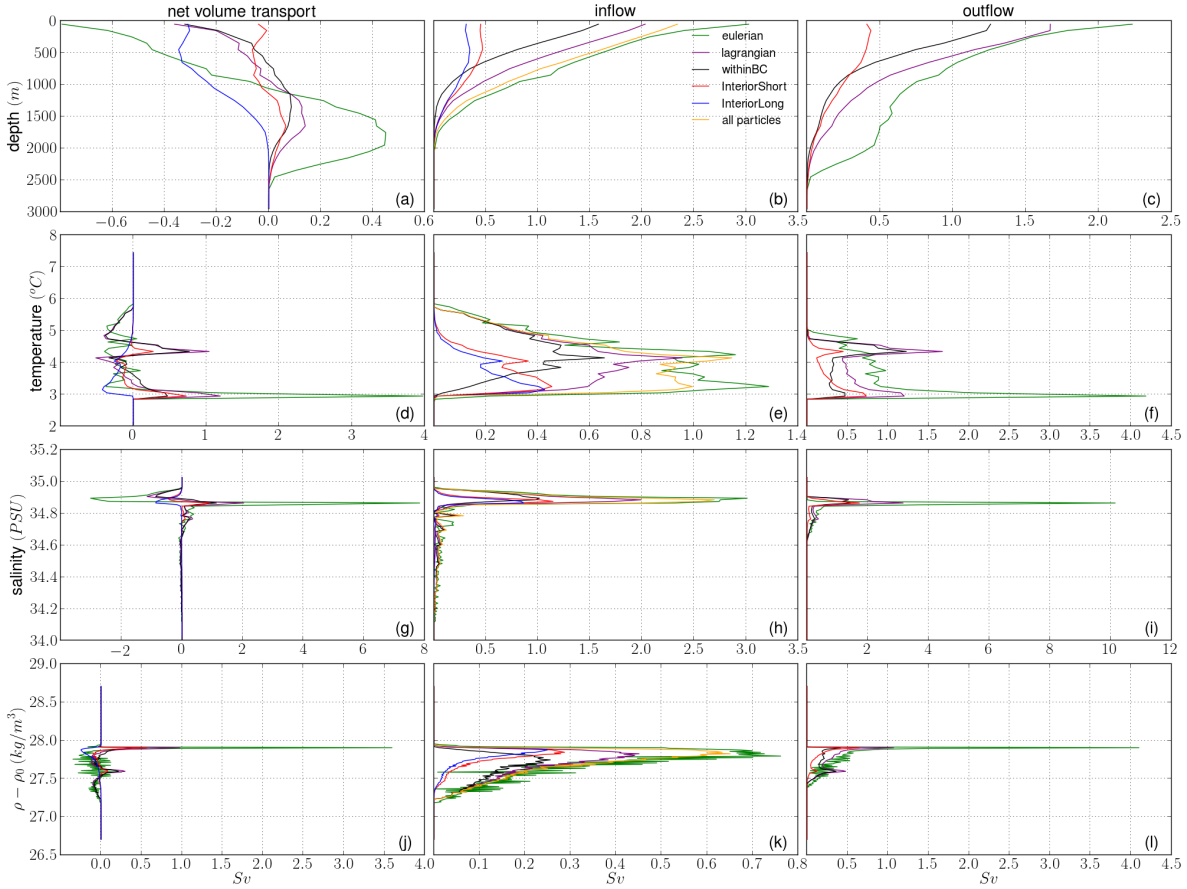

Figure B.6: Net overturning (left column), total inflow (middle column) and total outflow (right column) for Sconstant binned every 100m for depth space (a,b,c), 0,1 ^0C for temperature space (d,e,f) 0.01 PSU for salinity space (g,h,i) and 0.01 kg/m^3 for density space (j,k,l). Eulerian is the total calculated net transport (green line), withinBC particles are black, InteriorShort particles are red, their sum is the calculated Lagrangian flow (purple). The transport of the InteriorLong particles is also shown (blue dashed line). The yellow line at the inflow is Lagrangian + InteriorLong.

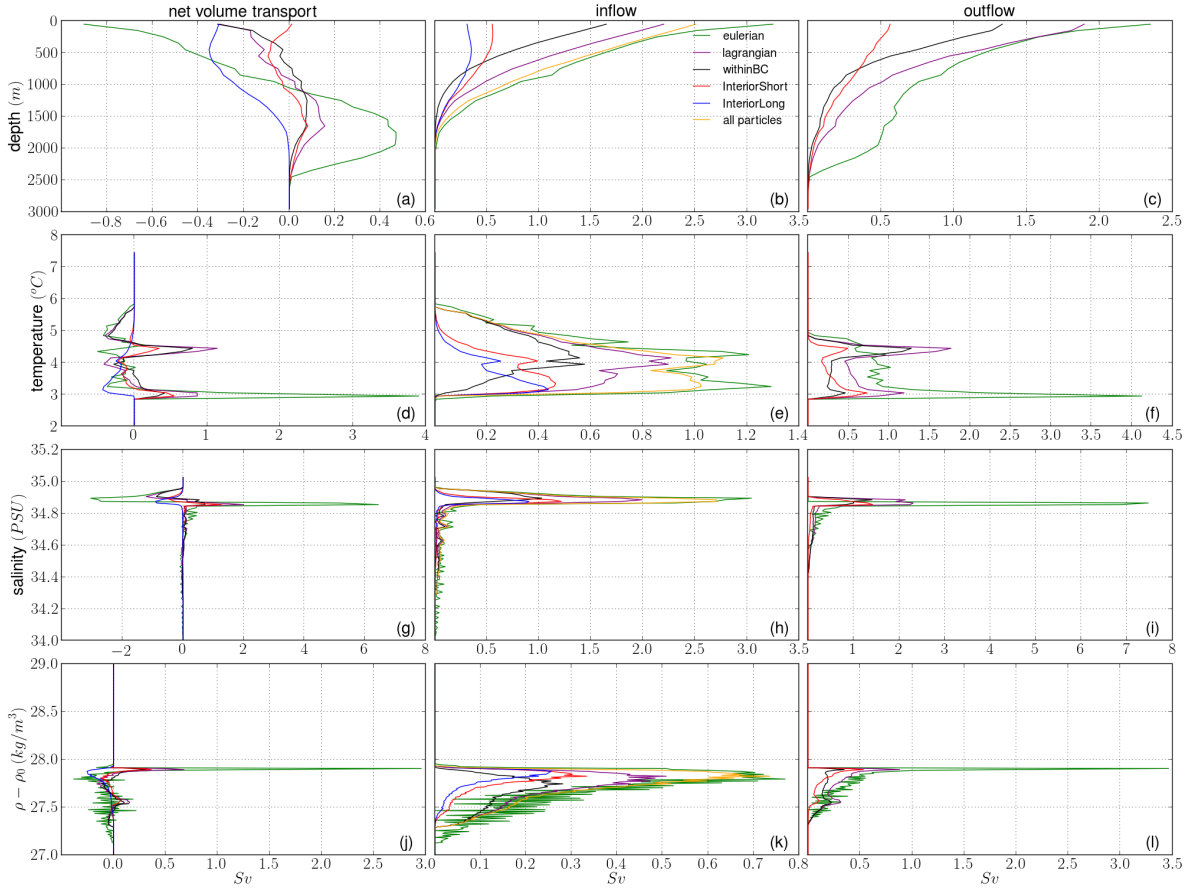

Figure B.7: Net overturning (left column), total inflow (middle column) and total outflow (right column) for Sseasonal binned every 100m for depth space (a,b,c), 0,1 ^0C for temperature space (d,e,f) 0.01 PSU for salinity space (g,h,i) and 0.01 kg/m^3 for density space (j,k,l). Eulerian is the total calculated net transport (green line), withinBC particles are black, InteriorShort particles are red, their sum is the calculated Lagrangian flow (purple). The transport of the InteriorLong particles is also shown (blue dashed line). The yellow line at the inflow is Lagrangian + InteriorLong.

B.4. Lateral transport of InteriorShort particles in area 1

Here the InteriorShort particles that leave, re-enter and and their net volume transport in area 1 is shown for the reference run (figure B.8) and Sseasonal (figure B.9).

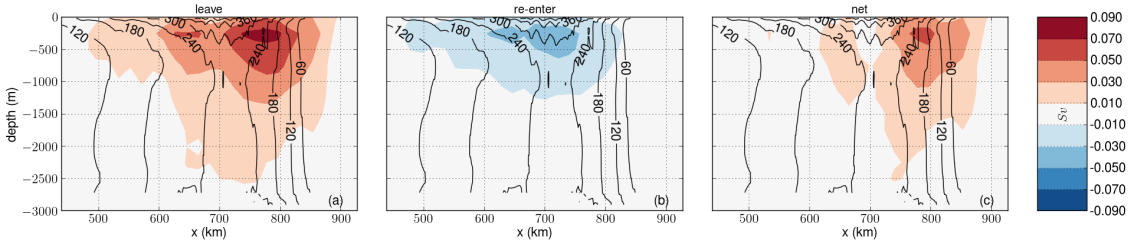

Figure B.8: Concentration of where volume transport leaves the BC (a), re-enters the BC (b) and net transport (c) of InteriorShort particles in area1 for the reference run. The contour lines show the EKE.

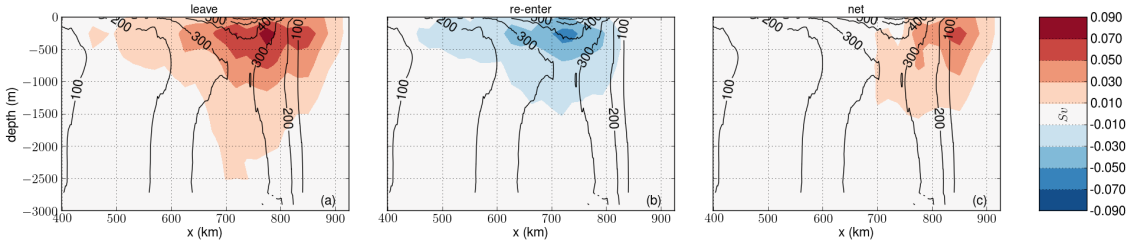

Figure B.9: Concentration of where volume transport leaves the BC (a), re-enters the BC (b) and net transport (c) of InteriorShort particles in area1 for Sseasonal. The contour lines show the EKE.

B.5. Net and cumulative volume transport of the top 110m waters

This section shows the net and cumulative volume transport in depth, temperature, salinity and density space for the reference run (figure B.10) and Sseasonal (figure B.11).

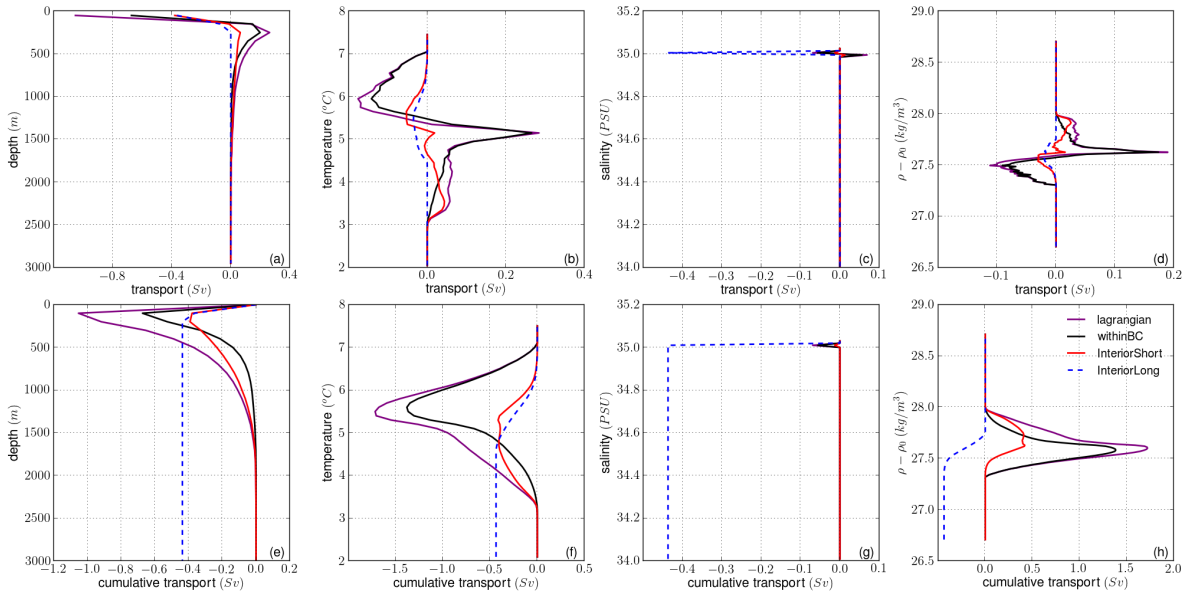

Figure B.10: Net overturning (top panels) and cumulative overturning (bottom panels) for particles starting in the top 110m at the inflow for the reference run binned every 100m for depth space (a,e), 0,1 ^0C for temperature space (b,f) 0.01 PSU for salinity space (c,g) and 0.01 kg/m^3 for density space (d,h). The withinBC particles are black, InteriorShort particles are red, their sum is the calculated Lagrangian flow (purple). The transport of the InteriorLong particles is also shown (blue dashed line).

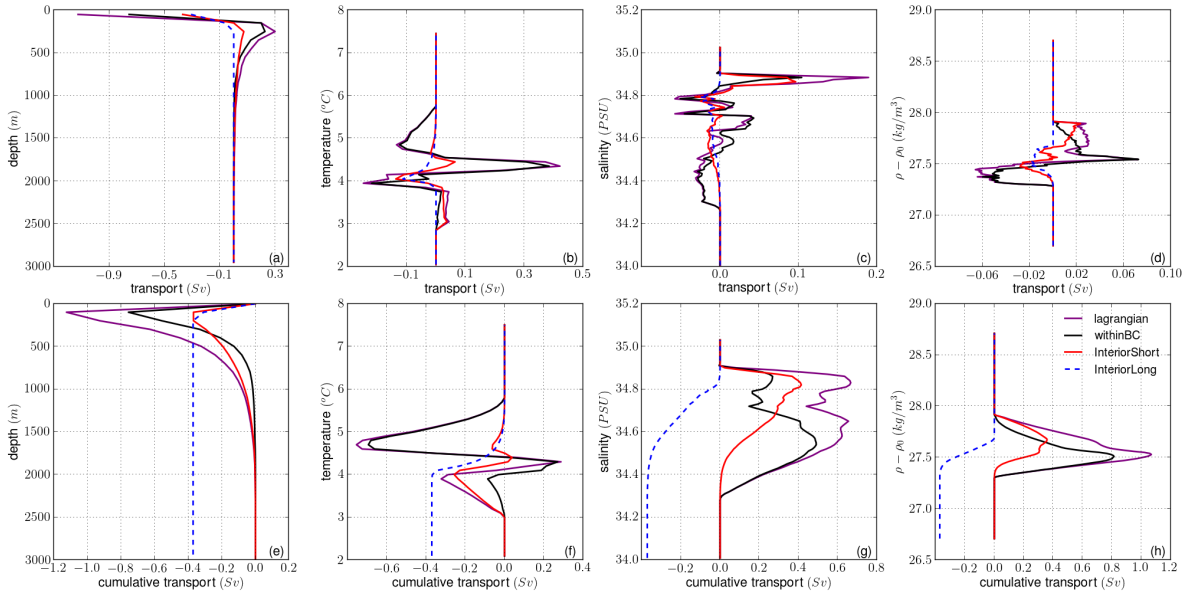

Figure B.11: Net overturning (top panels) and cumulative overturning (bottom panels) for particles starting in the top 110m at the inflow for Sseasonal binned every 100m for depth space (a,e), 0,1 ^0C for temperature space (b,f) 0.01 PSU for salinity space (c,g) and 0.01 kg/m^3 for density space (d,h). The withinBC particles are black, InteriorShort particles are red, their sum is the calculated Lagrangian flow (purple). The transport of the InteriorLong particles is also shown (blue dashed line).